ABSTRACT

Title of Document: MULTIPHOTON ABSORPTION: FABRICATION, FUNCTIONALIZATION AND APPLICATIONS

Linjie Li, Doctor of Philosophy, 2009

Directed By: Professor John T. Fourkas,
Department of Chemistry and Biochemistry

Despite the remarkable progress in micro/nano-scale fabrication that has occurred over the last decades, feature sizes are still restricted by the diffraction limit. The resolution in conventional photolithography is generally constrained to approximately one quarter of a wavelength (λ) of the light used. Multiphoton absorption polymerization (MAP) offers another option for high-resolution fabrication. Using nonlinear optical and chemical effects, MAP can generate features with a transverse dimension as small as 80 nm using 800-nm laser excitation. MAP has the additional capability of fabricating arbitrary 3D structures, which is essential in many applications. Details of MAP fabrication setup and process are described in this thesis. Novel optical devices have been fabricated with MAP.

One drawback of MAP is that the resolution in axial direction remains about three to five times poorer because of the shape of the laser focal point. A novel technique called Resolution Augmentation through Photo-Induced Deactivation

(RAPID) lithography has been developed to overcome this issue. With RAPID, resolution of 40 nm in axial direction has been achieved. The aspect ratio of the volume element of MAP has been reduced from about 3 to 0.5.

Selective functionalization of polymeric microstructure has been performed in two ways. In the first approach, microstructures are fabricated with hybrid resists that permits the chemical functionality only applies to one material. The second method is able to pattern both binary and gray-scale functionalities onto polymer surface. The density of the surface functional groups is determined by the intensity of the exposed light.

The nonlinear novelty of multiphoton absorption has not only been realized in MAP, it also shows promise for multiphoton absorption based microscopy. Photoluminescence from noble metal nanostructures has been used for two-photon imaging of living cells. Multiphoton Absorption Induced Luminescence (MAIL) has been used to monitor the targeting and endocytosis of goldnanoparticles to human umbilical vein endothelial cells. Field-enhanced phenomena have been studied with MAIL and MAP.

MULTIPHOTON ABSORPTION: FABRICATION, FUNCTIONALIZTION, AND APPLICATIONS

By

Linjie Li

Dissertation submitted to the Faculty of the Graduate School of the
University of Maryland, College Park, in partial fulfillment
of the requirements for the degree of
Doctor of Philosophy
2009

Advisory Committee:
Professor John T. Fourkas, Chair
Professor Sang Bok Lee
Professor Michael R. Zachariah
Professor Julius Goldhar
Professor Yuhuang Wang

Acknowledgements

It is a pleasure to thank those who made this thesis possible.

I would like to thank, from the bottom of my heart, my wife, Yan, for her love, understanding and support throughout my graduate study. I will never forget those "I-am-only-a-phone-call-away" days when we were apart by the oceans and continents. I am forever indebted to her for giving up her Ph. D. study and coming to this country to accompany me while I completed the work in this thesis. She has brought good time to my life and kept bad time away. I am confident that together we can weather any storm the 'real world' will present. Thank you, Yan. I love you.

I would also like to thank my parents for their life-long support. My parents instilled in me strong values of hard work, integrity, and they gave me the confidence to always strive for excellence. During my more than twenty years "student" career, they always build up an environment for me to concentrate on my work without any distractions.

I would like to deliver my numerous thanks to those people who have helped me with my research.

First and foremost I offer my sincerest gratitude to my supervisor, Dr. John Fourkas, who has supported me throughout my doctoral work with his breadth of knowledge, creativity and patience. Nearly all the clever ideas in this thesis were his, and I simply had the pleasure of turning them into a reality. One simply could not wish for a better or friendlier supervisor. I have enjoyed very much my five years in this lab under his advising.

I would also like to thank all the present and previous members of the Fourkas group that I had the pleasure to work with, particularly: Dr. Chris LaFratta, Dr. Erez Gershgoren, Dr. Rafael Gatass and Dr. George Kumi.

Dr. Chris LaFratta was my first American friend and teacher. He has patiently taught me almost everything he knows about the research in Fourkas group. I will forever remember those days when we worked together from 6 am to 2 am. I will forever remember all of the summer barbeques and his homemade delicious beers. He has set an example for me not only in science but also in daily life.

Dr. Erez Gershgoren has given me incredible help on RAPID project at the beginning stages. His broad knowledge and intelligence in science have driven all the projects to move forward. I was always amazed by his high efficiency: " I can finish it in fifteen milliseconds, or five microseconds---with coffee". I appreciate that he continues giving me great advice even after he left the country.

Dr. Rafael Gatass joined the group in my fourth year. I have to admit that I really wish I had known him much earlier. He passed me his attitude on science, which is brand new to me. He has taught me how to write and how to give a good presentation, which I believe will benefit my future career a lot. He has also brought his humor and enthusiasm to the whole group. Without Erez and Rafael, the RAPID project would be still only my proposal.

Dr. George Kumi, another postdoc who does not eat lunch, like Erez. He is also another great friend and scientist with broad knowledge in both physics and chemistry. He helped me a lot in microring resonator and surface patterning projects. He is also one of the two postdocs in the group who have been always joking with me

(the other one is Rafa for sure). But his attitude on research is one of the most scrupulous I have ever seen.

I would thank Juliet Znovena for teaching me a lot English and American culture. Many thanks go to Dr. Richard Farrer and Dr. Tommaso Baldacchini for their pioneer work of my project and their advise on my career. I would also thank Dr. Xiang Zhu for being such a good friend and mentor in many categories. A special thank would give to soon-to-be Dr. Qin Zhong, my great friend and five-year-long roommate. Together, we have explored this unknown lands from Boston to Maryland. Together, we have battled with many difficulties both in life and in Ph. D. study.

I am grateful to my colleagues who joined the group after me. I would thank Kathleen Monoca for all the helpful discussions and all the cup cakes. Thanks go to Mike Stoker for all the coffees and the free parking permit. And I really enjoyed the racket ball games we have played. I would also express my warmest thanks to Sanghee Nah for help with MAIL project; Meghan Driscoll and Ronald Hernandez for helps with amine pattern project; Sijia Qin for help with ring resonator fabrication; Hana Hwang for help with RAPID project. Thanks also go to other group members: Soner Erduran, Yunbo Shi, Xiaoxiao He, Pearl Hwang, Nteke Mulenga and Sheree Ibrahim.

I would like to thank many professors and their students in the chemistry department: Dr. Sang Bok Lee, Dr. Xia bai and Ran Liu for helpful discussion of electrodeposition; Dr. Philip DeShong, Dr. Juhee Park and Matthew Dowling for help

with cell imaging; Dr. Doug English for help with AFM; Dr. Robert Walker and Dr. Wendy Heiserman for help with fluorometer. Dr. Karen Gaskell for help with XPS.

I would like to thank professors and their students in the laboratory for physical sciences: Dr. Warren Herman, Dr. Ping-Tong Ho, Dr. Wei-Yen Chen and Dr. Tienan Ding for the helps with microring resonator project; Dr. Julius Goldhar, Dr. Yongzhang Leng and Dr. Victor Yun for help with photo mask fabrication; Dr. Weilou Cao for the help with nonlinearity measurement; Dr. Dong Park for helpful discussions.

I would like to thank professors and their students in the physics department: Dr. Ellen Williams, Dr. Brad Conrad and Jianhao Chen for helps with AFM measurement; Dr. Wolfgang Losert for help with amine patterning project.

I would like to thank professors and their students in the electrical engineering department: Dr. Reza Ghodssi, Dr. Lance Mosher and Stephan Koev for the helpful discussion on MEMS and gray-scale mask; Dr. Thomas Murphy for helpful discussions on stage stitching project.

Lastly, I would like to thank people who helped with SEM facility: Dr. Tim Maugel for helpful discussion on SEMs and American culture; Dr. Wen-An Chiou and Li-Chung Lai for help with SU-70 FESEM; Mr. Dave Myers for SEM maintenance.

Most of the work presented in this thesis was supported by funds from the National Science Foundation

Table of Contents

List of Figures

Chapter 1: Micro/Nano-scale Fabrication

1.1 Introduction

The information revolution has become a well-known term since the last decade of the twentieth century. It began with the inventions of integrated circuit (IC) chips and computer chips in 1960's.[1, 2] Those chips have changed and are changing our daily life dramatically. Turning into the twenty-first century, new miniaturization techniques are required to fulfill the demand of the smaller size of the chips and more components on each chip. Therefore, *nanotechnology* has become one of the most important technologies in this revolution.

Among all the aspects of nanotechnology, fabrication techniques are one of the most important. Innovations in the area of micro and nanofabrication have created opportunities to manufacture devices at the micrometer and nanometer scales. In 2008, state-of-the-art computers were made with over 2 billion transistors per chip, representing individual features on the scale of tens of nanometers.[3] These chips benefited from improvements in fabrication methods, such as lower cost, lower power consumption, faster response, and higher performance. These micro/nano-fabrication techniques have not only improved the chip industry but also opened a new era for many other fields. For instance, micro-electromechanical systems (MEMS) have

been developed for over two decades,[4-8] with interest increasing recently because of growing commercial applications. Micro-total analysis systems (μTAS)[9-11] are also drawing more and more attention, with many potential applications in biological areas.

Techniques for the fabrication of micro/nano-scale devices can be divided into two broad categories, including "bottom-up" methods and "top-down" methods. In "bottom-up" methods, the desired features are simply constructed from fundamental building blocks, such as atoms and molecules. In "top-down" methods, devices are fabricated via micro-miniaturization with advanced technologies, such as photolithography and laser micromachining, etc. Among all of these techniques, photolithography is the most widely used in the MEMS and μTAS fabrication. It has become a well-established technique for microscale patterning over the past fifty years.[12] It is capable of creating freestanding objects in silicon and other materials, with thickness and lateral dimensions down to tens of nanometers. This is truly a technological marvel. However, photolithography is essentially a planar technique. By combining layers or using special release techniques, patterns can be extend into the third dimension, but the control in the vertical dimension does not have as much freedom as that in the horizontal dimensions.

Several alternative patterning techniques have been developed to circumvent the 2-D constraint, such as ink-based writing,[13, 14] self-assembly,[15] layer-by-layer assembly,[16, 17] and X-ray lithography.[18, 19] Another technique based on the nonlinear absorption of light, multiphoton absorption polymerization (MAP), offers an alternative way to fabricate 3-D structures of arbitrary geometry.[12] MAP employs a

simple experimental setup and a straightforward fabrication scheme. It has also been shown that MAP is capable of fabricating features with resolution down to 80 nm, using 800nm laser.[20]

In this chapter, different advanced micro/nano-fabrication techniques will be presented, including their advantages and disadvantages. The details of MAP will be discussed.

1.2 Micro/nano-fabrication techniques

1.2.1 Bottom-up methods

Bottom-up fabrication techniques use chemical or physical forces operating at the nanoscale to transform basic units into large structures. It is usually unnecessary to use a pre-patterned mask in bottom-up processes. However, in order to obtain well-defined microscopic growth of nanostrutures, the growth mechanisms of the materials have to be well understood. There are several traditional processes used for bottom-up fabrication, such as chemical vapor deposition (CVD), sol-gel processing, plasma or flame spraying synthesis, etc. These methods are very effective to make large amounts of materials in one batch. The drawback of these techniques is the lack of 3-D control at large scales. In recent years, several new bottom-up methods have been developed to fabricate more controllable 3-D micro/nano-structures, such as self-assembly and template assisted growth.

Self-assembly is nature's way of building up materials. It is the "autonomous organization of components into patterns or structures without human intervention".[21] Self-assembly has the capability of creating arbitrarily complex 3-D patterns, as demonstrated by biological systems. It also shows promise for applications in the semiconductor industry. For instance, IBM recently reported the first-ever application of a self-assembly nanotechnology to build computer chips.[22] Self-assembly is a great tool for nanofabrication. However, it is currently best suited for *periodic* structures. It cannot be used to create more complex systems because of the lack of arbitrary control of the material growth.

Template-assisted growth offers another approach to fabricate nanostructures. Three-dimensional growth of nanoscale materials can be directed by the two-dimensional predesigned seed points or through periodically ordered arrays of holes as a growth template, such as a nano-pore filter.[23-26] The advantage of this technique is that it is inexpensive, simple and reliable. Multiple chemical functionalities can be achieved by growing different materials into final structures.[27] However, the shapes of the structures are dependent on the template utilized. Most common nanostructures made by this technique are nanoparticles or nanowires. Arbitrary complex structures are difficult to synthesize due to the limitation of the template.

In summary, the bottom-up methods are efficient ways to synthesize large-scale, uniformly size-distributed nanostructures. The 3-D devices can be complemented via a layer-by-layer scheme. However, in the microchips or MEMS fabrication, these methods are not widely employed because of this limitation in

making arbitrary devices. Besides, it is difficult to combine these nanostructures with full extension of their mechanical, electronic or optical properties.

1.2.2 Top-down methods

In contrast to bottom-up techniques, top-down methods start with bulk materials, and "machine" them down to micro/nano-scale devices. In principle, the structures can be generated in or on the surface of the substrate by *projection methods* or by *direct-write methods*. "Projection methods" use light, electrons or ions to apply to a photo- or particle-sensitive substrate (a resist) through a patterned mask. The patterns are transferred into the resist either positively (exposed area will be removed) or negatively (exposed area will stay). This method is able to mass-produce similar micro/nano-structures in one experimental process. The resolution is determined by the diffraction limit of the light or particle beams. In "direct-write methods", the electrons or ions are used to define the pattern directly, without a mask, on a point-by-point basis. The resolutions of the methods are determined by the scattering processes in the materials.

Photolithography, one of the "projection methods", has been considered as the "standard" top-down microfabrication method for many years. It was originally a silicon-based method in the IC and semiconductor field. However, photolithography has led to remarkable progress in many other fields too. Many materials have been utilized in photolithography, such as III-V semiconductors, polymers, noble metals, etc. The resolution of the photolithography has been improved to tens of nanometers.

The basic idea of photolithography is simple. Light is used to transfer a geometric pattern from a photomask to a thin film of photoresist on the substrate. Once the pattern is defined in the photoresist, it can be used as another photomask for the following treatment. Different etching techniques are applied to the substrate to form the required shape. A series of chemical treatments is then used to remove the photoresist to release the final microstructure. The process can be repeated many times to fabricate more complex patterns on the substrate.

While photolithography has been tremendously successful, it has several issues that limit its applications in some areas. The first drawback is the lack of chemical functionality over the patterned surfaces because most of the materials used in photolithography are semiconductors. Such control is important for chemical and biological applications, such as in μTAS devices. The second issue is the cost and facility requirements for photolithography, which are typically beyond the reach of most researchers. Third, although the resolution of the photolithography has been improved from a scale of several micrometers down to tens of nanometers, it is extremely difficult to fabricate at even better resolution. Finally, photolithography is an inherently two-dimensional technique. Patterns are duplicated from a 2-D mask, and while they can be stacked or released to create to layers in three dimensions, true 3-D fabrication cannot be simply accomplished with photolithography. Several other top-down approaches have been developed to overcoming the shortcomings of the conventional photolithography.

X-ray photolithography is one of the first attempts to extend fabrication into the

third dimension. IBM first made high-aspect ratio metal structures by combining electrode-position and x-ray lithography in 1969.[28] X-ray lithography is superior to photolithography because it employs shorter wavelengths and the exposure time and development conditions are not as strict.[29] The sources for x-ray lithography are usually from synchrotrons. Due to the short wavelength, the x-ray beam has a small divergence angle, resulting in micrometer-resolution patterning in photoresists with depths exceeding 1 cm. The aspect ratio, defined as the ratio between the height of the structure and its lateral dimension, is usually high, (e.g. > 100). X-ray lithography became well known with the development of LIGA, a German acronym for X-ray lithography (X-ray Lithographie), electroplating (Galvanoformung), and molding (Abformung), in 1980s.[19, 30, 31] As its name implies, LIGA uses X-rays to create patterns. The LIGA technique has been used to fabricate the parts of the MEMS devices, such as channels and gears, which can be used as molds to electro-deposit metals such as nickel.

Structures made by LIGA have good surface smoothness and sharp vertical features, but are of limited 3-D complexity because of the line-of-sight nature of the X-ray exposure. Besides, there are essentially no optics involved in x-ray lithography, so the pattern can only be transferred into the resist at a 1:1 ratio to the mask.

In the electron beam lithography, or EBL, a beam of electrons is used as the exposure source to generate micro/nano-structures in an electron resist. EBL is a maskless technique with high-resolution capabilities and a large depth of focus (DOF).[32] Due to its "direct writing" property, e-beam lithography is capable of

fabricating 3-D structures.[33-35] The primary advantage of EBL is the high resolution due to the short wavelength (<1 nm) used for fabrication. EBL can routinely make structures with feature sizes of 20 nm to 30 nm. With more careful experimental conditions, it reaches sub-10 nm fabrication resolution.

However, EBL has an issue with its low throughput. For example, it takes a very long time to expose an entire silicon wafer or glass substrate. Additionally, the equipment required for EBL are expensive. These limitations make EBL a perfect tool for production of photomasks and reticules for photolithography, or small-volume MEMS parts, but not a great method for real form 3-D fabrication.

Nanoimprint lithography (NIL) is a technique that is capable of producing three-dimensional features with high throughput and high resolution by "printing" materials.[36, 37] The basic principle of NIL is simple. A mask is first fabricated via lithographic techniques, followed by a pressure-induced transfer of the pattern on the mask into a thermoplastic polymer film heated above its glass-transition temperature. NIL can print a variety of polymeric materials, such as biomolecules, block copolymers, and conducting polymers.[38] One issue with the NIL is inhomogeneous sticking and missing material transport; thus, high temperature and high pressure are preferable in many cases. Another issue is the short lifetime of the mold. The mold needs to be replaced after about 50 consecutive imprints.

Another "printing" technique for fabricating 3-D structures is soft lithography, a class of techniques that includes micro-contact printing (μCP) and micromolding.[39]

Soft lithography uses a soft elastomer, typically polydimethylsiloxane (PDMS), to create a mold. One of the advantages of the soft lithography is that it is able to pattern on non-planar substrates.[40] This feature enables soft lithography to fabricate 3-D structures. Besides, if the master structure is fabricated with a membrane, even complex structures with closed loops can be replicated by μCP.[41] However, in most cases, soft lithography is unable to make *truly* 3-D patterns since the starting point is usually photolithography.

Microstereolithography (μSL) is another manufacturing process suited for the production of complex 3-D components.[42] Larger-scale versions also go by the name of rapid prototyping or 3-D printing. The basic idea of μSL is as follows. A laser is focused into a thin layer of a liquid prepolymer resin, photochemically inducing cross-linking. After patterning the desired 2-D image, additional liquid prepolymer is added to create a new layer of resin, and the process is repeated. The liquid resin is washed away after fabrication, yielding a 3-D microstructure. The feature size in the axial dimension is determined by the thickness of the added layer and is limited by the size of the laser focal spot in lateral dimension. Features that are submicron in all three dimensions have been demonstrated. One drawback of this technique is the speed of adding layers. For each layer, spreading a flat fresh prepolymer resin is crucial, which slows down the entire process. Generally, the resin has a low viscosity, but it still takes about 1 minute to reflow an additional layer.[42]

Another existing group of fabrication methods is based on the manipulation of materials at the microscale with nano-tips of scanning-probe microscopes. The materials delivered in these methods include colloids, polymers, polyelectrolyes and metals. Dip pen nanolithography (DPN)[43] is one of the most attractive techniques based on scanning-probe fabrication. In DPN, an atomic force microscope tip is used to transfer molecules to a surface via a solvent meniscus. Recently, massive parallel DPN patterning has been demonstrated, in which two-dimensional arrays of 55,000 tips were used.[44]

While 3-D control is accessible in scanning-probe fabrication, in practice the writing materials are not rigid enough to create structures with completely arbitrary geometries. For example, lattice type scaffolds have been demonstrated, but without compact structural support individual lines will not remain freestanding.

Multiphoton Absorption Polymerization, or MAP[12, 45-47], is a recently developed technique for *true* 3-D micro/nano-fabrication. MAP employs a focused laser beam, which is similar to μSL. However, it eliminates the need to reflow the resin by focusing directly inside the sample and polymerizing only at the focal point. MAP has a higher resolution than μSL and employs a simpler experimental setup. The inherent optical nonlinearity of multiphoton absorption allows such absorption to be localized in regions of high light intensity. This means that photochemical or photophysical transformations can be restricted to occur within the focal volume of a laser beam that has been focused through a microscope objective. By moving the

focal position in a prepolymer resin, intricate 3-D microstructures can be created through cross-linking.

MAP is able to generate arbitrarily complex 3-D structures. The polymeric materials used for fabrication enables chemical control of the devices made with MAP. Due to the optical and chemical nonlinearity of the MAP,[48] feature sizes as small as one tenth of wavelength (λ) used for fabrication have been achieved.[20]

Most of the work presented in this thesis is related to MAP. The principles of multiphoton absorption and MAP technique will be discussed in the following sections. The experimental setup and fabricate procedures will also be described in this chapter.

1.3 Multiphoton Absorption Polymerizaion

1.3.1 Fundamentals of multiphoton absorption

Maria Göppert-Mayer first predicted the existence of two-photon absorption (TPA) in 1931.[49] In honor of her work, the SI unit for the two-photon absorption cross section (δ) is named Göppert-Mayer (GM). A GM is equal to 10^{-58} m^4 s $photon^{-1}$, and for a typical molecule the peak value of δ is in the range of tenths to tens of GM for the lowest-lying electronic transition that is two-photon allowed. However, molecules that are designed to optimize TPA can have peak values of δ that are several orders of magnitude larger. Because of the high intensities required, the

experimental demonstration of TPA relied upon the invention of the laser and, therefore, did not take place until 1961.[50] With a continuous-wave laser, achieving a sufficient value of intensity squared to drive TPA to a significant extent requires high power. For this reason, although TPA was used for select applications, it did not find broad use for many years after its demonstration. This situation changed with the development of relatively simple, solid-state femtosecond lasers in the late 1980s and early 1990s.

The advantages of using ultrafast pulses to drive MPA are illustrated by the Ti:sapphire laser. A typical Ti:sapphire laser puts out pulses with a duration of 100 fs or less at a repetition rate of approximately 80 MHz. The time between pulses is therefore on the order of 12 ns. Thus, a sufficient peak intensity to drive efficient MPA can be realized at a low average laser power. While the output of a Ti:Sapphire laser is in the range of hundreds of milliwatts, two-photon excitation can generally be accomplished at average powers of a few milliwatts or less, depending on the focusing conditions and the species being excited. Most Ti:Sapphire lasers operate at a wavelength of about 800 nm, although with appropriate optics they can operate in the range of 700-1100 nm.

In practice, the first experiment showing localization due to TPA was performed with two-photon fluorescence microscopy in 1990.[51] In two-photon fluorescence microscopy an excitation wavelength is used that is approximately double the peak absorption wavelength of a given fluorophore. TPA occurs at the focal point, resulting in fluorescence that is then imaged. What is fundamental for two-photon fluorescence microscopy and for MAP is that excitation occurs only

within the focal volume. This is shown in Figure 1.1, where the total one-photon and two-photon absorption per transverse section of a focused laser beam are plotted as a function of axial position. Because the transition rate of two-photon absorption is proportional to the light intensity squared, maximum absorption occurs at the focal point.[52]

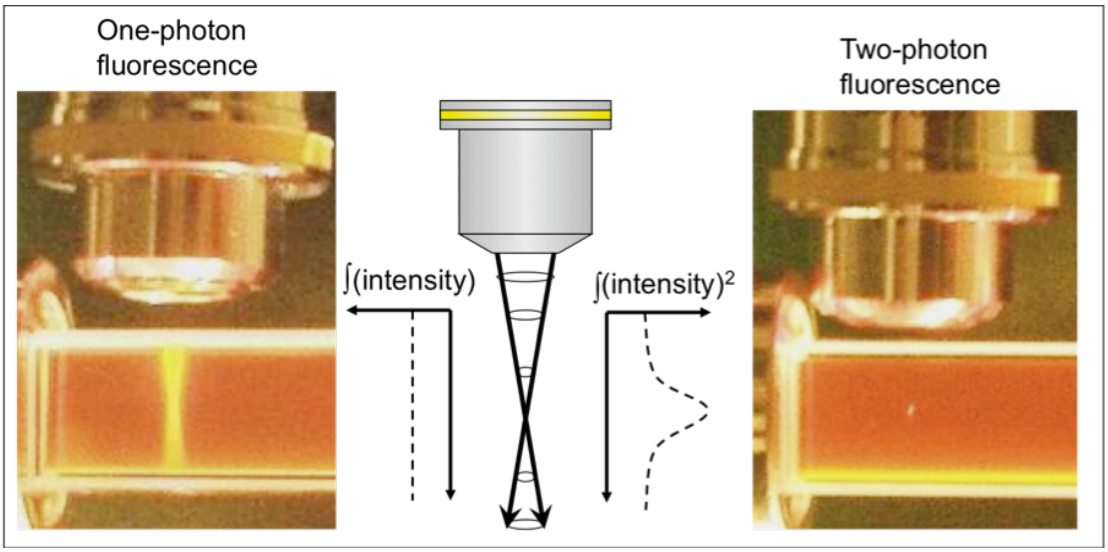

Figure 1.1 Fluorescence in a rhodamine B solution excited by single-photon excitation from a UV lamp (left) and by TPA of a mode-locked Ti:Sapphire laser tuned to 800 nm (right). In the former case, the integrated intensity is equal in all transverse planes, while in the latter case the integrated intensity squared is peaked in the focal region.

1.3.2 Multiphoton absorption polymerization

The most well developed multiphoton absorption (MPA) based fabrication technique is multiphoton absorption polymerization (MAP). In this technique, MPA

is used to expose a photoresist one volume element (voxel) at a time. Once the prescribed pattern has been scanned, the resist is developed to reveal the desired three-dimensional structure. A schematic demonstration of MAP is shown in Figure 1.2.

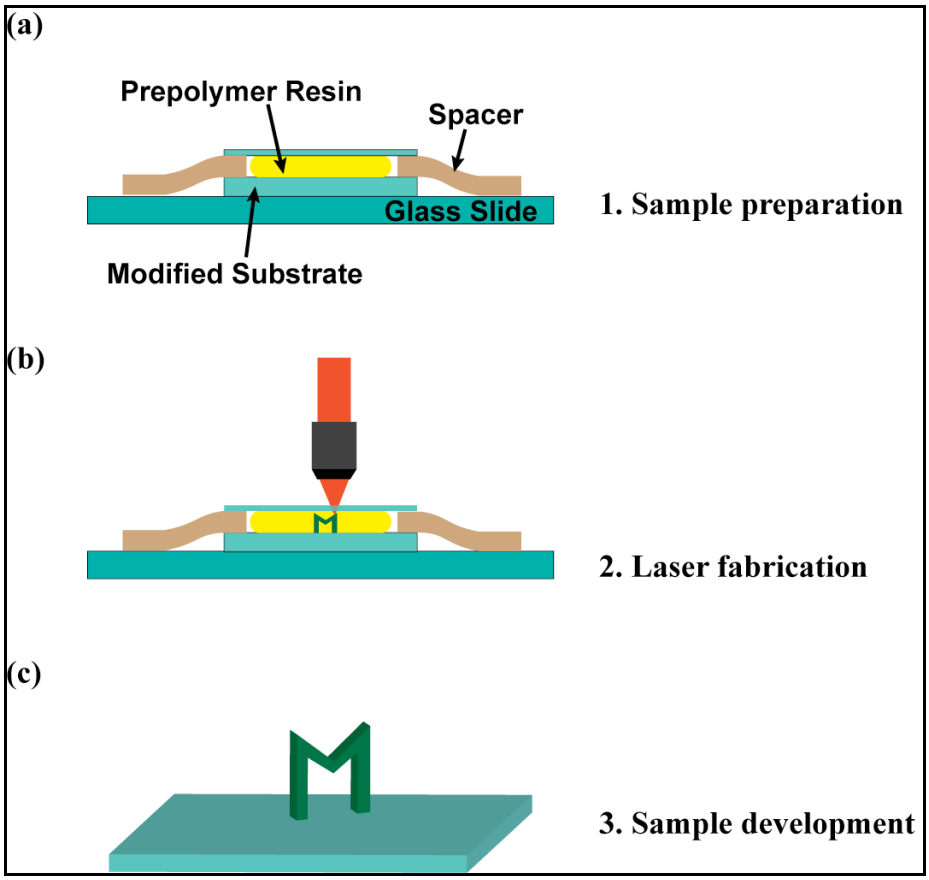

Figure 1.2 (a) In step 1 of MAP, a drop of prepolymer resin is sandwiched between a modified substrate and a cover slip with a layer of tape as spacer. (b) In step 2, the focal point of the laser is scanned in a 3-D pattern creating the desired part. (c) In step 3, the unpolymerized resin is washed away in solvent, leaving the freestanding structure.

Examples of structures fabricated with MAP are shown in Figure 1.3. Some of the structures are nearly impossible to make with conventional fabrication techniques, such as the micro-inductor in Figure 1.3 (a).

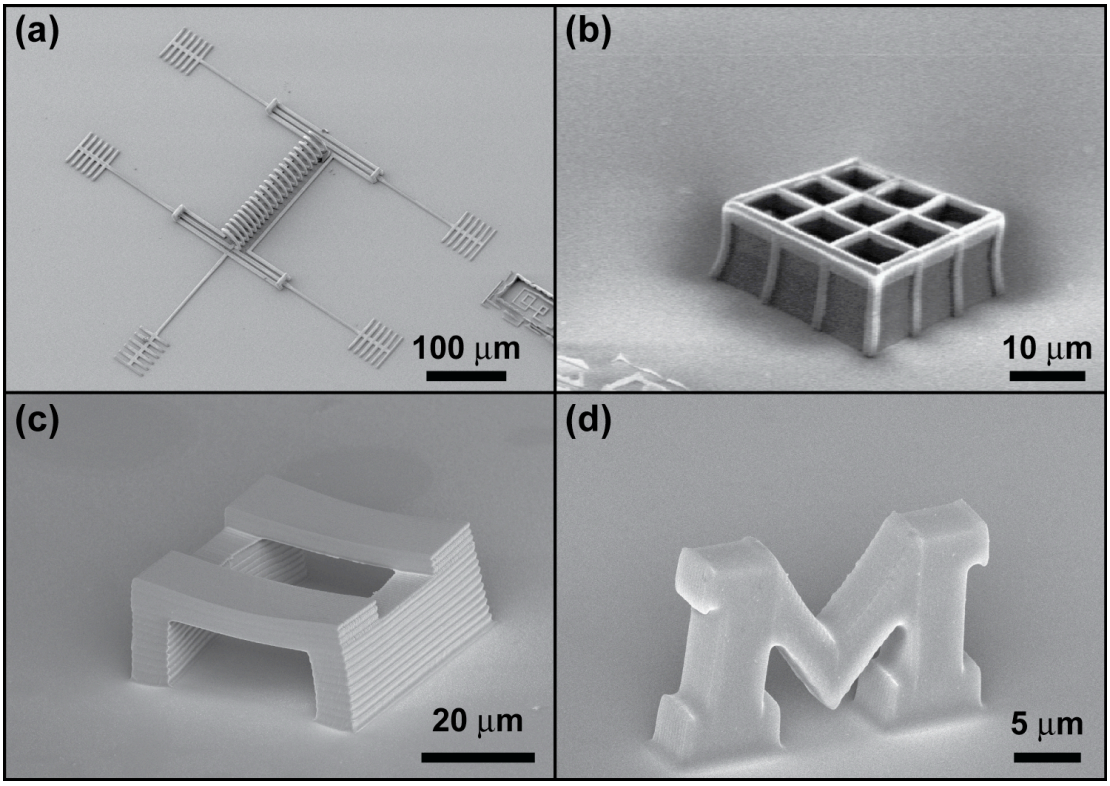

Figure 1.3 SEM images of the samples fabricated with MAP. (a) A micro-inductor with four probes system for measurement and a grounding wire. (b) A micro-scaffold. (c) A complex bridge structure. (d) A letter "M", showing the smoothness of the surface.

1.3.3 Experimental setup

A schematic of the experimental setup for performing MAP is shown in Figure 1.4. The excitation source is a Ti:sapphire oscillator. Optics may be placed in

the laser beam to prevent reflections from returning to the laser and to control the pulse length, intensity, and focal volume of the laser in the sample. The laser beam enters a microscope and is reflected through the objective into the sample, where it is focused. Three-dimensional patterns are scanned by moving the laser focus relative to the sample (with galvanometric mirrors, for instance), moving the sample relative to the laser (with a piezoelectric stage, for instance), or with some combination of the two. If the substrate upon which fabrication occurs is transparent, then the fabrication process can be monitored using transmitted light, as exposure of the photoresist generally leads to a visible change in refractive index.

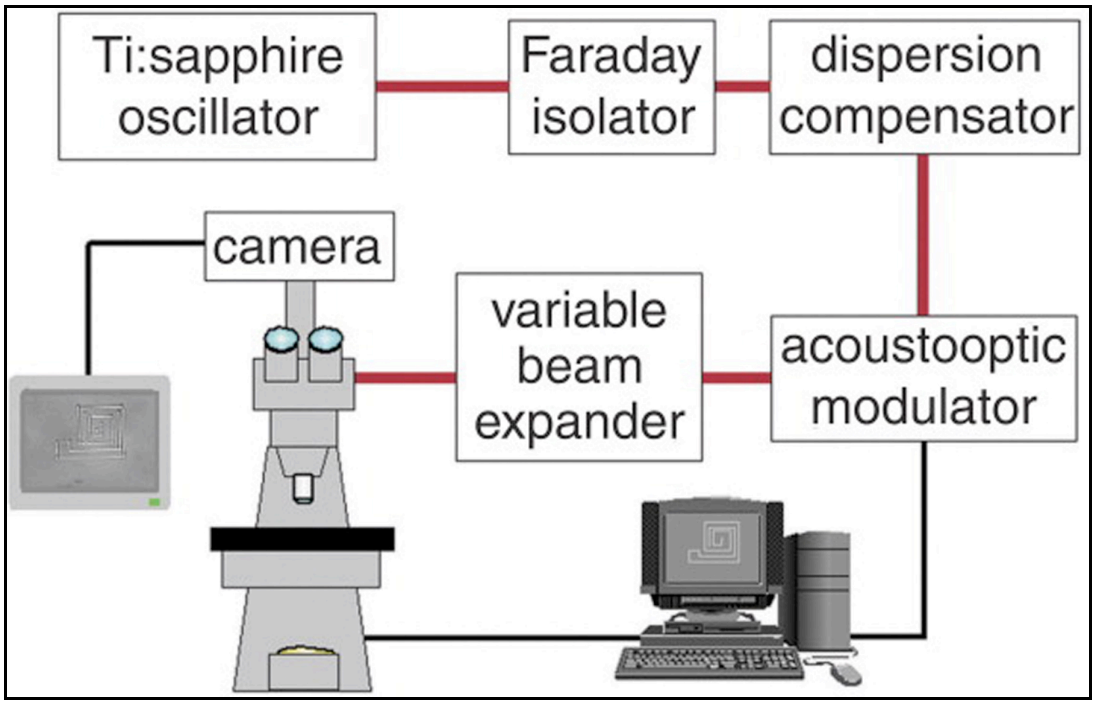

Figure 1.4 A typical setup for MAP. The excitation source is a Ti:sapphire oscillator. Elements in the optical path can be used to control the pulse length (e.g. a prism dispersion compensator), intensity (e.g. an acoustooptic modulator), and the focal volume (e.g. a variable beam expander). The position of the focal point is controlled

by computer using scanning mirrors or a three-dimensional stage. Fabrication can be observed in real time using reflected or transmitted light.

1.3.4 Materials for MAP

Negative-tone photoresists (also called prepolymer resins) used for MAP are generally either viscous liquids or amorphous solids (such as gels). A resin contains two key components: a photoinitiator that is excited via MPA and monomers and/or oligomers that react to form a solid that survives development. Resins may also contain other components, such as coinitiators or radical inhibitors, depending upon the nature of the initiation and polymerization reactions.

The majority of the materials used for MAP undergo radical polymerization. In this chemistry, MPA excites a photoinitiator that subsequently forms two or more radicals. These radicals in turn generate a chain reaction that causes the monomers/oligomers to cross-link. A highly cross-linked polymer is insoluble in the solvent used for development, and so will survive the washing steps. Commercial radical photoinitiators, while generally having only modest TPA cross sections, often work quite well for MAP.[48, 53] High radical quantum yields and initiation velocities tend to compensate for the low δ values of these initiators. Alternatively, some groups have focused on the synthesis of new initiators with TPA cross sections that may be orders of magnitude larger than those of commercial photoinitiators. In some cases, this allows polymerization to be accomplished at laser powers of significantly less than a milliwatt.[54, 55] The large δ values of these initiators balance their lower

radical yields and initiation velocities compared with commercial initiators. A number of strategies have been employed to increase δ, the most common of which is to create donor-acceptor-donor structures.[54]

Acrylates have been employed in the majority of MAP resins reported to date. A large range of acrylic monomers with different physical properties is available, and these materials can be polymerized readily. Most of the work reported in the thesis employed acrylate and methacrylate monomers, including ethoxylated(6) trimethylolpropane triacrylate (Sartomer), tris(2-hydroxy ethyl) isocyanurate triacrylate (Sartomer).

Cationic polymerization is also finding increasing use in MAP, particularly with epoxy resins[56, 57] such as SU-8. SU-8 is a convenient material for MAP because it is in an amorphous solid state during fabrication, circumventing the difficulties associated with flow of liquid resins. However, SU-8 also requires considerably more processing than liquid resins.

Also of note is the demonstration of positive-tone MPA lithography using a cationic initiator[58]. Positive-tone lithography makes the pattering of voids possible, as opposed to solid regions, and is therefore of use in applications such as microfluidic systems.

1.3.5 Incorporating other materials

For many applications it is desirable to be able to incorporate additional materials, such as metals or metal oxides, into three-dimensional structures. While

direct MPA fabrication with such materials is possible in some cases,[59, 60] the quality of structures created in this manner is generally considerably lower than those achieved using MAP. Consequently, the post-fabrication chemical modification of polymeric structures created with MAP has become a topic of considerable interest in recent years.

Several groups have developed methods for deposition of metals, including Ag, Au, and Cu, on polymeric structures created with MAP.[61, 62] If structures are fabricated from two different polymers, it is possible to perform selective chemical functionalization on one of those materials. The selective deposition of metals in such functionalized regions has been demonstrated and the extension of this technique to materials such as metal oxides or biomolecules should be straightforward.

1.3.6 Resolution of MAP

The resolution attainable with MAP is considerably finer than might be imagined based on the diffraction limit of the wavelength of light employed. Probably the most meaningful measure of the resolution attainable is the dimensions of an isolated voxel. With 800 nm light, it has proven possible to fabricate voxels with a transverse dimension smaller than 100 nm.[45, 63, 64] This feat is made possible by the nonlinearities inherent in the MAP exposure process. The fact that the polymerization efficiency depends nonlinearly upon the laser intensity provides some reduction in feature size. However, the most important nonlinearity is chemical in

nature. As a result of quenching, there is generally a threshold intensity below which complete exposure cannot occur. Thus, at low laser intensities exposure will only occur in the innermost regions of the focal volume, leading to smaller voxels. Considerably smaller features have been observed in suspended lines, although asymmetric shrinkage upon development is likely to play a considerable role in determining the dimensions in this case.[65]

As a result of optical constraints, the longitudinal dimension of a voxel is generally significantly greater than the transverse dimensions, causing the voxels to take on a cigar shape. Typical aspect ratios of voxels are on the order of 3:1 or greater.

In summary, MAP is a technique well-suited for micro/nano- scale fabrication with arbitrary 3-D capability. The polymeric microstructures produced by this method can also be functuionalized to produce a greater variety of devices. The resolution of the current MAP techniques is sub-100 nm. Nevertheless, there are still some issues to be solved in MAP. This thesis will introduce some applications of MAP, a strategy for chemical functinalization and a technique to enhance the resolution of MAP.

1.4 Thesis outline

MAP has been demonstrated by a number of groups and is a promising technology. It has been used as a method for fabricating photonic devices, including

photonic crystals, microlenses, and microlasers. Less attention has been focused on the use of MAP to create waveguide-based devices, although the fabrication of some elementary structures has also been reported. We have reported that MAP can be used to fabricate high performance, waveguide-based devices.[66] We fabricated microring resonators that show a quality competitive with that of devices created with more complex techniques. In Chapter 2, details of these experiments will be discussed.

Taking the advantage of optical and chemical nonlinear properties, MAP has been shown to have a fabrication resolution as fine as 80 nm. However, it is a challenge to acquire even better resolution using 800 nm laser light. Moreover, the voxel shape is not spherical, which limits MAP in some circumstances. A novel technique for higher resolution fabrication has been developed by introducing a second laser beam that is used to inhibit the polymerization. Furthermore, the aspect ratio of voxels has been reduced from more than 3 down to about 1/2. Chapter 3 will introduce this new method.

The chemical functionality for micro/nano-scale devices is critical in many for applications, such as conductive MEMS devices and many other optical and fluidic microdevices. It is also important for addressing biological issues such as cell motility, chemical signaling, cell growth and aggregation, and for biomedical applications such as tissue scaffolding. The acrylic polymer used in this dissertation work can be functionalized relatively simply. Different functionalities can be added to the surface of the devices fabricated with MAP, or photolithography. Chapter 4

will describe efforts to modify the surface chemistry of polymeric microstructures, enabling the incorporation of an assortment of functionality.

The nonlinear novelty of multiphoton absorption has not only been realized in MAP, it also shows promise for multiphoton absorption based microscopy. Photoluminescence from noble metal nanostructures has been used for two-photon imaging of living cells. We have demonstrated that multiphoton induced photoluminescence can be used to monitor the targeting and endocytosis of gold nanoparticles to human umbilical vein endothelial cells. The experimental details and results will be main subject of Chapter 5. Field enhancement from the metal nanostructures can be used to fabricate polymer nanostructures with feature sizes at the tens of nanometer scale. We discovered that it is the emission from gold nanoparticles, rather than field enhancement, that initiates photopolymerization. The experimental evidence of this phenomenon will also be discussed in Chapter 5.

Chapter 6 will summarize the projects that have been done, and will discuss future directions for some of the work going on in lab currently.

References:

(1) Kilby, J. S., Miniaturized Self-Contained Circuit Modules and Method of Fabrication. *U.S. Patent* **1964,** *3,138,744*.

(2) Noyce, R. N., Semiconductor Device-and Lead Structure. *U. S. Patent* **1961,** *No. 2,981,877*.

(3) Intel Corporation, Next-generation Intel® Itanium® processor (codenamed Tukwila) is the world's first 2-billion transistor microprocessor. 2008.

(4) Grabiec, P.; Domanski, K.; Janus, P.; Zaborowski, M.; Jaroszewicz, B., Microsystem technology as a road from macro to nanoworld. *Bioelectrochemistry* **2005,** *66* (1-2), 23-28.

(5) Esashi, M.; Ono, T., From MEMS to nanomachine. *Journal of Physics D: Applied Physics* **2005,** *38* (13), R223-R230.

(6) Elders, J. S., Vincent; Walsh, Steve Microsystems Technology (MST) and MEMS Applications: An Overview. *MRS Bulletin* **2001,** *26* (4), 4.

(7) Craighead, H. G., Nanoelectromechanical systems. *Science* **2000,** *290* (5496), 1532-1536.

(8) Petersen, K., From microsensors to microinstruments. *Sensors and Actuators, A: Physical* **1996,** *A56* (1-2), 143-149.

(9) Daw, R.; Finkelstein, J., Lab on a chip. *Nature* **2006,** *442* (7101), 367-367.

(10) Psaltis, D.; Quake, S. R.; Yang, C., Developing optofluidic technology through the fusion of microfluidics and optics. *Nature* **2006,** *442* (7101), 381-386.

(11) Whitesides, G. M., The origins and the future of microfluidics. *Nature* **2006,** *442* (7101), 368-373.

(12) LaFratta, C. N.; Fourkas, J. T.; Baldacchini, T.; Farrer, R. A., Multiphoton fabrication. *Angewandte Chemie International Edition* **2007,** *46* (33), 6238-6258.

(13) Gratson, G. M.; Garcia-Santamaria, F.; Lousse, V.; Xu, M.; Fan, S.; Lewis, J. A.; Braun, P. V., Direct-write assembly of three-dimensional photonic crystals: conversion of polymer scaffolds to silicon hollow-woodpile structures. *Advanced Materials* **2006,** *18* (4), 461-465.

(14) Therriault, D.; Shepherd, R. F.; White, S. R.; Lewis, J. A., Fugitive inks for direct-write assembly of three-dimensional microvascular networks. *Advanced Materials* **2005,** *17* (4), 395-399.

(15) Wang, T. C.; Cohen, R. E.; Rubner, M. F., Metallodielectric photonic structures based on polyelectrolyte multilayers. *Advanced Materials (Weinheim, Germany)* **2002,** *14* (21), 1534-1537.

(16) Fleming, J. G.; Lin, S. Y.; El-Kady, I.; Biswas, R.; Ho, K. M., All-metallic three-dimensional photonic crystals with a large infrared bandgap. *Nature* **2002,** *417* (6884), 52-55.

(17) Zhao, X. M.; Xia, Y.; Whitesides, G. M., Fabrication of three-dimensional microstructures. Microtransfer molding. *Advanced Materials* **1996,** *8* (10), 837-840.

(18) Tolfree, D. W. L., Microfabrication using synchrotron radiation. *Reports on Progress in Physics* **1998,** *61* (4), 313-351.

(19) Hruby, J., LIGA technologies and applications. *MRS Bulletin* **2001,** *26* (4), 337-340.

(20) Xing, J. F.; Dong, X. Z.; Chen, W. Q.; Duan, X. M.; Takeyasu, N., Improving spatial resolution of two-photon microfabrication by using photoinitiator with high initiating efficiency. *Applied Physics Letters* **2007,** *90*, 3.

(21) Whitesides, G. M.; Grzybowski, B., Self-assembly at all scales. *Science* **2002,** *295* (5564), 2418-2421.

(22) Black, C. T.; Ruiz, R.; Breyta, G.; Cheng, J. Y.; Colburn, M. E.; Guarini, K. W.; Kim, H.; Zhang, Y., Polymer self assembly in semiconductor microelectronics. *IBM Journal of Research and Development* **2007,** *51* (5), 605-633.

(23) Mao, Y.; Park, T.; Zhang, F.; Zhou, H.; Wong, S. S., Environmentally friendly methodologies of nanostructure synthesis. *Small* **2007,** *3* (7), 1122-1139.

(24) Che, G. L.; Lakshmi, B. B.; Fisher, E. R.; Martin, C. R., Carbon nanotubule membranes for electrochemical energy storage and production. *Nature* **1998,** *393* (6683), 346-349.

(25) Wirtz, M.; Martin, C. R., Template-fabricated gold nanowires and nanotubes. *Advanced Materials* **2003,** *15* (5), 455-458.

(26) Hou, S. F.; Wang, J. H.; Martin, C. R., Template-synthesized protein nanotubes. *Nano letters* **2005,** *5* (2), 231-234.

(27) Bauer, L. A.; Reich, D. H.; Meyer, G. J., Selective functionalization of two-component magnetic nanowires. *Langmuir* **2003,** *19* (17), 7043-7048.

(28) Cerrina, F., Application of Xrays to Nanolithography. *Proceedings of the IEEE* **1997,** *84* (4), 644-651.

(29) Madou, M. J., *Fundamentals of Microfabrication: the Science of Miniaturization*. 2 ed.; CRC Press: 2002; p 723.

(30) Becker, E. W.; Ehrfeld, W.; Muenchmeyer, D. *Accuracy of x-ray lithography using synchrotron radiation for the fabrication of technical separation nozzle elements*; Inst. Kernverfahrenstech.,Kernforschungszent. Karlsruhe G.m.b.H.,Karlsruhe,Fed. Rep. Ger.: 1984; p 92 pp.

(31) Ehrfeld, W.; Becker, E. W., The LIGA process for fabricating microstructure devices with extreme aspect ratio and great structural height. *KFK-Nachrichten* **1987,** *19* (4), 167-79.

(32) Ito, T.; Okazaki, S., Pushing the limits of lithography. *Nature* **2000,** *406* (6799), 1027-1031.

(33) Chen, K.-S.; Lin, I.-K.; Ko, F.-H., Fabrication of 3D polymer microstructures using electron beam lithography and nanoimprinting technologies. *Journal of Micromechanics and Microengineering* **2005,** *15*, 1894-1903.

(34) Chou, S. Y.; Keimel, C.; Gu, J., Ultrafast and direct imprint of nanostructures in silicon. *Nature* **2002,** *417*, 835-837.

(35) Yamazaki, K.; Namatsu, H., Two-axis-of-rotation drive system in electron-beam lithography apparatus for nanotechnology applications. *Microelectronic Engineering* **2004,** *73-74*, 85-89.

(36) Chou, S. Y.; Krauss, P. R.; Renstrom, P. J., Imprint Lithography with 25-Nanometer Resolution. *Science* **1996,** *272* (5258), 85-87.

(37) Schift, H., Nanoimprint lithography: An old story in modern times? A review. *Journal of Vacuum Science and Technology B* **2008,** *26* (2), 458-480.

(38) Gates, B. D.; Xu, Q.; Stewart, M.; Ryan, D.; Willson, C. G.; Whitesides, G. M., New Approaches to Nanofabrication: Molding, Printing, and Other Techniques. *Chemical Reviews* **2005,** *105* (4), 1171-1196.

(39) Xia, Y.; Whitesides, G. M., Soft lithography. *Angewandte Chemie International Edition* **1998,** *37* (5), 550-575.

(40) Rogers, J. A.; Nuzzo, R. G., Recent progress in soft lithography. *Materials Today* **2005,** *8* (2), 50-56.

(41) LaFratta, C. N.; Li, L.; Fourkas, J. T., Soft-lithographic replication of 3D microstructures with closed loops. *Proceedings of the National Academy of Sciences of the United States of America* **2006,** *103* (23), 8589-8594.

(42) Bertsch, A.; Jiguet, S.; Bernhard, P.; Renaud, P., Microstereolithography: A review. *Materials Research Society Symposium Proceedings* **2003,** *758* (Rapid Prototyping Technologies), 3-15.

(43) Piner, R. D.; Zhu, J.; Xu, F.; Hong, S. H.; Mirkin, C. A., "Dip-pen" nanolithography. *Science* **1999,** *283* (5402), 661-663.

(44) Salaita, K.; Wang, Y.; Fragala, J.; Vega, R. A.; Liu, C.; Mirkin, C. A., Massively Parallel Dip-Pen Nanolithography with 55 000-Pen Two-Dimensional Arrays. *Angewandte Chemie International Edition* **2006,** *45* (43), 7220-7223.

(45) Kawata, S.; Sun, H.-B.; Tianaka, T.; Takada, K., Finer features for functional microdevices. *Nature* **2001,** *412* (6848), 697-698.

(46) Li, L.; Fourkas, J. T., Multiphoton polymerization. *Materials Today* **2007,** *10* (6), 30-37.

(47) Maruo, S.; Fourkas, J. T., Recent progress in multiphoton microfabrication. *Laser Photonics Reviews* **2008,** *2* (1-2), 100-111.

(48) Baldacchini, T.; LaFratta, C. N.; Farrer, R. A.; Teich, M. C.; Saleh, B. E. A.; Naughton, M. J.; Fourkas, J. T., Acrylic-based resin with favorable properties for three-dimensional two-photon polymerization. *Journal of Applied Physics* **2004,** *95* (11), 6072-6076.

(49) Goppert-Mayer, M., Annalen der Physik. *(Berlin, Germany)* **1931,** *9*, 273.

(50) Kaiser, W.; Garrett, C. G. B., Two-photon excitation in CaF2:Eu++. *Physical Review Letters* **1961,** *7*, 229-31.

(51) Denk, W.; Strickler, J. H.; Webb, W. W., Two-photon laser scanning fluorescence microscopy. *Science* **1990,** *248* (4951), 73-6.

(52) Soeller, C.; Cannell, M. B., Two-photon microscopy: imaging in scattering samples and three-dimensionally resolved flash photolysis. *Microscopy Research and Technique* **1999,** *47* (3), 182-195.

(53) Schafer, K. J.; Hales, J. M.; Balu, M.; Belfield, K. D.; Van Stryland, E. W.; Hagan, D. J., Two-photon absorption cross-sections of common photoinitiators. *Journal of Photochemistry and Photobiology, A: Chemistry* **2004,** *162* (2-3), 497-502.

(54) Cumpston, B. H.; Ananthavel, S. P.; Barlow, S.; Dyer, D. L.; Ehrlich, J. E.; Erskine, L. L.; Heikal, A. A.; Kuebler, S. M.; Lee, I. Y. S.; McCord-Maughon, D.; Qin, J.; Rockel, H.; Rumi, M.; Wu, X.-L.; Marder, S. R.; Perry,

J. W., Two-photon polymerization initiators for three-dimensional optical data storage and microfabrication. *Nature (London)* **1999,** *398* (6722), 51-54.

(55) Belfield, K. D.; Ren, X.; Van Stryland, E. W.; Hagan, D. J.; Dubikovsky, V.; Miesak, E. J., Near-IR Two-Photon Photoinitiated Polymerization Using a Fluorone/Amine Initiating System. *Journal of the American Chemical Society* **2000,** *122* (6), 1217-1218.

(56) Teh, W. H.; Duerig, U.; Drechsler, U.; Smith, C. G.; Guentherodt, H. J., Effect of low numerical-aperture femtosecond two-photon absorption on (SU-8) resist for ultrahigh-aspect-ratio microstereolithography. *Journal of Applied Physics* **2005,** *97* (5), 054907/1-054907/11.

(57) Witzgall, G.; Vrijen, R.; Yablonovitch, E.; Doan, V.; Schwartz, B. J., Single-shot two-photon exposure of commercial photoresist for the production of three-dimensional structures. *Optics Letters* **1998,** *23* (22), 1745-1747.

(58) Yu, T.; Ober, C. K.; Kuebler, S. M.; Zhou, W.; Marder, S. R.; Perry, J. W., Chemically amplified positive resists for two-photon three-dimensional microfabrication. *Advanced Materials (Weinheim, Germany)* **2003,** *15* (6), 517-521.

(59) LaFratta, C. N.; Lim, D.; O'Malley, K.; Baldacchini, T.; Fourkas, J. T., Direct Laser Patterning of Conductive Wires on Three-Dimensional Polymeric Microstructures. *Chemistry of Materials* **2006,** *18* (8), 2038-2042.

(60) Formanek, F.; Takeyasu, N.; Tanaka, T.; Chiyoda, K.; Ishikawa, A.; Kawata, S., Three-dimensional fabrication of metallic nanostructures over large areas by two-photon polymerization. *Optics Express* **2006,** *14* (2), 800-809.

(61) Formanek, F.; Takeyasu, N.; Tanaka, T.; Chiyoda, K.; Ishikawa, A.; Kawata, S., Selective electroless plating to fabricate complex three-dimensional metallic micro/nanostructures. *Applied Physics Letters* **2006,** *88* (8), 083110/1-083110/3.

(62) Farrer, R. A.; LaFratta, C. N.; Li, L.; Praino, J.; Naughton, M. J.; Saleh, B. E. A.; Teich, M. C.; Fourkas, J. T., Selective functionalization of 3-D polymer microstructures. *Journal of the American Chemical Society* **2006,** *128* (6), 1796-1797.

(63) Juodkazis, S.; Mizeikis, V.; Seet, K. K.; Miwa, M.; Misawa, H., Two-photon lithography of nanorods in SU-8 photoresist. *Nanotechnology* **2005,** *16* (6), 846-849.

(64) Sun, H.-B.; Maeda, M.; Takada, K.; Chon, J. W. M.; Gu, M.; Kawata, S., Experimental investigation of single voxels for laser nanofabrication via two-photon photopolymerization. *Applied Physics Letters* **2003,** *83* (5), 819-821.

(65) Tan, D.; Li, Y.; Qi, F.; Yang, H.; Gong, Q.; Dong, X. Z.; Duan, X. M., Reduction in feature size of two-photon polymerization using SCR500. *Applied Physics Letters* **2007,** *90*, 071106/1-071106/3.

(66) Li, L.; Gershgoren, E.; Kumi, G.; Chen, W.; Ho, P.; Herman, W. N.; Fourkas, J. T., High-Performance Microring Resonators Fabricated with Multiphoton Absorption Polymerization. *Advanced Materials* **2008,** *20* (19), 3668-3671.

Chapter 2: Microring resonators fabricated with MAP

2.1 Introduction

In the last chapter, I presented the basic theory and experimental setup for multiphoton absorption polymerization (MAP). In this chapter, I will discuss the applications of MAP to microring resonator fabrication.

MAP[1-6] has been used as a method for fabricating photonic devices, including photonic crystals,[7-9] microlenses,[10] and microlasers.[11] Less attention has been focused on the use of MAP to create waveguide-based devices, although the fabrication of some elementary structures has also been reported.[12-14] While high-performance photonic crystals have been created by introducing other materials into structures created with MAP,[9] the performance of polymeric photonic structures created with MAP has generally not rivaled that of devices created with more conventional fabrication techniques. Discussed in this chapter is a demonstration of MAP as a technique to fabricate high performance, waveguide-based devices. The microring resonators shown here display a quality competitive with that of devices created with more complex techniques.[15-22]

In MAP, an ultrafast laser is focused through a microscope objective into a negative-tone photoresist.[1-6] Due to the nonlinear intensity dependence of the multiphoton absorption process, the resist is exposed only within the focal region of

the laser beam. Because photoresists have an intensity threshold for exposure, it is possible to create features smaller than 100 nm with 800 nm light.[23] Three-dimensional structures can be created by moving the laser beam relative to the substrate. After fabrication of the desired pattern, the photoresist is developed and a free-standing structure is left behind.

With an appropriate photoresist, MAP can be used to fabricate structures of high optical clarity with a surface roughness that is considerably smaller than optical wavelengths.[10] I have used an acrylic resin similar to one we have reported previously[24] to fabricate waveguide structures on top of a low-index, polydimethylsiloxane (PDMS) substrate.

2.2 Microring resonator

2.2.1 Overview

Microring resonators are promising photonic elements with applications such as optical filters and switches. They have gained considerable prominence in photonic applications such as optical logic gates[16, 25, 26] and sensors.[15, 27-29] A typical microring resonator is a ring-shaped or racetrack-shaped waveguide, as shown in Figure 2.1. Light introduced into the input port is partially coupled into the ring through coupler 1. The optical wave in the ring is partially coupled into the straight waveguide through coupler 2 and an output is observed from the drop port.

If the wavelength λ_i satisfies the resonant condition, then,

$$n_{eff} L = m\lambda_i \qquad \text{(Eq. 2.1)}$$

Here n_{eff} is the effective index of the bending waveguide, L is length of the ring, and m is an integer. The coupling of waves that satisfy Eq. 2.1 will be enhanced and all others will be suppressed. As a result, only the wavelengths meeting this condition will be dropped from drop port, while the rest of the wavelengths will pass through and output from Terminal 4.

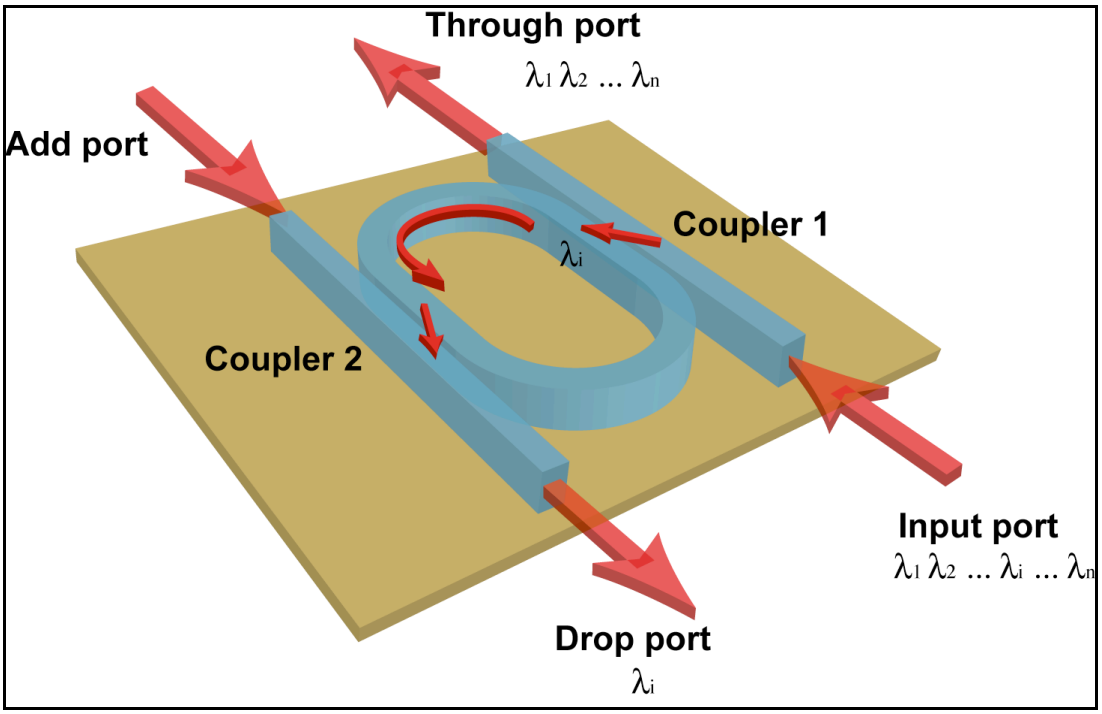

Figure 2.1 Illustrated diagram of a microring resonator.

2.2.2 Materials

Various materials have been used for microring resonators fabrication, including semiconductors and different kinds of polymer.[19, 30-32] Semiconductor materials have been mostly used in microring technology because of their well-developed fabrication and processing. However, the scattering loss of

semiconductors is huge (>3dB/cm).[33] Compared with semiconductors, silica-based materials feature extremely low propagation loss and simpler processing. Additionally, the refractive index of silica can be tuned by using different deposition recipes. Nevertheless, the low optical nonlinearity of silica-based materials restricts their use to passive devices in integrated photonic circuits.

Low-loss polymers with different refractive indices have been developed and are attractive for their cost-effectiveness.[34] Polymers with C–H bond vibrations exhibit material absorption at the wavelength of 1550 nm, but the absorption can be significantly reduced by employing fluorinated or deuterated polymers.[35] The low refractive index of polymers reduces the scattering losses associated with waveguide roughness and increases the coupling efficiency between waveguides, providing a looser processing requirement on coupling gaps. In terms of device fabrication, a variety of techniques are available for polymer processing: photolithography,[19] soft lithography,[21] imprinting,[36] photobleaching,[37] and multiphoton absorption polymerization.[38] Finally, polymers are promising materials for realization of active and nonlinear microring devices because of their large nonlinear optical effects. The acrylic polymers I have used in fabrication have relative low scattering losses and are ready to mix with some organic nonlinear materials.

2.2.3 Characteristics of microring resonators

Free spectral range: Free spectral range (FSR) is one of the key specifications of the ring resonator. It is spectral range between to resonant peaks. For a racetrack type microring resonator, FSR is defined as:

$$FSR = \frac{\lambda_i^2}{n_{eff} L} \approx \frac{\lambda_i^2}{n_{eff}(2\pi R + 2L_c)} \quad \text{(Eq. 2.2)}$$

where R is the ring radius and L_c is the coupler length. Because FSR is inversely proportional to the size of the ring resonator, the ring must be small in order to achieve a high FSR.

Finesse: The finesse (F) is another key specification of the ring resonator and it is defined as:

$$F = \frac{FSR}{\Delta\lambda_{FWHM}} = \frac{\pi}{2\sin^{-1}(\frac{1-K}{2\sqrt{K}})} \quad \text{(Eq. 2.3)}$$

Where

$$K = e^{-\alpha}(1-\kappa) \quad \text{(Eq. 2.4)}$$

Here $\Delta\lambda_{FWHM}$ is the bandwidth of the resonance at wavelength of λ, α is the total amplitude attenuation coefficient for each round trip, and κ is the normalized coupling coefficient of the coupler. Equation 2.2 shows that F is dependent on both the internal loss and the coupling (that is, the external loss) of the resonator. The higher the total losses are, the lower the finesse of the resonator.

It is advantageous to reduce both the internal and external losses in order to obtain higher finesse. However, the external loss due to coupling is necessary and therefore cannot be removed if the resonator is to operate as an optical filter. Also, if the external loss is smaller than the internal loss, the coupled power will be lost inside the cavity and no power will be coupled out. Because of these constraints, a ring resonator with a very small radius must use a strongly guided waveguide to minimize the bending loss.

Quality factor: The quality factor of a microring resonator Q, defined as the ratio of the stored energy to the energy lost per round trip, indicates the ability of a resonator to store energy. It can be written as:

$$Q = \frac{n_{eff} L}{\lambda} F \qquad \text{(Eq. 2.5)}$$

The quality factor is dependent on the dimension of the resonator and resonance wavelength. Therefore, the finesse, instead of the quality factor, will be used to make judgment on the quality of microring resonators.

2.3 Experiment and results

2.3.1 Device fabrication

We have fabricated acrylic polymeric (n~1.49) microring resonator devices in an "IOU" geometry, as shown schematically in Figure 2.2. The input bus is a straight waveguide (the "I"). The microring is shaped like a racetrack (the "O"), and the output bus is shaped like a "U" so that the drop port can be monitored from the side of the device opposite to the input port. The performance of the devices can be controlled via the length of the coupling regions (the straight segments of the ring), the radius of curvature of the semicircular regions, and the widths of the gaps in the coupling regions. The "IOU" structures were fabricated on PDMS substrates (n~1.41).

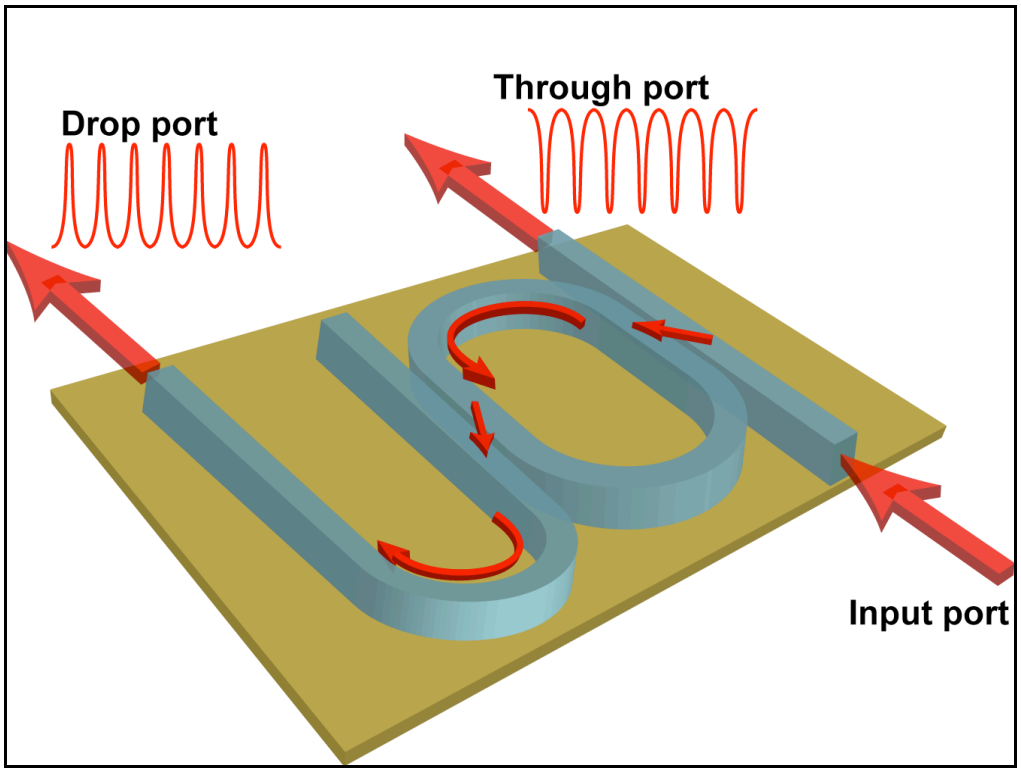

Figure 2.2 Illustration of an "IOU" device.

To make the PDMS substrates, a few grams of Sylgard 184 (Dow Corning) were mixed in a 10:1 mass ratio of prepolymer to curing agent. The resulting mixture was centrifuged for several minutes to remove air bubbles. The PDMS was poured onto a glass cover slip that had been treated with an oxygen plasma. A silicon wafer was treated overnight in an evacuated desiccator with (tridecafluoro-1,1,2,2-tetrahydrooctyl) dimethylchlorosilane.[39] A 200 μm-thick spacer separated the glass slide from the wafer that was used to cover the PDMS. The sandwiched PDMS was placed in an oven at 110 °C for 20 min to cure, after which the silicon wafer was removed. The PDMS substrate was again subjected to an oxygen plasma, after which it was treated with (3-acryloxypropyl)trimethoxysilane to improve adhesion of the acrylic polymer. A razor blade mounted on a micrometer

translation stage was used to cut a 250 μm wide stripe in the PDMS that served as the substrate for fabrication.

For microring resonator fabrication, the acrylic resin employed was composed of 54 wt% dipentaerythritol pentaacrylate (Sartomer), 43 wt% tris (2-hydroxy ethyl) isocyanurate triacrylate (Sartomer), and 3 wt % Lucirin TPO-L (BASF). After thorough mixing, the resin was placed on the PDMS substrate and covered by a thin cover slip with a spacer. The slide with acrylic resin was then placed on a piezoelectric motorized stage (PI-USA) that was mounted on an upright microscope. The excitation source was a Ti:Sapphire laser (Coherent Mira 900-F) producing 100-fs pulses with a center wavelength of 800 nm at a repetition rate of 80 MHz. The beam was expanded to overfill the back aperture of a 100x, 1.45 NA, oil immersion objective (Zeiss). The piezoelectric stage was controlled by a LabView program, moving point by point to fabricate a microring resonator. A typical fabrication power at the sample was <2 mW. After fabrication, the unexposed resin was washed away with dimethylformamide and then ethanol.

2.3.2 Device characterization

The waveguide devices were characterized using an Agilent 8164A Lightwave Measurement System tunable from 1530 nm to 1570 nm. The light was coupled into and out of the devices using tapered, single-mode fibers. The output intensity was also measured by the Agilent 8164A. After the optical measurement, the device was coated with gold and imaged with a SEM.

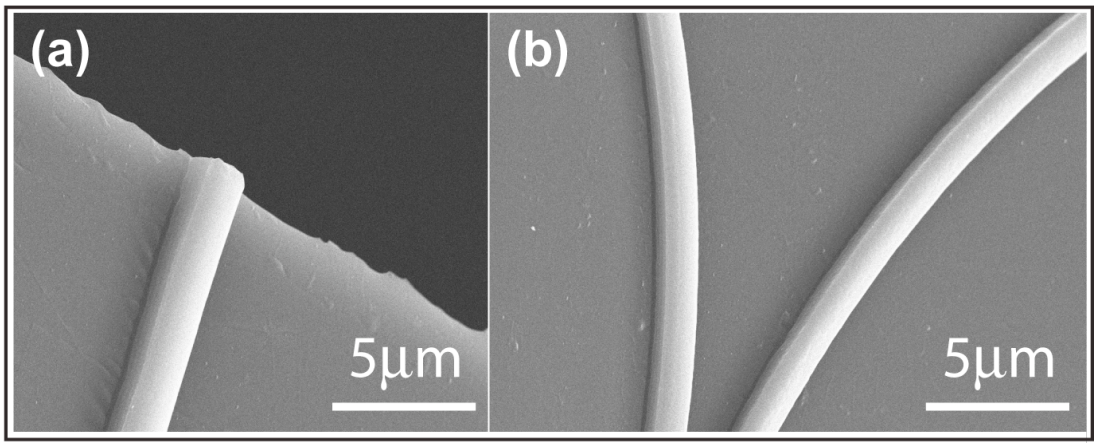

Figure 2.3 SEM images of straight and curved waveguides. (a) The end of a straight waveguide fabricated on PDMS substrate; (b) two curved waveguides.

2.3.3 Results and Discussions

The straight waveguide section shown in Figure 2.3 (a) illustrates the degree of smoothness that can be attained routinely in structures fabricated with MAP. This waveguide was created by fabricating 15 parallel lines separated by increments of 100 nm. As demonstrated in Figure 2.3 (b), it is also straightforward to create waveguides of equally high quality that have local curvature and can be of an essentially arbitrary overall shape.

Test structures were fabricated on PDMS platforms that were several hundreds of µm thick and as wide as the test structures were long, typically 200 to 300 µm. This design was selected such that optical fibers can be brought into close proximity to the inputs and outputs of the test structures, allowing for efficient optical coupling. To assess the mode quality in our test structures, a straight waveguide 250 µm in length, 1.8 µm high and 1.8 µm wide was fabricated and the spatial mode structure at a wavelength of 1.55 µm was measured at its output. As can be seen

from Figure 2.4, the mode quality remains excellent after propagation over 250 μm distance.

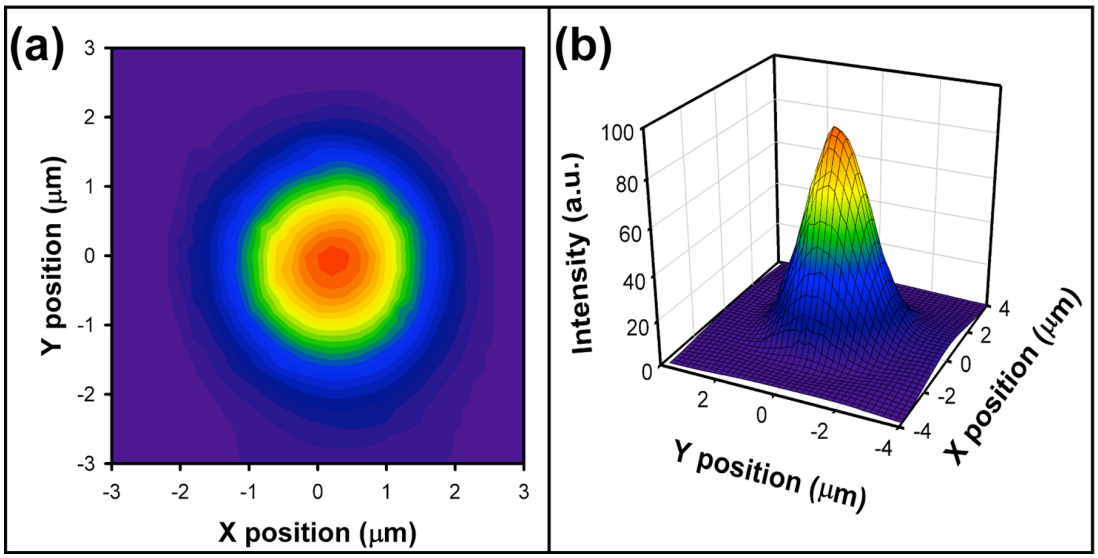

Figure 2.4 Output mode of a straight waveguide. (a) Contour image of top view; (b) 3-D plot.

There are a number of possible loss mechanisms for these waveguides.[40] Vibrational overtones in acrylic polymers in the 1.55 μm spectral region can lead to absorptive losses.[41] Inhomogeneities or surface roughness can cause scattering losses. Curved regions of waveguides can exhibit bending loss, and the vicinity of the input of a waveguide is also susceptible to coupling losses. To determine whether our waveguides have appreciable absorptive or scattering losses, we fabricated test structures to isolate the effects of these two loss mechanisms. The test structures, a schematic of which is shown in Figure 2.5 (a), consisted of a linear input region, a 90° bend, a straight region of variable length, a 90° bend in the opposite direction, and a linear output region. Varying the length of the central linear region 5 μm to

125 μm resulted in no measurable change in propagation loss. We therefore conclude that on the distance scale relevant to the devices discussed here, absorption and scattering losses are insignificant. We also use these s-shape structures to test the bending loss by varying the curvature of the bending parts. Figure 2.5 (b) shows the bending losses from the different curved radii. The bending loss increases dramatically for radii smaller than 8 μm while remaining stable for radii greater than 8 μm.

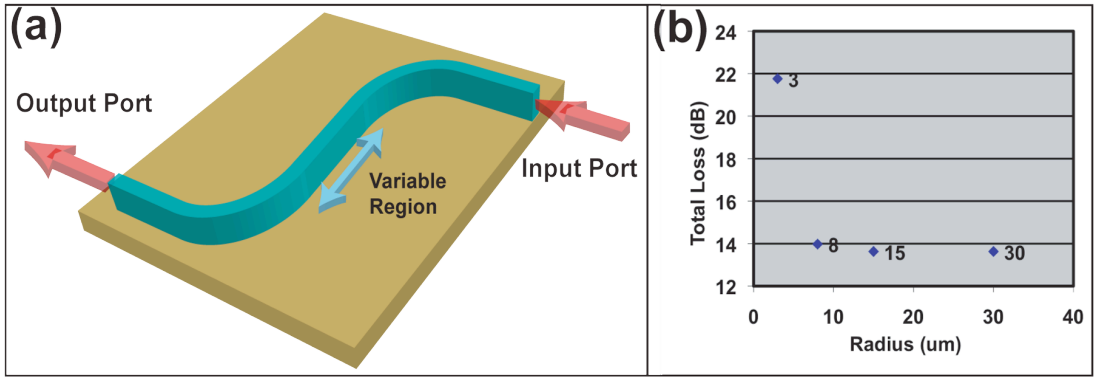

Figure 2.5 (a) Schematic design of a test structure for determining the loss in straight waveguides, (b) Bending loss of different radii.

Representative sets of IOU devices with a range of architectures are shown in Figure 2.6. The radius of curvature of the microrings in these devices ranges from 10 μm to 70 μm, and the length of the coupling region from 0 μm (i.e., a circular microring) to 100 μm. In all of the devices shown here the coupling gap is 500 nm, although smaller gaps can be fabricated if desired. These images demonstrate the versatility of MAP in creating such devices. With MAP it is straightforward to fabricate microring resonators with a broad range of parameters on a single substrate.

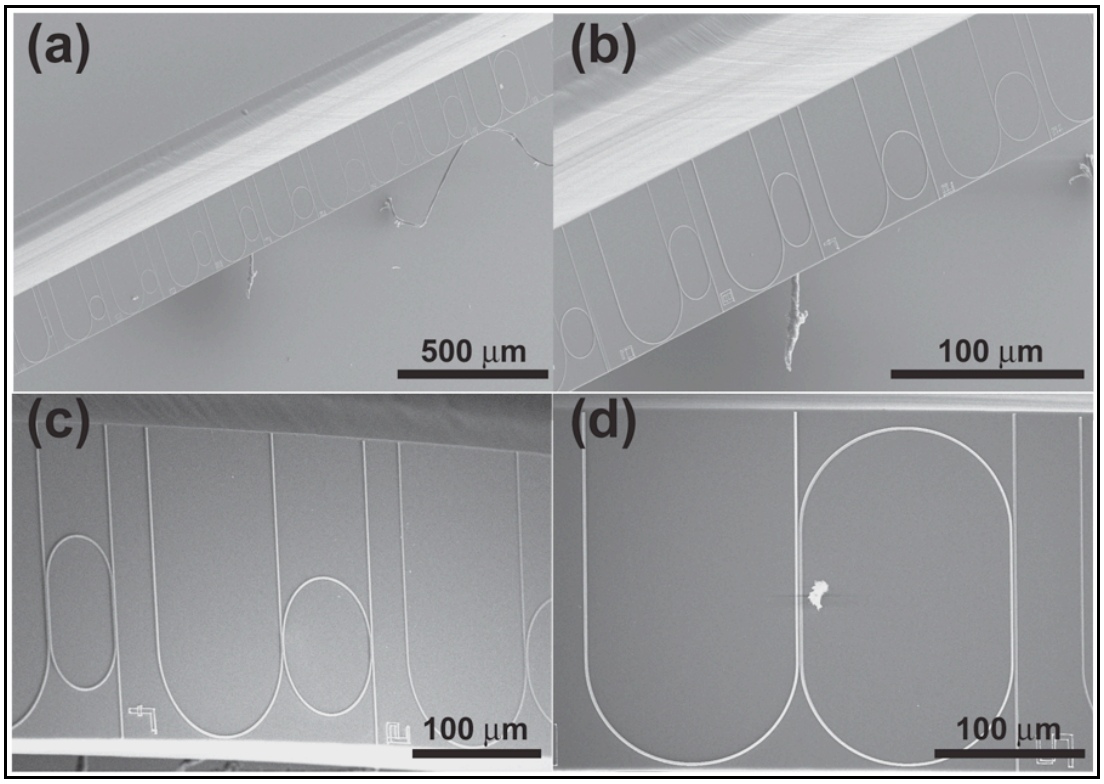

Figure 2.6 IOU microring resonator devices. (a) (b) Electron microscopy image of a set of IOU structures with different ring designs; (c) (d) Close-up views of two different IOU devices.

Shown in Figure 2.7 are data obtained from representative devices. In Figure 2.7 (b) we show extinction data (filled circles) obtained from the through port of a microring resonator with a 50 μm radius of curvature and a coupling region 10 μm long, along with a fit to the data with a standard microring resonator model (line).[19] The extinction is greater than 20 dB for every resonance, which is significantly better than the highest previously reported (12 dB) for an air-clad, supported polymeric device[21, 42] and is competitive with all but the best semiconductor-based devices.

The finesse of the device is approximately 2.5.

The drop port spectrum for the above device is plotted in Figure 2.7 (a) (filled circles) along with a fit using the same parameters as in Figure 2.7 (a) (line). Based on these fits, the round-trip power loss in the microring is approximately 16% and the coupling efficiency is approximately 70%. The modest finesse of this device is in fact a direct result of this strong coupling, which can easily be decreased with different designs. Such strong coupling is difficult to achieve with conventional lithography due to the narrow gaps required, but can easily be attained with devices fabricated with MAP.

By changing the design parameters, we can also create devices with narrower resonances. For instance, shown in Figure 2.7 (c) is the drop port spectrum (filled circles) from a device with a radius of curvature of 70 μm and a coupling region 90 μm long, as well as a fit to the data (line). The finesse of this device is approximately 15, further demonstrating the high performance that can be attained in microring devices fabricated with MAP.

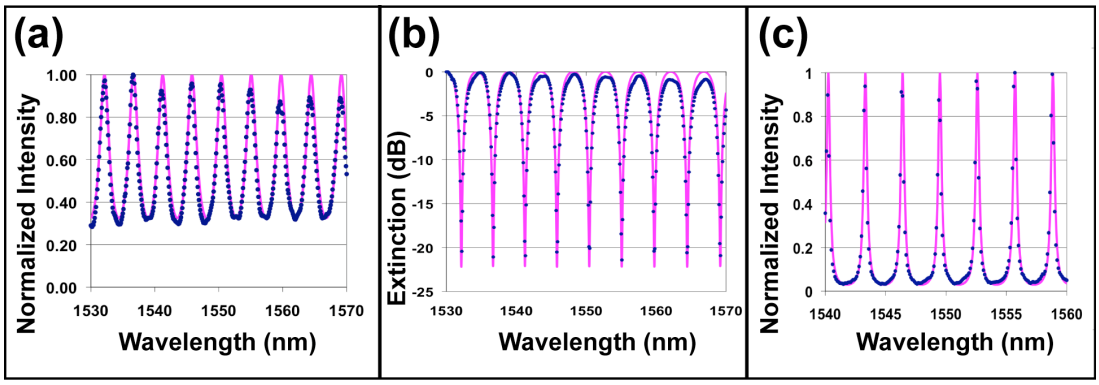

Figure 2.7 Data from typical IOU devices. (a) Through-port extinction spectrum (filled circles) and fit (line) for a device with a 50 μm radius of curvature and a 10mm coupling region; (b) Drop port spectrum for the same device (filled circles) and a fit to the data (line); (c) Drop port spectrum (filled circles) and fit (line) for a device with a 70 μm radius of curvature and a 90μm coupling region.

2.4 Conclusion

The chapter demonstrates the use of MAP for fabricating high-performance optical devices. Those devices require supported waveguides with micron-scale diameters and tight tolerances. While the devices reported here were made from a single polymer, it is readily possible to create different portions of devices from different polymeric materials while maintaining excellent registry. The ability to integrate two or more different polymers in these devices enables the introduction of additional functionality. For instance, to create optical logic gates, a nonlinear optical material can be incorporated in the microring. For sensing applications, the microring can instead be fabricated with a material than can be selectively chemically

functionalized.[43] The ability to use MAP to fabricate high-performance, polymeric microring resonators will make possible a wide range of new applications for these devices.

References:

(1) Sun, H. B.; Kawata, S., Two-photon laser precision microfabrication and its applications to micro-nano devices and systems. *IEEE/OSA Journal of Lightwave Technology* **2003,** *21* (3), 624-633.

(2) LaFratta, C. N.; Fourkas, J. T.; Baldacchini, T.; Farrer, R. A., Multiphoton Fabrication. *Angewandte Chemie International Edition* **2007,** *46* (33), 6238-58.

(3) Marder, S. R.; Bredas, J. L.; Perry, J. W., Materials for multiphoton 3D microfabrication. *MRS Bulletin* **2007,** *32*, 561-565.

(4) Maruo, S.; Fourkas, J. T., Recent progress in multiphoton microfabrication. *Laser Photonics Reviews* **2008,** *2* (1-2), 100-111.

(5) Li, L.; Fourkas, J. T., Multiphoton polymerization. *Materials Today* **2007,** *10* (6), 30-37.

(6) Yang, D.; Jhaveri, S. J.; Ober, C. K., Three-dimensional microfabrication by two-photon lithography. *MRS Bulletin* **2005,** *30* (12), 976-982.

(7) Cumpston, B. H.; Ananthavel, S. P.; Barlow, S.; Dyer, D. L.; Ehrlich, J. E.; Erskine, L. L.; Heikal, A. A.; Kuebler, S. M.; Lee, I. Y. S.; McCord-Maughon, D.; Qin, J. Q.; Rockel, H.; Rumi, M.; Wu, X. L.; Marder, S. R.; Perry, J. W., Two-photon polymerization initiators for three-dimensional optical data storage and microfabrication. *Nature* **1999,** *398* (6722), 51-54.

(8) Deubel, M.; Freymann, G. v.; Wegener, M.; Pereira, S.; Busch, K.; Soukoulis, C. M., Direct laser writing of three-dimensional photonic-crystal templates for telecommunications. *Nature Materials* **2004,** *3* (7), 444-447.

(9) Tétreault, N.; Freymann, G. v.; Deubel, M.; Hermatschweiler, M.; Pérez-Willard, F.; John, S.; Wegener, M.; Ozin, G. A., New Route to Three-Dimensional Photonic Bandgap Materials: Silicon Double Inversion of Polymer Templates. *Advanced Materials* **2006,** *18*, 457-460.

(10) Guo, R.; Xiao, S.; Zhai, X.; Li, J.; Xia, A.; Huang, W., Micro lens fabrication by means of femtosecond two photon photopolymerization. *Optics Express* **2006,** *14* (2), 810-816.

(11) Yokoyama, S.; Nakahama, T.; Miki, H.; Mashiko, S., Fabrication of three-dimensional microstructure in optical-gain medium using two-photon-induced photopolymerization technique. *Thin Solid Films* **2003,** *438-439*, 452-456.

(12) Ishihara, J.; Komatsu, K.; Sugihara, O.; Kaino, T., Fabrication of three-dimensional calixarene polymer waveguides using two-photon assisted polymerization. *Applied Physics Letters* **2007,** *90*, 033511/ -033511/3.

(13) Klein, S.; Barsella, A.; Leblond, H.; Bulou, H.; Fort, A.; Andraud, C.; Lemercier, G.; Mulatier, J. C.; Dorkenoo, K., One-step waveguide and optical circuit writing in photopolymerizable materials processed by two-photon absorption. *Applied Physics Letters* **2005,** *86* (21), 211118/1-211118/3.

(14) Serbin, J.; Gu, M., Superprism phenomena in waveguide-coupled woodpile structures fabricated by two-photo polymerization. *Optics Express* **2006,** *14* (8), 3563-3568.

(15) Chen, L.; Sherwood-Droz, N.; Lipson, M., Compact bandwidth-tunable microring resonators. *Optics letters* **2007,** *32* (22), 3361-3.

(16) Ibrahim, T. A.; Grover, R.; Kuo, L. C.; Kanakaraju, S.; Calhoun, L. C.; Ho, P. T., All-optical AND/NAND logic gates using semiconductor microresonators. *IEEE Photonics Technology Letters* **2003,** *15* (10), 1422-1424.

(17) Xiao, S.; Khan, M. H.; Shen, H.; Qi, M., Compact silicon microring resonators with ultra-low propagation loss in the C band. *Optics Express* **2007,** *15* (22), 14467-14475.

(18) Vander Rhodes, G. H.; Goldberg, B. B.; Ünlü, M. S.; Chu, S. T., Internal Spatial Modes in Glass Microring Resonators. *IEEE Journal of Selected Topics in Quantum Electronics* **2000,** *6* (1), 46-53.

(19) Chen, W. Y.; Grover, R.; Ibrahim, T. A.; Van, V.; Herman, W. N.; Ho, P. T., High-finesse laterally coupled single-mode benzocyclobutene microring resonators. *IEEE Photonics Technology Letters* **2004,** *16* (2), 470-472.

(20) Chen, W.; Van, V.; Herman, W. N.; Ho, P., Periodic microring lattice as a bandstop filter. *IEEE Photonics Technology Letters* **2006,** *18* (17-20), 2041-2043.

(21) Poon, J. K. S.; Huang, Y. Y.; Paloczi, G. T.; Yariv, A., Soft lithography replica molding of critically coupled polymer microring resonators. *IEEE Photonics Technology Letters* **2004,** *16* (11), 2496-2498.

(22) Song, H. C.; Oh, M. C.; Ahn, S. W.; Steier, W. H.; Fetterman, H. R., Flexible low-voltage electro-optic polymer modulators. *Applied Physics Letters* **2003,** *82* (25), 4432-4434.

(23) Xing, J. F.; Dong, X. Z.; Chen, W. Q.; Duan, X. M.; Takeyasu, N., Improving spatial resolution of two-photon microfabrication by using photoinitiator with

highinitiating efficiency. *Applied Physics Letters* **2007,** *90*, 131106/1-131106/3.

(24) Baldacchini, T.; LaFratta, C. N.; Farrer, R. A.; Teich, M. C.; Saleh, B. E. A.; Naughton, M. J.; Fourkas, J. T., Acrylic-based resin with favorable properties for three-dimensional two-photon polymerization. *Journal of Applied Physics* **2004,** *95* (11), 6072-6076.

(25) Li, C.; Zhou, L.; Poon, A. W., Silicon microring carrier-injection-based modulators/switches with tunable extinction ratios and OR-logic switching by using waveguide cross-coupling. *Optics Express* **2007,** *15* (8), 5069-5076.

(26) Mikroulis, S.; Simos, H.; Roditi, E.; Syvridis, D., Ultrafast all-optical AND logic operation based on four-wave mixing in a passive InGaAsP-InP microring resonator. *IEEE Photonics Technology Letters* **2005,** *17* (9), 1878-1880.

(27) Chao, C. Y.; Guo, L. J., Biochemical sensors based on polymer microrings with sharp asymmetrical resonance. *Applied Physics Letters* **2003,** *83* (8), 1527-1529.

(28) Zhu, H.; White, I.; Suter, J.; Zourob, M.; Fan, X., Opto-fluidic micro-ring resonator for sensitive label-free viral detection. *Analyst* **2008,** *133* (3), 356-360.

(29) Yalcin, A.; Popat, K. C.; Aldridge, J. C.; Desai, T. A.; Hryniewicz, J. V.; Chbouki, N.; Little, B. E.; King, O.; Van, V.; Chu, S. T.; Gill, D.; Anthes-Washburn, M.; Unlu, M. S., Optical sensing of biomolecules using

microring resonators. *IEEE Journal of Selected Topics in Quantum Electronics* **2006,** *12* (1), 148-155.

(30) Little, B. E.; Foresi, J. S.; Steinmeyer, G.; Thoen, E. R.; Chu, S. T.; Haus, H. A.; Ippen, E. P.; Kimerling, L. C.; Greene, W., Ultra-compact Si-SiO2 microring resonator optical channel dropping filters. *IEEE Photonics Technology Letters* **1998,** *10* (4), 549-551.

(31) Laine, J. P.; Little, B. E.; Haus, H. A., Etch-eroded fiber coupler for whispering-gallery-mode excitation in high-Q silica microspheres. *IEEE Photonics Technology Letters* **1999,** *11* (11), 1429-1430.

(32) Turner, A. C.; Foster, M. A.; Gaeta, A. L.; Lipson, M., Ultra-low power parametric frequency conversion in a silicon microring resonator. *Optics Express* **2008,** *16* (7), 4881-4887.

(33) DERI, R. J. K., E., Low-Loss III-V Semiconductor Optical Waveguides. *IEEE Journal of Quantum Electronics* **1991,** *27* (3), 626-640.

(34) Chen, W., Benzocyclobutene Microring Resonators. *Ph.D. Thesis* **2007**.

(35) Robitaille, L. C., Claire L.; Noad, Julian P., Polymer waveguide devices for WDM applications. *SPIE Proceedings Series* **1998,** *3281*, 14-24.

(36) Chao, C. Y.; Guo, L. J., Polymer microring resonators fabricated by nanoimprint technique. *Journal of Vacuum Science and Technology B* **2002,** *20* (6), 2862-2866.

(37) Zhou, J.; Pyayt, A.; Dalton, L. R.; Luo, J.; Jen, A. K. Y.; Chen, A., Photobleaching fabrication of microring resonator in a

chromophore-containing polymer. *IEEE Photonics Technology Letters* **2006,** *18* (21-24), 2221-2223.

(38) Li, L.; Gershgoren, E.; Kumi, G.; Chen, W.; Ho, P.; Herman, W. N.; Fourkas, J. T., High-Performance Microring Resonators Fabricated with Multiphoton Absorption Polymerization. *Advanced Materials* **2008,** *20* (19), 3668-3671.

(39) Zhuang, Y. X.; Hansen, O.; Knieling, T.; Wang, C.; Rombach, P.; Lang, W.; Benecke, W.; Kehlenbeck, M.; Koblitz, J., Thermal stability of vapor phase deposited self-assembled monolayers for MEMS anti-stiction. *Journal of Micromechanics and Microengineering* **2006,** *16* (11), 2259-2264.

(40) Van, V.; Absil, P. P.; Hryniewicz, J. V.; Ho, P. T., Propagation loss in single-mode GaAs-AlGaAs microring resonators: measurement and model. *Journal of Lightwave Technology* **2001,** *19* (11), 1734-1739.

(41) Eldada, L.; Shacklette, L. W., Advances in polymer integrated optics. *IEEE Journal of Selected Topics in Quantum Electronics* **2000,** *6* (1), 54 - 68.

(42) Kim, D. H.; Im, J. G.; Lee, S. S.; Ahn, S. W.; Lee, K. D., Polymeric microring resonator using nanoimprint technique based on a stamp incorporating a smoothing buffer layer. *IEEE Photonics Technology Letters* **2005,** *17* (11), 2352-2354.

(43) Farrer, R. A.; LaFratta, C. N.; Li, L. J.; Praino, J.; Naughton, M. J.; Saleh, B. E. A.; Teich, M. C.; Fourkas, J. T., Selective functionalization of 3-D polymer microstructures. *Journal of American Chemical Society* **2006,** *128* (6), 1796-1797.

Chapter 3: Resolution Augmentation through Photo-Induced Deactivation (RAPID) Lithography

3.1 Introduction

The demand for increasingly powerful integrated circuits has spurred remarkable progress in lithographic techniques in the past decades.[1] However, progress towards higher resolution has proven to be increasingly difficult and expensive as feature sizes decrease. To improve resolution in photolithography, chemical nonlinearity can be employed to create a sharp intensity threshold for exposure.[2] However, diffractive effects still limit feature sizes in conventional photolithography to approximately a quarter of a wavelength (λ) of the light used to expose the photoresist.

Here we introduce a technique called Resolution Augmentation through Photo-Induced Deactivation (RAPID) lithography.[3] In RAPID lithography, one laser beam is used to initiate polymerization in a negative-tone photoresist. A second laser beam is used to deactivate the photoinitiator, preventing photopolymerization from occurring. By spatial shaping of the phase of the deactivation beam, features with resolution far below the diffraction limit can be fabricated. This chapter discusses RAPID lithography, including background, experimental apparatus and results.

3.2 Motivation of RAPID lithography

3.2.1 Fabrication resolution of MAP

Due to the optical nonlinearity of multiphoton absorption and the existence of an intensity threshold for polymerization, MAP can be used to create volume elements (voxels) with a resolution that is considerably smaller than the wavelength of the light used. For instance, 800 nm light has been used with MAP to create voxels with a transverse dimension of 80 nm,[4] corresponding to $\lambda/10$ resolution. Even finer resolution has been reported for suspended lines, although based on the tapered nature of these lines at their attachment points it is likely that shrinkage during the developing stage plays a role in this case.[5] Using light of a shorter wavelength for MAP can also improve resolution.[6] Due to the shape of the focal region of the laser beam, the resolution of MAP along the beam axis is usually a factor of at least three times poorer than the transverse resolution.[7]

In principle, the smaller the focal volume of the laser is, the higher the resolution. There are several factors that can influence effective focal volume, such as the numerical aperture (N.A.) of the objective, the index of refraction of the resin and the intensity of laser. In order to get high resolution, an objective with a high N.A. and a resin with refractive index matching to the objective immersion oil are preferable. The laser intensity should be close to polymerization threshold so that a small voxel can be made. We have examined these resolution enhancement techniques in our MAP system; the best resolution we achieved with them is about 100 nm.

3.2.2 Alternative means to improve resolution: STED

To improve the resolution of the MAP beyond 80 nm, we have to find a means to overcome the diffraction limit. Our inspiration for this comes from Stimulated Emission Depletion (STED) fluorescence microscopy.[8-10] In STED, fluorescent molecules are excited from the ground state to the first excited electronic state by a femtosecond or picosecond laser pulse. A second laser pulse, which is tuned to a significantly longer wavelength than the first pulse, is used to de-excite the molecules through stimulated emission. This depletion pulse must arrive after vibrational relaxation is complete in the excited electronic state but before significant spontaneous emission to ground state (fluorescence) has occurred. In a typical STED microscopy setup,[8] the excitation beam is tuned to 560 nm and STED pulse is tuned to 760 nm for the specific fluorescent molecule.

Spatial phase shaping of the depletion beam causes de-excitation to occur everywhere except in a small region at the center of the original focal volume, localizing fluorescence to a zone that can be much smaller than the diffraction limit.[8-10] Figure 3.1 demonstrates how the STED technique generates a "smaller" effective focal volume in fluorescent microscopy.

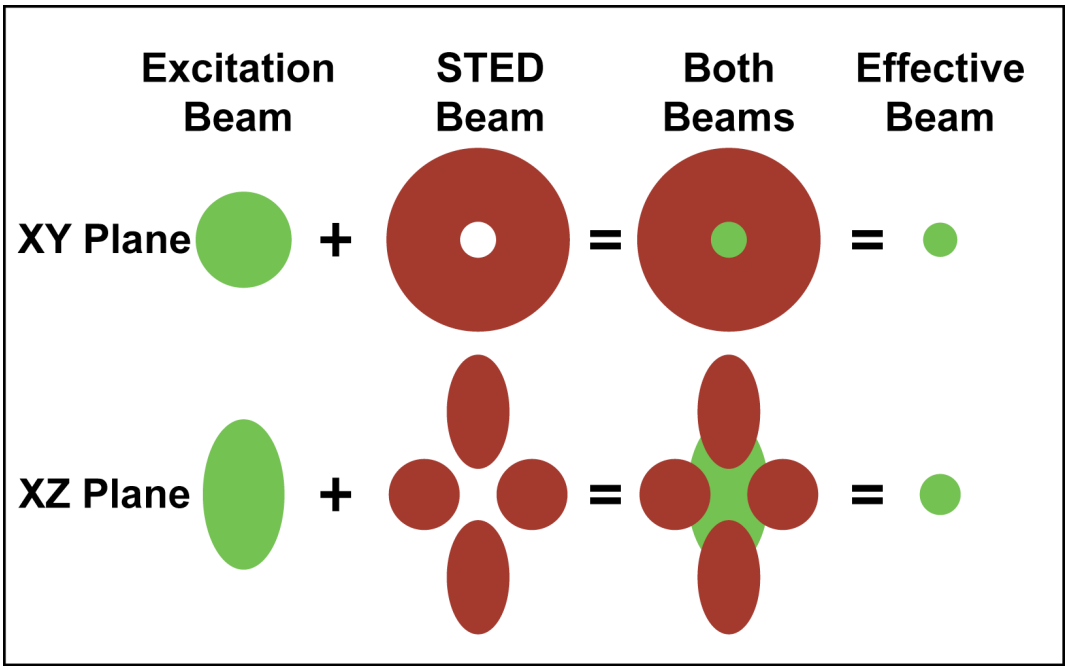

Figure 3.1 Schematic diagrams of the point spread functions of the beams in STED microscopy. The size of the effective beam is smaller than the original excitation beam.

3.2.3 Stop polymerization in MAP

In principle, STED should work equally well to deactivate polymerization in MAP or even in conventional, single-photon photopolymerization. Typical radical photoinitiators undergo intersystem crossing to a triplet state on a time scale on the order of 100 ps.[11] The radicals that lead to polymerization are formed in the triplet state, and so de-excitation of molecules before intersystem crossing occurs will turn off photopolymerization. Furthermore, radical photopolymerization only occurs above a threshold concentration of radicals, so de-excitation of a small fraction of

excited photoinitiator molecules could be sufficient to halt polymerization if the concentration of excited molecules is just above this threshold.

In practice, however, to achieve efficient de-excitation, stimulated emission must dominate over absorption from the first excited electronic state to higher excited states, which will only happen when the oscillator strength between the ground and first excited electronic states is large.[12] This oscillator strength condition is met for the strongly fluorescent molecules used for STED. However, radical photoinitiators generally have relatively small oscillator strengths between the ground and first excited states. Therefore these molecules are more likely to be excited from the first excited state to higher levels than de-excited to the ground state due to the higher oscillator strengths. The higher-lying electronic states have faster intersystem crossing times so that the deactivation beam causes faster polymerization as opposed to inhibiting polymerization in typical photoinitiators.

To solve the oscillator strength problem, we searched for molecules with large absorption cross-sections that are not typically used as radical photoinitiators, but that can still generate radicals upon photoexcitation. We focused our search on molecules with a low fluorescence quantum yield, on the premise that one of the non-radiative processes might lead to radical generation. We identified a number of such dyes that could act as photoinitiators for MAP, including Brilliant Green, Lucirin TPO-L, Rose Bengal, Irgacure 369, Irgacure 184, Isopropylthioxanthone, and Tris(bipyridine)ruthenium(II) dichloride. We then tested whether a second laser beam could be used to deactivate any of these molecules after the initial excitation. For one of the dye molecules tested, malachite green carbinol base, we were able to

use the deactivation beam to reduce polymerization or, at high enough intensity, to inhibit polymerization completely (Figure 3.2). The detailed experimental methods will be discussed in the following sections.

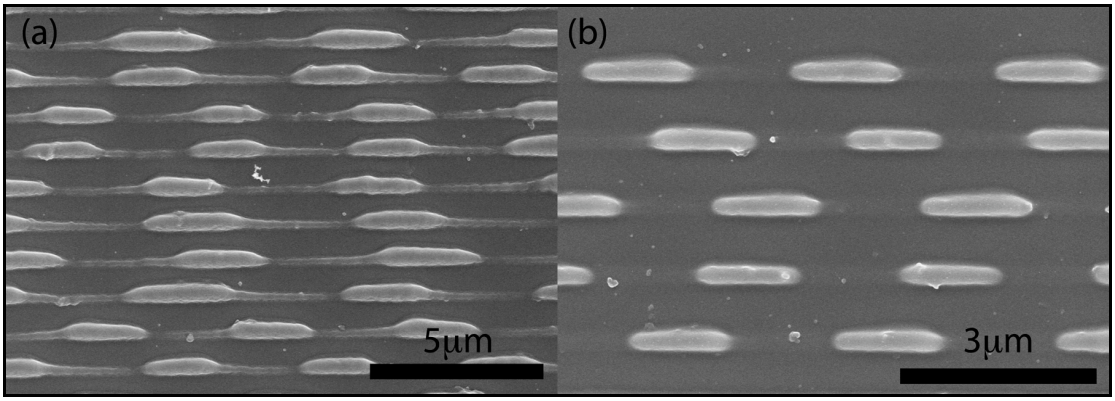

Figure 3.2 (a) Top-view scanning electron micrograph (SEM) of lines written using with offset 200-fs excitation pulses and 50 ps deactivation pulses. The deactivation beam was chopped. The excitation intensity was 7 mW and the deactivation intensity 70 mW; (b) Top-view SEM of lines written with coincident, 200 fs excitation pulses and a CW deactivation beam that was chopped to turn polymerization off and on. The excitation intensity was 5 mW and the deactivation intensity 34 mW.

3.3 RAPID lithography

3.3.1 Experimental setup

At the early stage of the project, we employed two tunable, synchronized Ti:sapphire lasers for these experiments (Figure 3.3), based on the STED idea. The

synchronization was realized through a Coherent SynchroLock apparatus. The excitation laser produced pulses of 200 fs duration centered at 800 nm. The output of the second laser was stretched to a duration of approximately 50 ps to enhance the effectiveness of the stimulated emission process by allowing time for vibrational relaxation in the electronic ground state,[8] and was tuned over a range of wavelengths to search for evidence of deactivation. The two laser beams were combined by a polarizing beam cube before they were sent into a 100x oil-immersion objective (Zeiss α Plan-FLUAR) on an inverted microscope (Zeiss Axiovert 100). The sample was mounted on a 3-D piezo-nanostage (Physik Instrumente) that was in turn mounted on a motorized microscope stage (Ludl). Both the stages and a z drive for the objective (Ludl) were computer controlled. Laser beams were introduced into the microscope through the reflected light-source port.

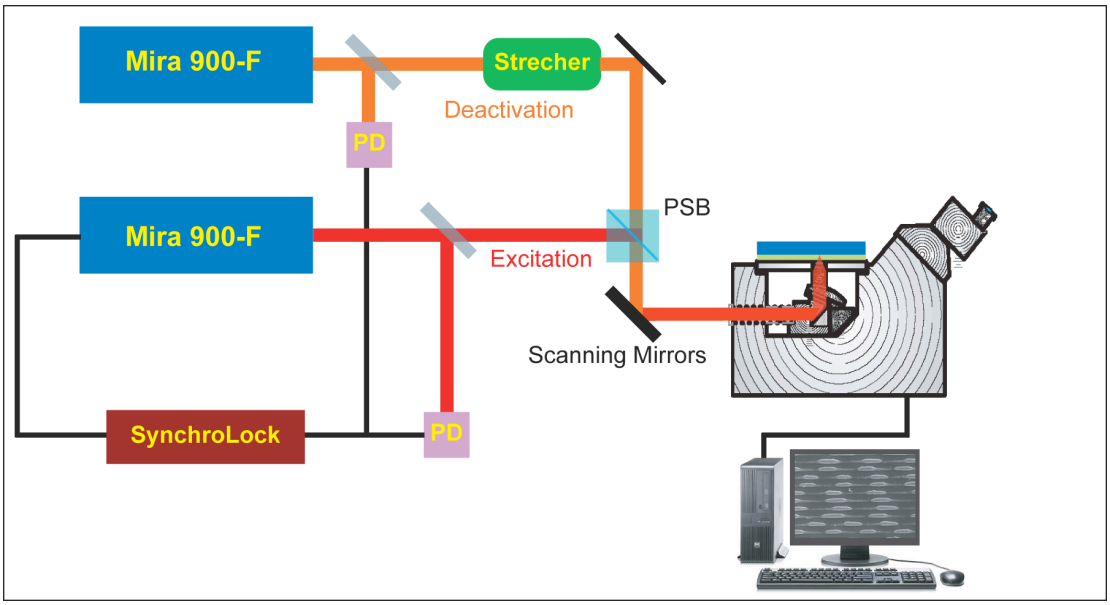

Figure 3.3 First generation of experimental setup for RAPID, in which two synchronized pulsed lasers were used. PD = Photodiode; Stretcher = a glass tube containing CCl_4; PBC = polarizing beam cube

Figure 3.4 shows the schematic illustration of the two beams on the sample. The excitation and deactivation beams are focused in the prepolymer resin with a lateral separation of Δx. The substrate is translated perpendicular to the separation axis to fabricate polymer lines.

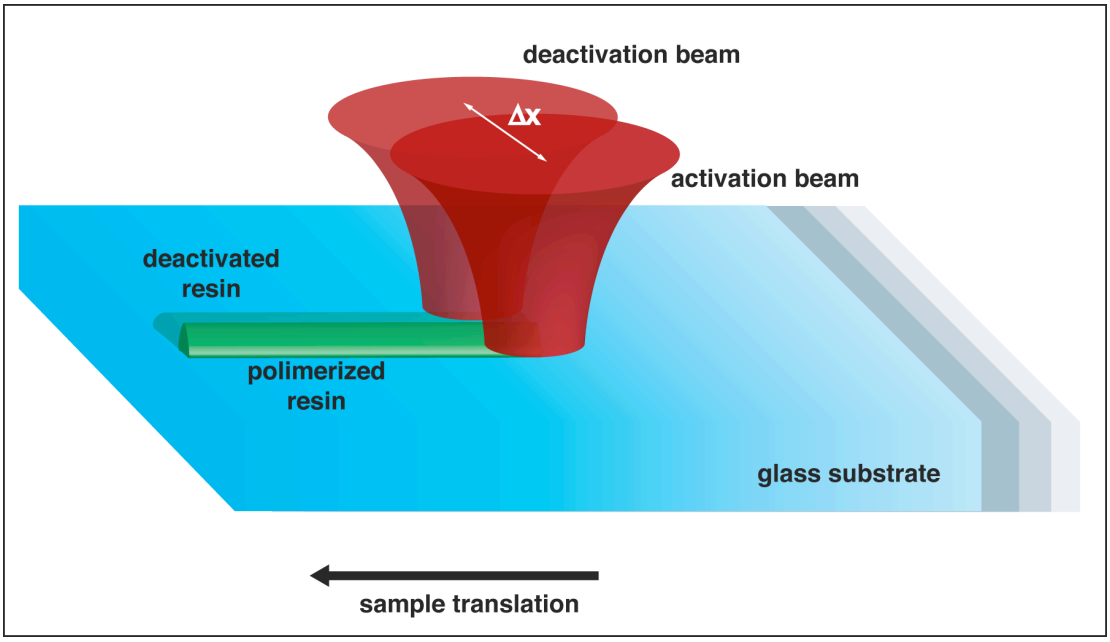

Figure 3.4 Illustration of two beams overlap on the sample in RAPID photolithograph.

3.3.2 Materials and experiment procedures

Pre-processing: For RAPID fabrication, we employed an acrylic resin that was composed of 48.7 wt% ethoxylated(6) trimethylolpropane triacrylate (Sartomer), 48.7 wt% tris(2-hydroxy ethyl) isocyanurate triacrylate (Sartomer), and 1.6 wt% malachite green carbinol base (Aldrich). After thorough mixing, the resin was filtered with a 200-nm pore-size syringe filter. The resin was sandwiched between a cover slip and a substrate that had been treated with (3-acryloxypropyl)trimethoxysilane to improve adhesion of the final voxels.[13]

Beam alignment: The overlap of the two beams is critical for RAPID lithography. The overlap was ensured using multiphoton-absorption-induced luminescence (MAIL);[14] more details about MAIL will be discussed in Chapter 5. A drop of solution containing gold nanoparticles with a diameter of 70 nm was put on a No. 2 cover slip. After the solvent evaporated, a small amount of UV curable adhesive (Norland) was dropped on the cover slip. A piece of No. 1 cover slip was used to cover the glue before the sandwiched sample was put under the UV lamp for 1 minute. This procedure ensured that the gold particles were fixed when performing the MAIL scanning. Because of the high efficiency of MAIL, the lasers should be tuned down to their minimum intensity. The laser focal point was scanned over a gold nanoparticle using either the scanning mirrors and the piezo stage, either in the xy or xz planes. The signal was collected by a single-photon-counting avalanche photodiode (EG&G) and was transferred to a computer by a data acquisition board (National Instruments). Data collection was performed by a program written in LabView (National Instruments).

Fabrication: The basic fabrication procedure is similar to the one described in Chapter 1 and Chapter 2. A second shutter was needed to control the deactivation beam.

Post-processing: After fabrication, the top cover slip was removed and the substrate with fabricated structures was rinsed in dimethylformamide for three minutes twice, followed by two three-minutes rinses in ethanol. If the structure had a suspended component, a 30 seconds rinse in hexamethyldisilazane was performed at the end to avoid capillary effects. For SEM imaging, samples were first coated with approximately 25 nm of palladium-platinum in a sputter coater. All AFM images were acquired in tapping mode.

3.3.3 Results and Discussions

We first verified that continuous-wave (CW) radiation from the laser did not lead to polymerization with the photoinitiator, which ensured that photoinitiation occurred through multiphoton absorption. We then examined deactivation beam wavelengths ranging from 760 nm to 840 nm, and in all cases were able to inhibit polymerization. The capacity to initiate polymerization with fs pulses and inhibit polymerization with considerably longer pulses of the same wavelength confers the advantage that the entire process can be accomplished with the output of a single ultrafast laser if desired.

To demonstrate photoinduced deactivation of polymerization, we fabricated polymer lines with excitation and deactivation beams that were either offset or

spatially coincident (Figure 3.4). Shown in Figure 3.2 (a) are lines drawn with an offset between the beams. The deactivation beam was blocked at regular periods with an optical chopper wheel. The resultant modulation of the polymer line demonstrates the effectiveness of the deactivation process.

In Figure 3.5 we show lines drawn by scanning the sample stage at a constant velocity with no deactivation beam (bottommost line) and with different timings between the excitation and deactivation pulses. The deactivation beam was set at an intensity that resulted in only partial inhibition of polymerization so that the dependence of the deactivation efficiency on timing could be determined. The efficiency of deactivation did not change noticeably for excitation/deactivation delays between 0 and 13 ns. The maximum delay time of 13 ns is determined by the 76 MHz laser repetition rate. This result implies that the photoinitiator goes through an intermediate state between optical excitation and the initiation of polymerization. The lifetime of this intermediate state must be considerably longer than 13 ns, making it likely that the state is deactivated through a process other than stimulated emission. Once a structure was polymerized it could not be erased by subsequent application the deactivation beam, indicating that for deactivation to be effective it must occur while the dye molecule is in this intermediate state. However, a region in which deactivation was used to prevent polymerization can be polymerized subsequently by the excitation beam.

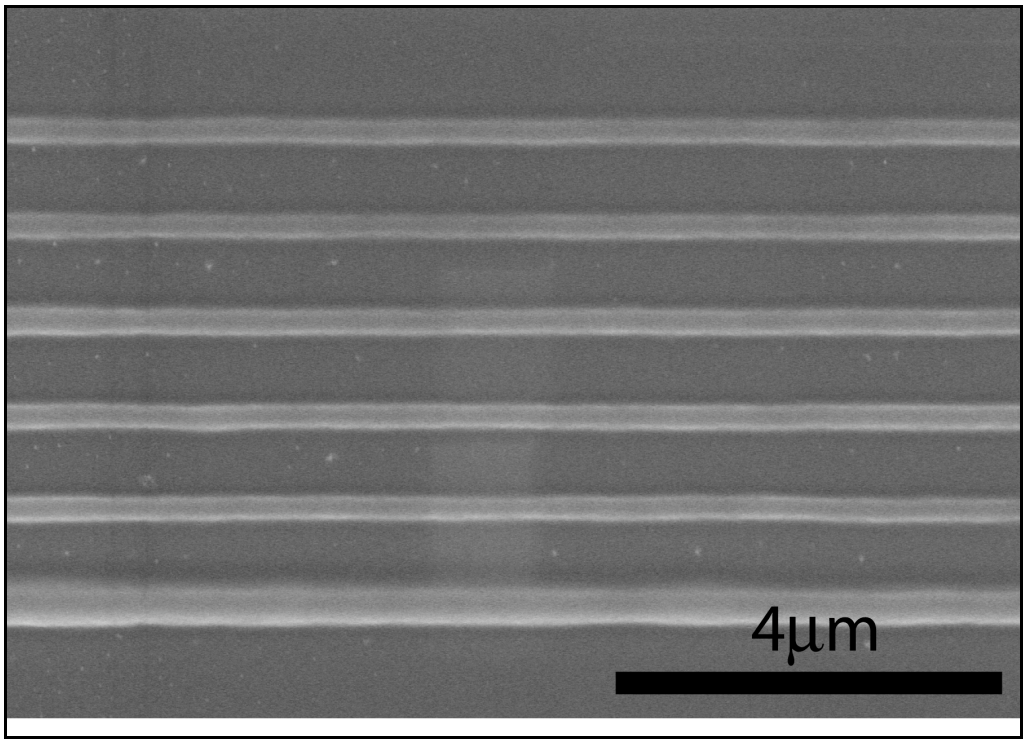

Figure 3.5 Top-view SEM of lines written with different timings between the excitation and deactivation pulses. The deactivation beam was at a low enough intensity to inhibit polymerization incompletely. The bottom line was written without a deactivation beam, and the remaining lines were with written with delay times, from bottom to top, of 7 ns, 12 ns, 0 ns, 1 ns and 6 ns; all delay uncertainties are < 1 ps. The excitation intensity was 7 mW and the deactivation intensity 50 mW.

Even with 50 ps pulses, at high enough average power the deactivation beam caused increased polymerization, presumably through two-photon absorption. Based on the observation that delays as long as 13 ns did not affect the deactivation efficiency, we tested whether deactivation could be driven by CW radiation, for

which considerably higher deactivation intensities would be feasible. As shown in Figure 3.2 (b) for spatially coincident excitation and deactivation beams (with the latter beam chopped), CW radiation is indeed effective for deactivation. This result is important because it allows RAPID to be performed without the need to establish any timing between the excitation and deactivation lasers, and also implies that RAPID lithography should be feasible with single-photon absorption using CW excitation and deactivation beams.

Figure 3.2 (a) gives a clear indication of how using different spatial intensity patterns for these two beams can improve resolution. We therefore next explored spatial phase shaping of the deactivation beam to alter its intensity distribution in the focal region. The 2nd generation of experimental setup for RAPID lithography, with a pulsed excitation beam and a phase-shaped, CW deactivation beam, is shown in Figure 3.7. This setup employs two Ti:sapphire lasers tuned to 800 nm, one operating in pulsed mode for multiphoton excitation and one operating in CW mode for deactivation. The outputs of the two lasers were set to orthogonal polarizations and combined in a polarizing beam cube. The beams were focused into the sample with a high numerical aperture objective, the back aperture of which was overfilled by the excitation beam and filled completely by the deactivation beam.

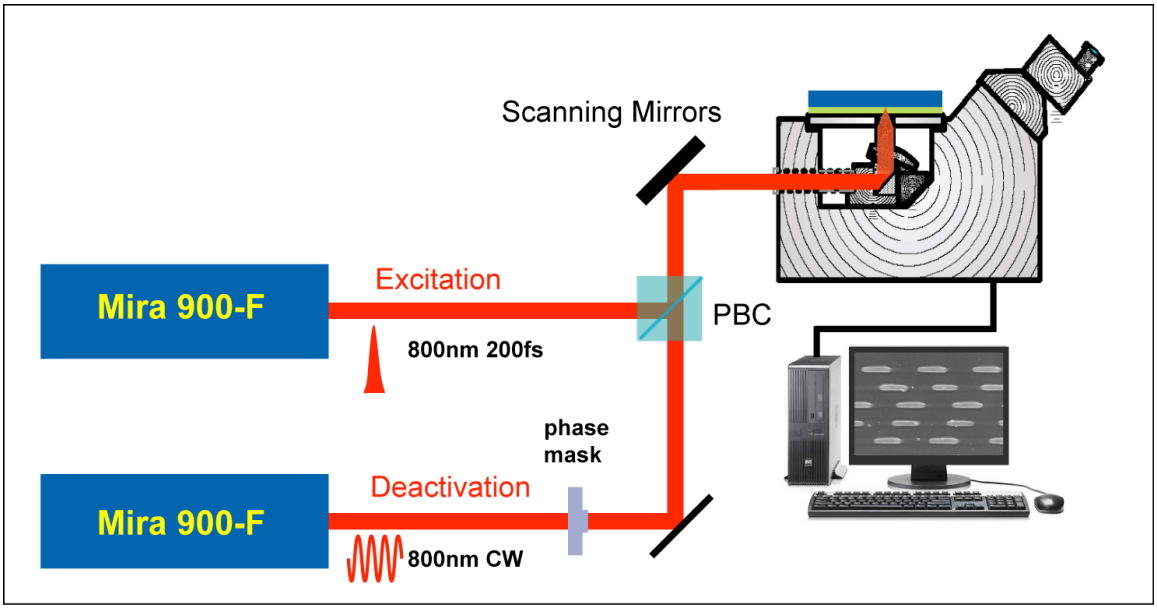

Figure 3.6 Schematic experimental setup for 2nd generation of RAPID lithography with a pulsed excitation beam and a phase-shaped, CW deactivation beam. PBC = polarizing beam cube.

We employed a spatial phase mask[8] that is designed to improve resolution along the optical axis of the fabrication system, which we will designate z. The mask consists of a flat substrate with a central circular region of an appropriate thickness to create a half-wave delay at 800 nm. The point-spread functions (PSFs) of the two beams were measured using MAIL from a gold nanoparticle (Figure 3.7). Because MAIL from gold nanoparticles is a 3-photon process at 800 nm, the images show the cubes of the PSFs. The majority of the intensity of the deactivation beam lies outside of the center of the focal region. As can be seen from these images, there is no overlap between the excitation and deactivation PSFs in the xy plane, but there is considerable overlap along the z direction.

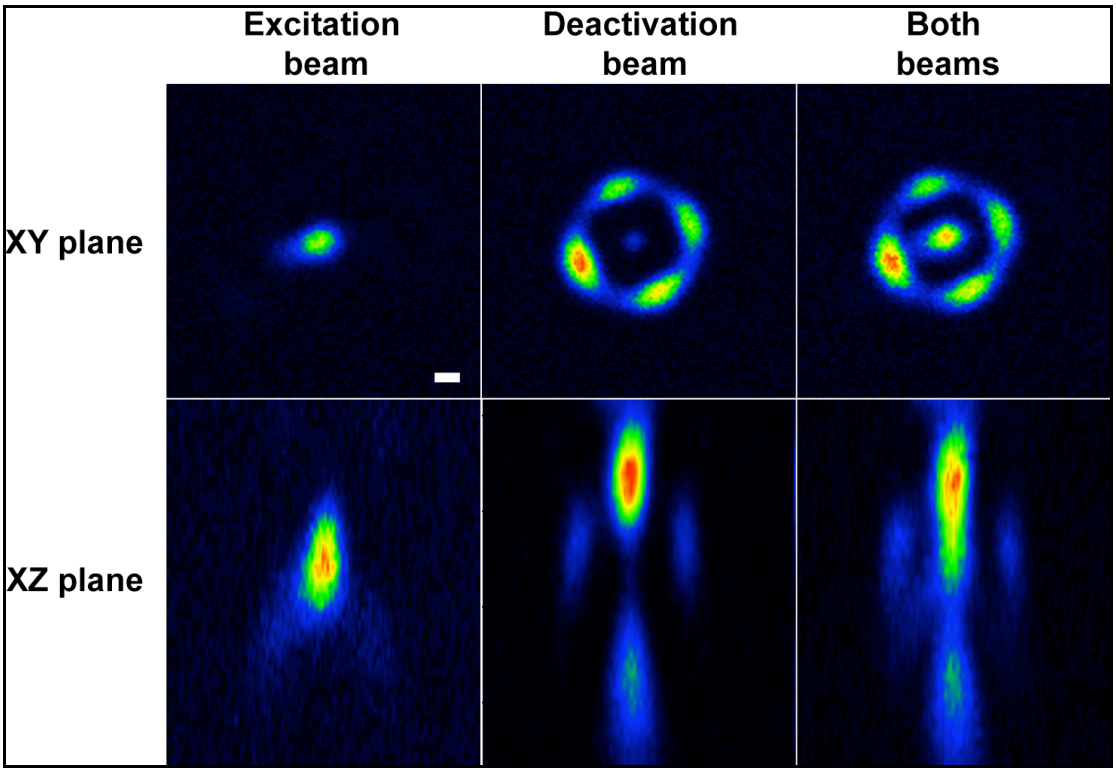

Figure 3.7 Mulitphoton-absorption-induced luminscence images of the cubes of the point spread functions of the excitation beam, the deactivation beam, and both beams together. The scale bar is 200 nm.

To assess the resolution enhancement of RAPID lithography with this phase mask, we studied the sizes and shapes of voxels created with different excitation and deactivation powers. In order to observe the voxel shapes, we employed an ascending-scan method, in which identical, isolated voxels are created at different heights relative to the substrate.[7] At some particular height the voxel will barely be attached to the substrate. If the aspect ratio of the voxel is greater than unity it will fall over, allowing its dimensions to be determined readily with scanning electron microscopy (SEM) or atomic force microscopy (AFM).

Figure 3.8 shows SEM images from one such voxel study at a fixed excitation power (time averaged) of 10 mW and different deactivation beam powers. To fabricate the voxels, the excitation beam was exposed on the resin for 38 ms. As would be expected for the phase mask employed, deactivation did not have a substantial effect on the transverse dimensions of the voxels. However, with increasing deactivation power the z dimension of the voxel decreased more than three-fold. For a given excitation intensity, deactivation intensity, and height relative to the substrate, voxels were either present at every exposed spot or were absent at every exposed spot. The variation in voxel dimensions for a fixed set of fabrication parameters was approximately ±5%.

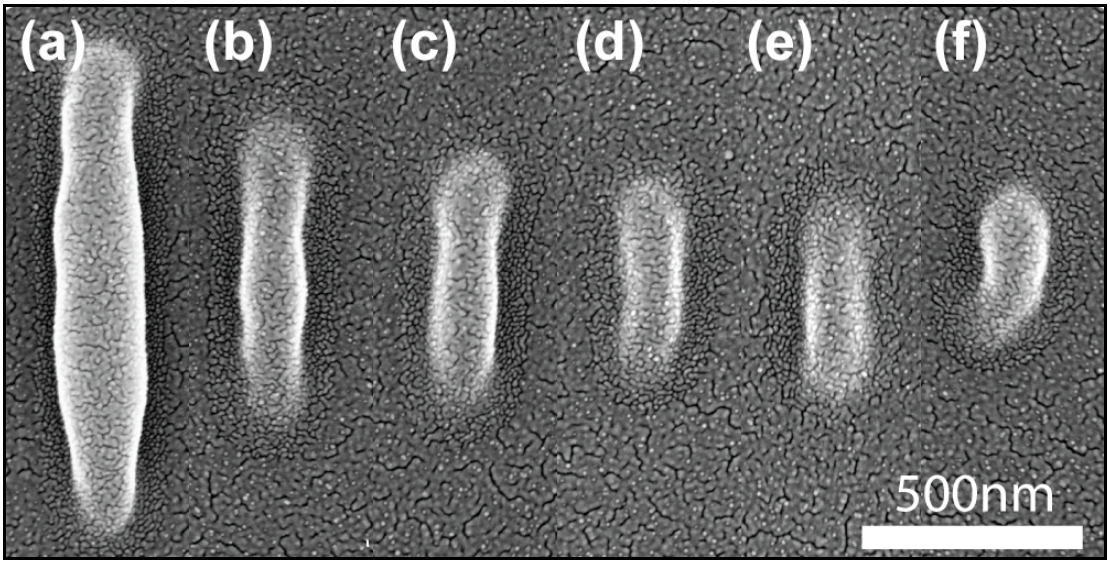

Figure 3.8 SEM images of voxels created with excitation power of 10mW and deactivation beam powers of 0 mW, 17 mW, 34 mW, 50 mW, 84 mW and 100 mW, from (a) to (f), respectively.

Because our voxel studies were performed on a glass cover slip (which is transparent but not electrically conductive), voxels had to be coated with metal for SEM imaging. Thus, to measure the smallest voxels that could be fabricated and to avoid size distortions from the coating step, we used an AFM. Shown in Figure 3.9 (a) is the smallest voxel that we were able to fabricate reproducibly with RAPID lithography using 800 nm light. The slight asymmetry of the voxel is due to our use of linearly-polarized light for fabrication.[15] For comparison, the corresponding smallest voxel that could be fabricated reproducibly without the deactivation beam is shown in Figure 3.9 (b). While the voxel in Figure 3.9 (a) is standing, the voxel in Figure 3.9 (b) has fallen over due to its high aspect ratio. The resin used here is composed of low-molecule-weight monomers that exhibit low shrinkage. To test whether shrinkage takes on an increased importance at small feature sizes, we fabricated suspended polymer lines, shown in Figure 3.9 (c), with cross-sectional dimensions similar to those of the voxels in Figure 3.9. The widths of the lines did not increase substantially at their attachment points to the supporting structures, indicating that shrinkage is not responsible for the small voxel sizes observed here.

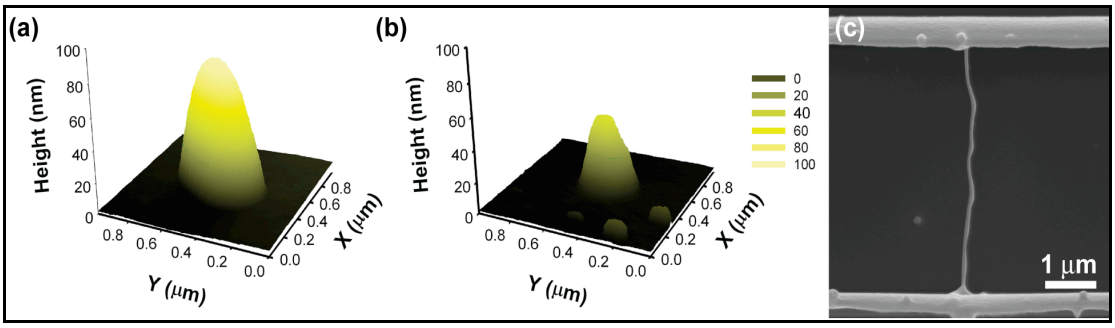

Figure 3.9 (a) 3-dimensional AFM images of the smallest voxel that could be created with conventional MAP; (b) Corresponding images of the smallest voxel that could be created with RAPID lithography. Note that the X and Y dimensions of the voxels are exaggerated due to the width of the AFM tip, whereas the Z dimension (height) is accurate. (c) SEM image of a suspending polymer wire fabricated with RAPID.

In Figure 3.10 we plot the height and aspect ratio of voxels measured in AFM experiments as a function of deactivation power. Note that when the aspect ratio of a voxel is less than unity, it will not fall over even when barely attached to the substrate. We were able to reduce the voxel height from nearly 600 nm with no deactivation beam to 40 nm with a deactivation power of 93 mW, representing a resolution of $\lambda/20$. The aspect ratio was correspondingly reduced from over 3 to 0.5.

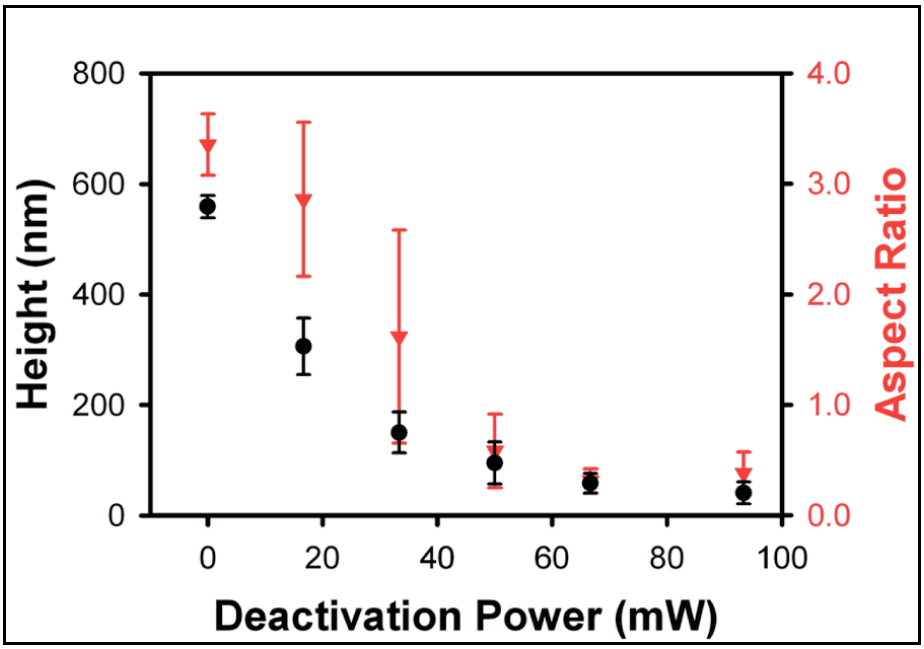

Figure 3.10 The height and aspect ratio of voxels vs. the power of the deactivation beam. The error bars represent $\pm\sigma$ based on measurements of four voxels.

To demonstrate the capability of fabricating 3-D structures with RAPID, we designed a tower structure with three rings on the surface. In Figure 3.11 (a), the rings are fabricated with conventional MAP, while the RAPID was used to fabricated the structure shown in Figure 3.11 (b) It can be observed that the enhancement of resolution and aspect ratio can also be achieved in 3-dimensional structures.

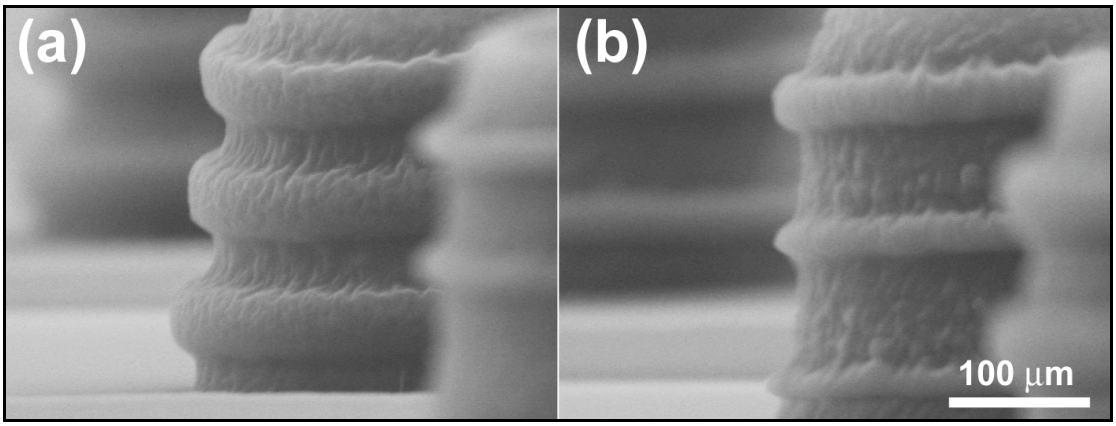

Figure 3.11 SEM images of 3-D objects. (a) Tower with rings created with conventional MAP; (b) Tower with rings created with RAPID.

We have observed that above a certain excitation power, it becomes impossible to inhibit polymerization fully even at high deactivation beam power (Figure 3.12). This result implies that there are two different channels for photoinitiation, only one of which is deactivatable. So long as the concentration of radicals from the non-deactivatable channel is below the polymerization threshold, the deactivation beam can inhibit polymerization completely. We have further observed that the irreversible channel is weaker in more viscous resins. While research into the nature of the photophysics of this system is ongoing, we believe that excitation of the photoinitiator leads to an electron transfer process that creates two relatively stable radicals. Due to their stability, these radicals initiate polymerization on a time scale that is considerably longer than the 13 ns repetition time of our laser system. So long as the radicals do not diffuse apart, absorption of a photon from the deactivation beam can lead to back transfer of the electron, depleting the radicals

before they can react. If the radicals do diffuse apart, deactivation can no longer occur, accounting for the non-deactivatable channel.

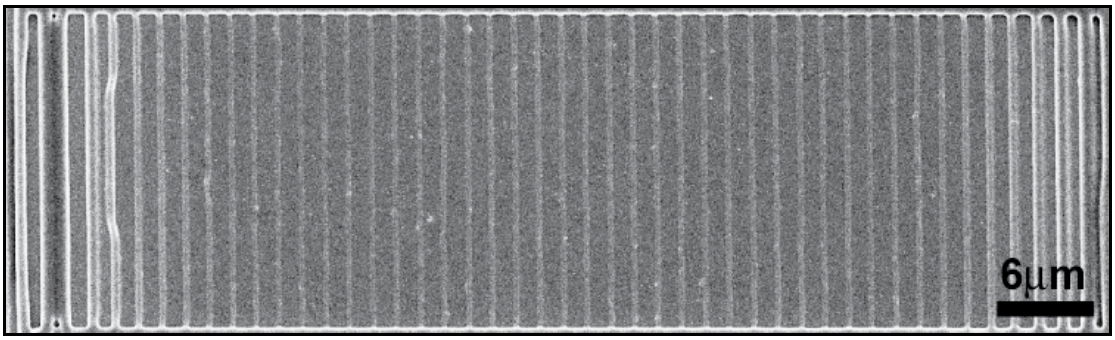

Figure 3.12 SEM image of polymeric lines fabricated with vary depletion beam power. The depletion powers are increasing by 5 mW from line to line, varying from 10 mW to 100 mW from left to right, respectively.

Given the high peak intensity of the short excitation pulses, two-photon initiation dominates over one-photon deactivation. Due to their considerably greater duration and correspondingly weaker peak intensity, the energy of 50-ps deactivation pulses can be much greater than that of the excitation beam without causing polymerization. Thus, for these longer pulses deactivation can dominate over initiation. Use of a CW beam allows for the use of a correspondingly larger energy for deactivation.

3.4 Conclusion

In this chapter, the background and experimental details of RAPID lithography were described. We demonstrated that λ/20 resolution had been achieved

by the RAPID technique. With the phase mask used here, RAPID lithography can clearly produce features with heights as small as $\lambda/20$ along the optical axis. In analogy with results from STED microscopy, comparable transverse resolution should be attainable by employing a different phase mask, such as a spiral phase element.[16] By using two phase-masked deactivation beams[17] it should further be possible to attain this resolution in all dimensions. The use of shorter excitation and deactivation wavelengths should improve resolution further.

A current limiting factor in the resolution attainable is that even a CW deactivation beam can cause polymerization at high enough intensity. Since the resolution enhancement of RAPID lithography is based on an optical saturation effect, making the deactivation process more efficient should lead to finer features. In principle, the resolution of RAPID will ultimately be limited by material properties, particularly the minimum size of a self-supporting polymer voxel. With this limitation in mind, we believe that resolution on the order of 10 nm can be attained through full optimization of the photoresist properties and the optical configuration. Resolution on this scale may be attractive for next-generation lithography, particularly considering that RAPID lithography can be implemented with a tabletop instrument.

Reference:

(1) Thompson, S. E.; Parthasarathy, S., Moore's law: the future of Si microelectronics. *Materials Today* **2006,** *9* (6), 20-25.

(2) Ito, H.; Marty, J. D.; Mauzac, M., *Microlithography, molecular imprinting*. Springer-Verlag Berlin: Berlin, 2005; Vol. 172.

(3) Li, L.; Gattass, R.; Gershgoren, E.; Hwang, H.; Fourkas, J. T., Achieving λ /20 Resolution by One-Color Initiation and Deactivation of Polymerization *Science* **2009**.

(4) Xing, J. F.; Dong, X. Z.; Chen, W. Q.; Duan, X. M.; Takeyasu, N., Improving spatial resolution of two-photon microfabrication by using photoinitiator with high initiating efficiency. *Applied Physics Letters* **2007,** *90*, 131106/1-131106/3.

(5) Tan, D.; Li, Y.; Qi, F.; Yang, H.; Gong, Q.; Dong, X. Z.; Duan, X. M., Reduction in feature size of two-photon polymerization using SCR500. *Applied Physics Letters* **2007,** *90*, 071106/1-071106/3.

(6) Haske, W.; Chen, V. W.; Hales, J. M.; Dong, W.; Barlow, S., 65 nm feature sizes using visible wavelength 3-D multiphoton lithography. *Optics Express* **2007,** *15* (6), 3426-3436.

(7) Sun, H. B.; Tanaka, T.; Kawata, S., Three-dimensional focal spots related to two-photon excitation. *Applied Physics Letters* **2002,** *80* (20), 3673-3675.

(8) Klar, T. A.; Jakobs, S.; Dyba, M.; Egner, A.; Hell, S. W., Fluorescence microscopy with diffraction resolution barrier broken by stimulated emission.

Proceedings of the National Academy of Sciences of the United States of America **2000,** *97* (15), 8206-8210.

(9) Hell, S. W., Far-field optical nanoscopy. *Science* **2007,** *316*, 1153-1158.

(10) Hell, S. W., Microscopy and its focal switch. *Nature Methods* **2009,** *6* (1), 24-32.

(11) Colley, C. S.; Grills, D. C.; Besley, N. A.; Jockusch, S.; Matousek, P.; Parker, A. W.; Towrie, M.; Turro, N. J.; Gill, P. M. W.; George, M. W., Probing the reactivity of photoinitiators for free radical polymerization: Time-resolved infrared spectroscopic study of benzoyl radicals. *Journal of American Chemical Society* **2002,** *124* (50), 14952-14958.

(12) Hirschfelder, J. O.; Curtiss, C. F.; Bird, R. B., *Molecular theory of gases and liquids*. Wiley: New York, 1954; p 890.

(13) Baldacchini, T.; LaFratta, C. N.; Farrer, R. A.; Teich, M. C.; Saleh, B. E. A.; Naughton, M. J.; Fourkas, J. T., Acrylic-based resin with favorable properties for three-dimensional two-photon polymerization. *Journal of Applied Physics* **2004,** *95* (11), 6072-6076.

(14) Farrer, R. A.; Butterfield, F. L.; Chen, V. W.; Fourkas, J. T., Highly efficient multiphoton-absorption-induced luminescence from gold nanoparticles. *Nano Letters* **2005,** *5* (6), 1139-1142.

(15) Sun, H. B.; Maeda, M.; Takada, K.; Chon, J. W. M.; Gu, M.; Kawata, S., Experimental investigation of single voxels for laser nanofabrication via two-photon photopolymerization. *Applied Physics Letters* **2003,** *83* (5), 819-821.

(16) Beijersbergen, M. W.; Coerwinkel, R. P. C.; Kristensen, M.; Woerdman, J. P., Helical-wave-front Laser-beams Produced with a Spiral Phaseplate. *Optics Communications* **1994,** *112* (5-6), 321-327.

(17) Harke, B.; Ullal, C. K.; Keller, J.; Hell, S. W., Three-dimensional nanoscopy of colloidal crystals. *Nano Letters* **2008,** *8* (5), 1309-1313.

Chapter 4: Selective Functionalization of Microstructures

4.1 Introduction

Previous chapters have shown that MAP is an effective technique for fabrication of arbitrary, 3-D, polymeric micro-/nano-structures. The ability to pattern chemical functionality on polymer surfaces is essential for many applications, such as conductive MEMS devices and many other optical and fluidic microdevices. This capability is also important for addressing biological issues such as cell motility, chemical signaling, cell growth and aggregation, and for biomedical applications such as tissue scaffolding.

In this chapter, a technique for selective functionalization of polymer microstructures will be discussed. These microstructures can be fabricated by either MAP or the conventional photolithography.

4.2 Selective metallization of MAP devices

The acrylate-based resins we have used for MAP fabrication have multiple functional groups. After the crosslinking of the monomers caused by laser irradiation, there are still unreacted actylate groups left on the surface of the final polymeric structure. Each surface acrylate group can undergo Michael addition with ethylene diamine, leaving a free amine group on the polymer surface. The ability to

react with these free amines of these free acrylate groups is a starting point for chemical functionalizaion.

4.2.1 Michael addition reaction

The Michael addition reaction is a nucleophilic addition to an α, β unsaturated carbonyl compound. It belongs to the larger class of conjugate additions. The reaction of acrylate groups with nucleophiles, such as primary amines, has been demonstrated via a Michael addition.[1, 2] Scheme 4.1 shows the Michael addition reaction between a nucleophilic compound and an acrylate group.

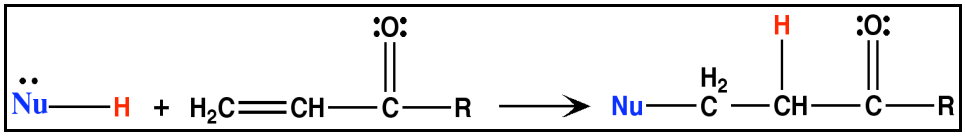

Scheme 4.1 Typical Michael addition reaction.

We employed a similar idea here to functionalize our polymer surface. By reacting acrylic microstructures with diamines, such as ethylene diamine (Figure 4.1), one amine group of the molecule should react with an acrylate group thereby appending a primary amine to the polymer.

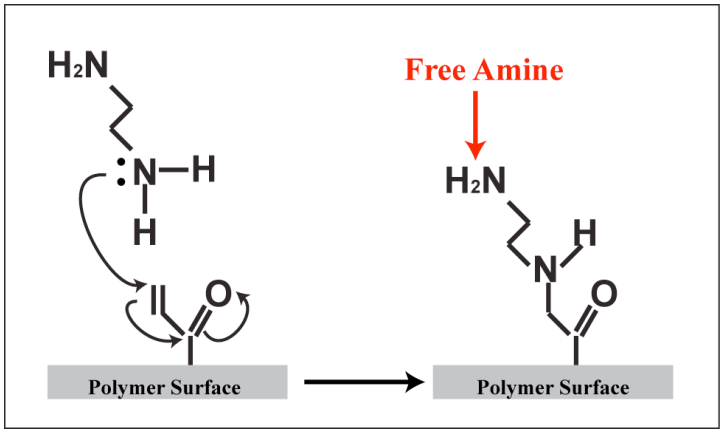

Figure 4.1 Michael addition of ethylene diamine onto an acrylate surface.

To create polymeric structures that would not react with amines, we introduced another type of monomer, Sartomer SR348, which is a difunctional methacrylate. Ethylene diamine can also react with methacrylates via Michael addition. However, the reaction rate is almost negligible compared with that of acrylates. Thus, we can selectively functionalize the surface of microdevices by fabricating different regions with different monomer components.[3]

4.2.2 Visualizations of amines

Here, we employ the dansyl chloride as a fluorescent dye to visualize the amines on the polymer surface. Dansyl chloride was chosen for several reasons: (1) it becomes fluorescent upon reaction with primary amines, avoiding the need for expensive analytical equipments (e.g. XPS[4, 5]) to test for the presence of amines; (2) it is nonfluorescent before reaction with a primary amine, reducing background; (3) it has moderate two-photon cross section, so that we are able to image functionalized microstructure with a multiphoton microscope.[6]

To make the dansyl chloride solution, 1 mL of dimethylformamide and 12.5 μL of diisopropylethylamine were added to a test tube containing 18 mg of dansyl chloride. After thorough mixing, the solution was dropped on the surface of the aminated sample for 2 minutes. Then the sample was rinsed with methanol for 3 minutes twice, following by thorough drying in air.

Figure 4.2 shows examples of fluorescent images of amine coated polymeric structures. The dansyl chloride that has reacted with amines shows strong fluorescence under excitation of the UV light. The sample in Figure 4.2 (a) was made by single-polymerization, while the structures in Figure 4.2 (b) were fabricated with MAP. The width of the lines in Fig. 4.2 (b) is about 1 μm, showing the high resolution of the detection method.

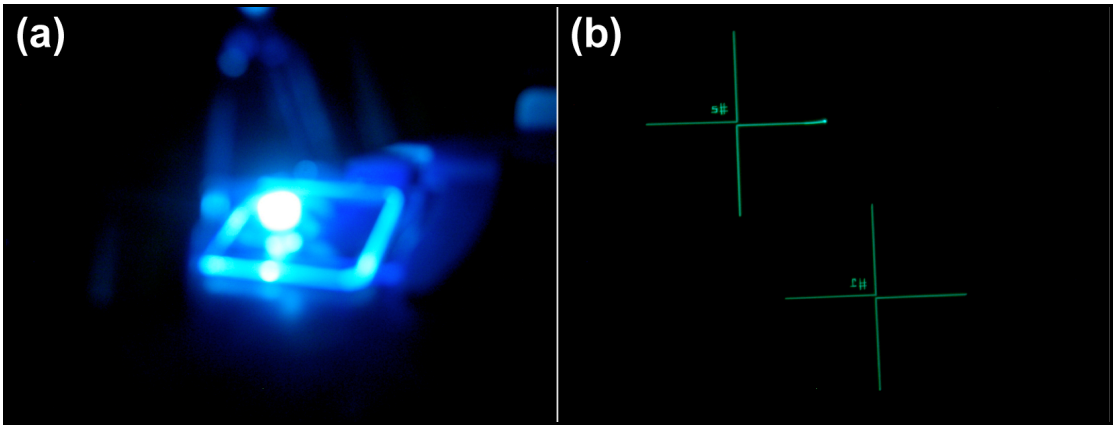

Figure 4.2 Fluorescent images of the dansyl chloride coated amine surfaces. (a) a drop of the resin polymerized by single-photon absorption; (b) crosses fabricated with MAP.

4.2.3 Metallization of polymeric devices

Reactive amine-coated surfaces can be used for the seeding of a catalyst for metallization. The most common catalyst used is palladium. Palladium can form a metal complex with amines rapidly under mild reaction conditions. This reaction occurs simply by immersing an amine-coated acrylate sample in a solution of palladium chloride for about 15 minutes. The palladium cation Pd^{2+} is reduced to Pd^{0} for the purpose of catalyzing the electroless metal deposition on the polymer surface.

The experimental details for this metallization procedure are as follows. The microstructures are fabricated with MAP as described in the previous chapters. The resin used consists of equal parts Sartomer SR-368 and Sartomer SR-399 with 3 wt. % Lucirin TPO-L (BASF). To protect the glass substrate from being coated with metal, we modify the substrate with 3-methacryloxypropyltrimethoxysilane. After fabrication, samples are washed in dimethylformamide and then in ethanol. The sample is submerged in a 20% (by vol.) solution of ethylene diamine in DI water for 45 minutes, followed by three 1-minute rinses in water. The amine-coated samples are then placed in an aqueous solution composed of 0.1 g/L $PdCl_2$ and 0.1 mL/L of concentrated HCl for 15 minutes. The samples are rinsed in water twice for a minute each before being placed in an 85 °C solution of 0.1 M NaH_2PO_2 for 10 min. Following that, the samples are washed in water three times for 1 min each. The final step is to dip the samples into the copper solution under stirring for 5 minutes or more depending on the desired amount of copper. The copper solution consists of 0.6 M

$NaKC_4H_4O_6 \cdot 4H_2O$ (Rochelle salt), 0.14 M NaOH, 0.28 M $CuSO_4 \cdot 5H_2O$, and 0.3 M EDTA.[5]

Selective coating has been achieved when fabricating structures in which portions are fabricated with acrylate monomers and other portions with methacrylate monomers. Figure 4.3 shows examples of selective metallization. In Figure 4.3 (a), the letters 'U' and 'D' were made with an acrylic resin and then the letter 'M' was made from a methacrylic resin. The hybrid sample was metallized following the procedure described above. This image was taken using a reflecting optical microscope and shows that no copper was deposited on the methacrylic 'M'. In Figure 4.4 (b), the 1st and 3rd circle from the center were fabricated with an acrylic resin while the other two were fabricated with a methacrylic resin.

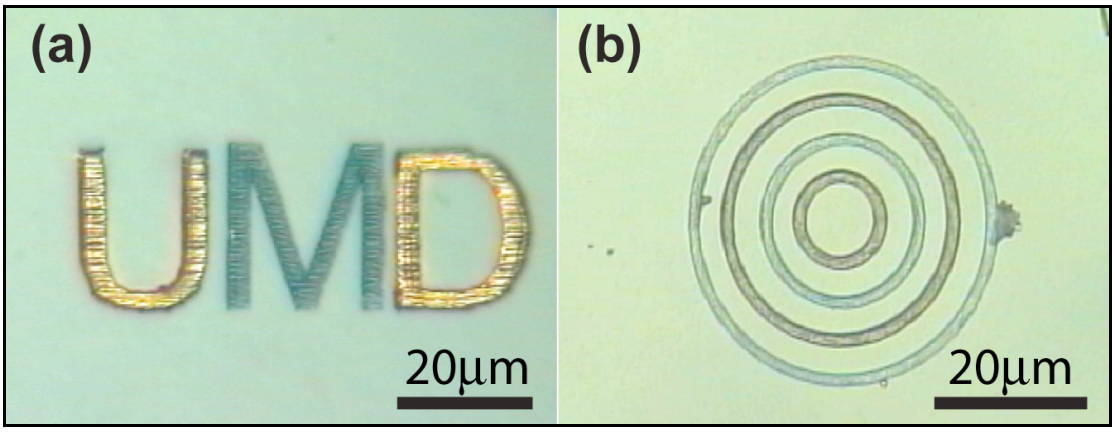

Figure 4.3 Example of selective metallization.

4.2.4 How the method of fabrication affects metallization

The reaction between free acrylate groups and ethylenediamine is the first step for the metallization of the polymer microstructure; therefore, the number of free

acrylate groups is an important factor for metallization. We observed that fabrication with higher laser intensities and faster stage translation speeds generated structures with more free acrylate groups. Figures 4.4 (a) and 4.4 (b) are the fluorescent images of dansyl chloride/amine coated polymer microarrays. The 10 x 10 μm squares were fabricated at different speeds and laser intensities. The square made at 18 mW with a 70 μm/sec writing speed shows the strongest fluorescence. A similar test was performed by metalizing microarrays, showing that a square fabricated at 20 mW with a 50 μm/sec speed got more metal than others (Figure 4.4 (c)).

The explanation for this phenomenon is as follows. At high fabrication speeds, the crosslinking of the monomers is less complete and more free acrylate groups are left on the surface. When fabricating at high power, the voxel size becomes larger, which also can generate more areas of free acrylate groups.

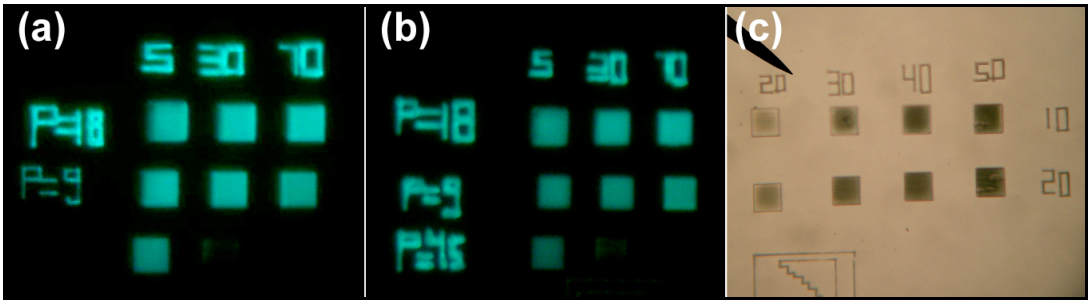

Figure 4.4 Images of squares fabricated at vary speeds and laser intensities. (a) (b) Dansyl chloride-Amine fluorescent images of 10 x 10 μm sqaures fabricated with speeds of 5, 30 and 70 μm/sec from left to right, and powers of 4.5, 9 and 18 mW from bottom to top, respectively; (c) Metallized squares, fabricated with speeds from 20 to 40 μm/sec and powers from 10 and 20 mW.

Other factors that affect the metallization of acrylic microstructures have been addressed in previous published work.[3, 7] After demonstration of the selective metallization of polymeric devices made with MAP, we looked into techniques to functionalize polymer surfaces that were fabricated by single-photon photolithography.

4.3 New strategy for patterning of chemical functionality

4.3.1 Overview

As discussed above, the surfaces of structures created with MAP receive less light exposure than do the interior regions. Thus, each unreacted surface acrylate group can undergo Michael addition with ethylene diamine, leaving a free amine group on the polymer surface. By the same token, we can generate a polymer structure with different acrylate density on the surface by exposing different regions to different intensities of light in single-photon lithography. The amines are then patterned on the polymer surface by reacting with acrylates. We have generated both binary and gray-scale amine patterned surfaces in this way.

A number of methods exist for creating binary (on/off) patterns of chemical functionality on surfaces, but in many instances it is desirable to be able to create gray-scale patterns of functionalization with high dynamic range. Most approaches for gray-scale patterning of functionality rely upon effects such as diffusion to create simple gradient patterns.[8-13] Other methods can create more sophisticated patterns,[14] but generally not with high resolution and dynamic range. One exception[15] is a

technique based on the creation of a self-assembled monolayer on glass using a specially-synthesized molecule with photouncageable amine groups. Here we show a technique that is rapid, uses inexpensive, commercially available components, and avoids the use of photolabile protecting groups.

In bulk photopolymerization, the surfaces of the sample receive as much light exposure as does the interior. However, if a surface is exposed to a radical quencher such as O_2 during polymerization, then the radical chain reaction will proceed less efficiently there, potentially leaving unreacted acrylate groups. Figure 4.5 demonstrates how O_2 affects single-photon polymerization. A small amount of acrylate resin (Sartomer SR368 and SR399 with 3% TPO-L) was dropped on a glass substrate followed by exposing to UV light for about 1 minute. The sample in Figure 4.5 (a) was covered with glass cover slips while the samples in Figure 4.5 (b) was exposed to UV directly without being covered. The cured polymer dots were then dipped in ethylene diamine solution (20% by volumn in H_2O) followed by dansyl chloride treatment. As seen from the figures, only the outer ring of the covered polymer dot fluoresces under UV light since the side of the dot was exposed to air. However, the entire surface area of the uncovered polymer dot shows the strong fluorescence.

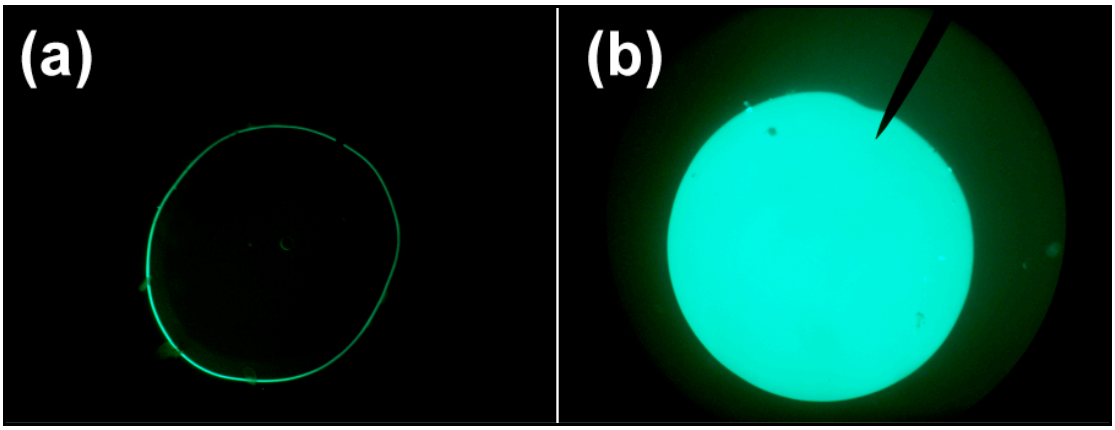

Figure 4.5 Fluorescent images of Dansyl-aminated polymer surface under UV irradiation. (a) the top surface of prepolymer resin was covered with a cover slip to prevent oxygen from inhibiting crosslinking; (b) the prepolymer resin was open to air while polymerizing.

The surface density of unreacted acrylates in any region of the surface will depend upon the total light exposure, providing a means for photolithographic patterning of chemical functionality.

4.3.2 Experimental details

Protocol: Our scheme for patterning of functionalization is illustrated in Figure 4.6. The substrates were glass microscope cover slips functionalized with (3-acryloxypropyl)trimethoxysilane to promote adhesion. The prepolymer resin were spin coated on the substrate at 1500 rpm for 1 min to create a thin film. For ease of handling, the resin was prepolymerized with 365 nm light at an intensity of 10 mW/cm^2 for 10 sec. A mask was then placed in direct contact with the prepolymerized sample for photopatterning. After photopatterning, the sample was immersed for 10 minutes in a solution of 20% by volume of ethylene diamine in

water. The sample was then rinsed with water three times for 5 minutes each. The details of the experiments are as follows.

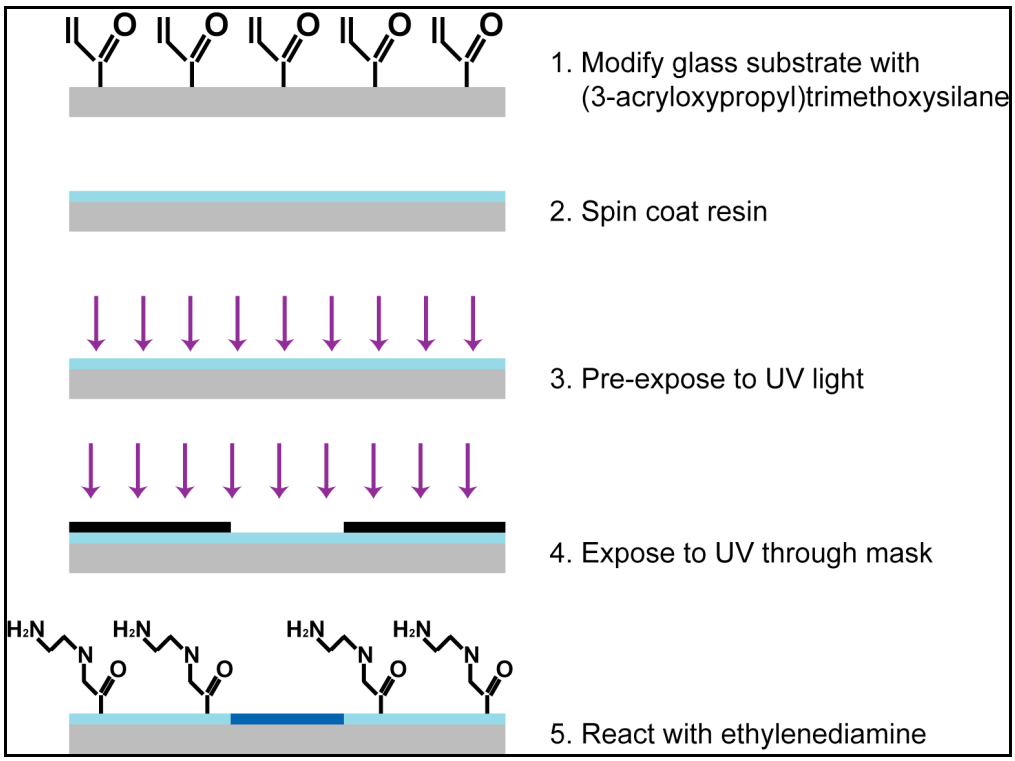

Figure 4.6 Strategy for binary and gray-scale patterning of amines on the surface of acrylic polymer films. The dark blue regions of the polymer film represent areas that have received higher UV exposure.

Functionalization of cover slips: To promote adhesion of the final film, the cover slips were modified prior to spin coating. First, the glass cover slips were cleaned in an oxygen plasma cleaner for 2 min at 200 millitorr. They were then immersed in a solution containing 2% of (3-acryloxypropyl)trimethoxysilane, 5% of water and 93% of ethanol (by volume) for 24 hours. Finally, the cover slips were rinsed with ethanol for 1 hour followed by baking at 100 ˚C for 1 hour.

Sample preparation: The acrylic resin was composed of 54 wt % dipentaerythritol pentaacrylate (Sartomer), 43 wt % tris (2-hydroxy ethyl) isocyanurate triacrylate (Sartomer), and 3 wt % Lucirin TPO-L (BASF). 5 grams of resin was mixed in a test tube and agitated for 12 hours. Several drops of the resin were put on a modified glass cover slip. The resin was then spread by spinning at 1500 rpm for 1 min followed by prepolymerization for 10 sec with a Hamamatsu Lightningcure 200 UV spot light source producing radiation at 365 nm. The purpose of the prepolymerization was to rigidify the resin enough to make it easy to work with during photopatterning.

Photopatterning: Photolithographic patterning can be accomplished with either a contact mask or a projection mask. We have employed both commercial, reflective contact masks and absorptive contact masks created on laser printer transparencies. The light source was a Hamamatsu Lightningcure 200 UV spot light source producing radiation at 365 nm. The light source was placed 10 cm away from the mask, giving an intensity of 10 mW/cm^2. For binary patterning a positive USAF 1951 high resolution target (Edmund Scientific A58-198) was used as the mask, and the exposure time was 1 min. For gray-scale patterning, a color digital image (Figure 4.7a) was converted to gray-scale (Figure 4.7b) and then printed out in negative (Figure 4.7c) on a transparency using a high-definition laser printer. The exposure time for the gray-scale mask was 45 sec.

Figure 4.7 Washington Monument scene used for gray-scale patterning. The original color image is shown in (a), the gray-scale version is shown in (b), and the negative mask used for patterning is shown in (c).

Amine visualization: After photopatterning, the sample was immersed for 10 minutes in a solution of 20% by volume of ethylene diamine in water. The sample was then rinsed with water three times for 5 minutes each. The aminated sample was immersed in the dansyl chloride solution for 2 minutes followed by rinsing twice with methanol.

Sample imaging: Samples were imaged on an upright microscope at a magnification of 8x while under UV illumination. The fluorescent pattern was recorded using a digital camera through eyepiece of the microscope. A filter was used to eliminate the UV light at the camera.

4.3.3 Results and discussions

Shown in Figure 4.8 (a) is a fluorescent image of a binary pattern created with a reflective Air Force test pattern mask. The contrast between bright and dark regions in the pattern is greater than 100. The finest features in the pattern that are well

resolved have a width of 10 μm, demonstrating the high resolution attainable. Shown in Figure 4.8 (b) is a gray-scale image of Testudo created using a laser-printed, absorptive mask. Mask regions of different optical density are well resolved in the image, as are fine features. In Figure 4.8 (c) we show a pattern created with a reflective, gray-scale test mask in which consecutive panels have increasing transmission. The large variation in intensity going across the image demonstrates the dynamic range of this technique, which exceeds 20 dB.

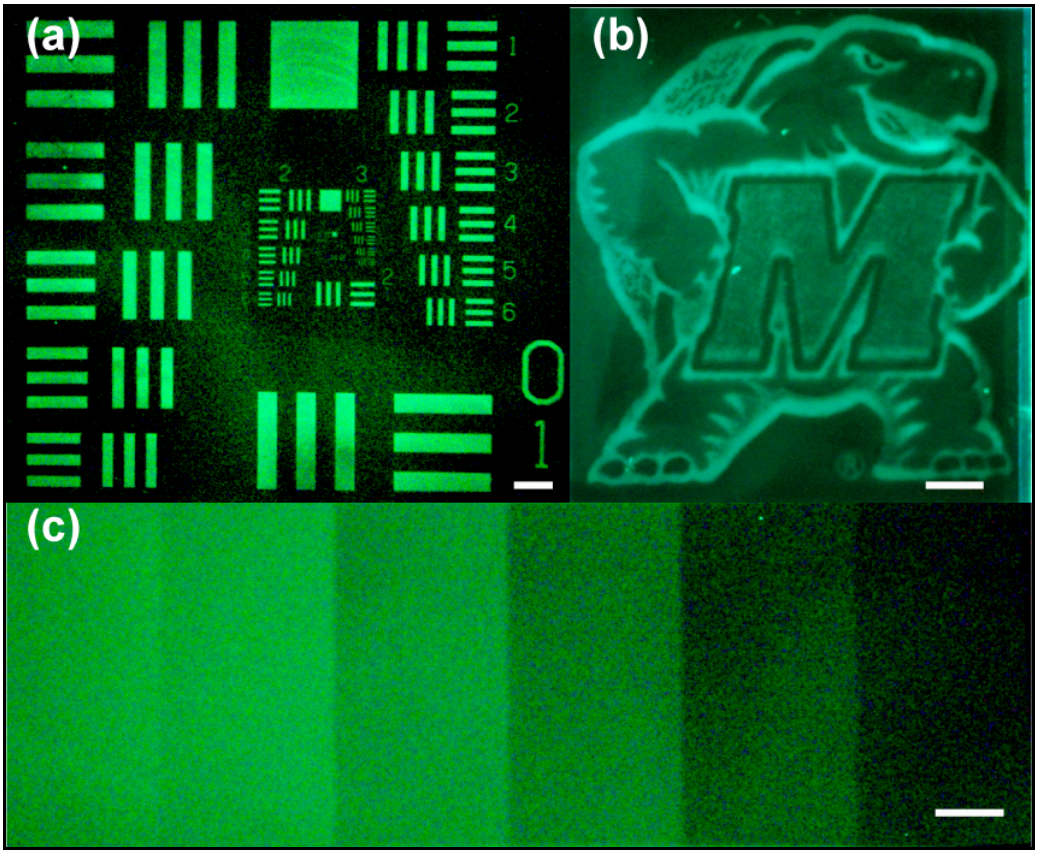

Figure 4.8 Representative fluorescent images of photolithographically patterned polymer surfaces. (a) Dansyl chloride patterned with a binary Air Force test mask.

(b) Dansyl chloride patterned with a gray-scale image mask. (c) Dansyl chloride patterned with a gray-scale mask. All scale bars are 1 mm.

Fluorescence spectroscopy was used to estimate the dynamic range of our patterning technique using samples that had been reacted with dansyl chloride. We should note that this technique likely underestimates the total dynamic range, as quenching can occur at high densities of bound fluorophores. To prepare the fluorescent samples, films were prepared that were polymerized for 10 sec, 30 sec, 270 sec, 810 sec and 2430 sec. The films were all treated with 20% ethylene diamine in water for 10 min and then with dansyl chloride for 2 min. The films were mounted on the sample holder of the fluorimeter using tape. The sample was mounted at an angle of 45° to the excitation beam path. An excitation wavelength of 365 nm was used. The emission was collected through a 1.2 mm slit at wavelengths ranging from 400 nm to 650 nm at 2 nm increments with an integration time of 0.2 sec. The excited area was about 5 mm × 1.2 mm. The results of the fluorescence measurements are shown in Figure 4.9. The red line is the background level of counts for a control polymer sample that was not treated with either ethylene diamine or dansyl chloride. The circles are fluorescence intensity data for samples with different exposure times. Based on these data, the dynamic range of our technique is greater than 100 (20 dB).

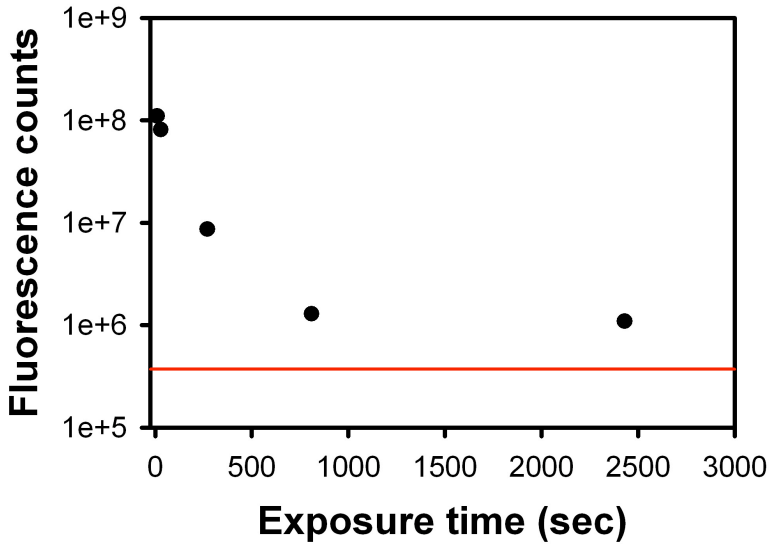

Figure 4.9 Integrated fluorescence counts as a function of UV exposure for dansyl-functionalized polymer films (black circles) and counts from an unfunctionalized film (red).

We have also performed an X-ray photoelectron spectroscopy (XPS) study on the surface containing different densities of amines. The data were collected on a Kratos AXIS 165 operating in the hybrid mode using non-monochomatized Al Kα radiation (1486.6 eV). Charge neutralization was required to compensate for sample charging and the UHV chamber was operated at a pressure of 1 x 10^{-6} Pa or lower. Survey spectra and high resolution spectra were collected with energies of 80 eV and 20 eV, respectively. Peak fitting was performed using CASA XPS, using peaks with a 50%/50% Gaussian/Lorentzian line-shape after removal of a Shirley background. All peaks were calibrated with reference to the hydrocarbon peak at 285.0 eV. XPS studies on unpatterned surfaces revealed a maximum surface density of about one primary amine per 2 to 3 nm^2. The details of the calculation of surface amine density are as follows.

Based on the formula weight and density of SR-399 and SR-368, the molecular volumes of these compounds are 0.731 nm^3 and 0.540 nm^3, respectively. If we treat the molecules as being cubic in shape, then the corresponding surface area for one face of the cube for SR-399 is 0.812 nm^2 and for SR-368 is 0.663 nm^2. We assume that the two monomers have equal surface activity, which means that there is one molecule of SR-368 per 0.812 nm^2 + 0.663 nm^2 = 1.48 nm^2 in the cured polymer. Each molecule of SR-368 has 3 nitrogen atoms, leading to a surface density of 2 nitrogen atoms/nm^2. We use this number as our internal standard.

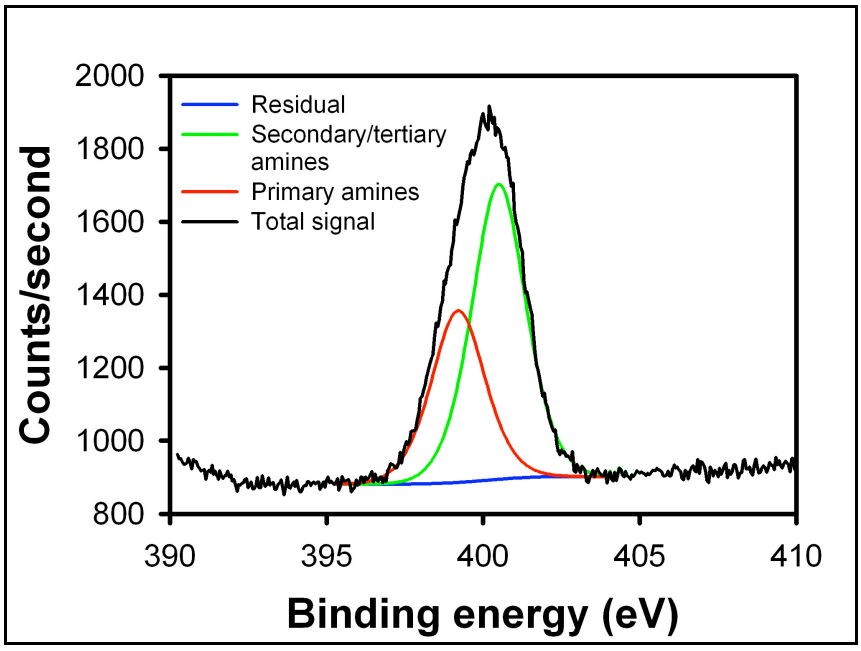

Figure 4.10 Nitrogen XPS data for an amine-functionalized polymer film. The black line is the XPS data and the red and green curves are fits to the peaks for primary amines and secondary/tertiary amines, respectively. The blue line is the residual.

XPS data for a sample with a 10 sec exposure time are shown in Figure 4.10. It is important to note that XPS may probe to a depth of as much as 10 nm in a polymer film. As ethylene diamine is a small molecule, some of it may penetrate into the polymer before reaction, leaving inaccessible primary amines. To test whether such inaccessible amines exist, we created samples in which the surfaces were in contact with a cover slip during curing. This procedure prevents oxygen from quenching polymerization at the surface of the sample. Samples that have been prepared in this manner that are then treated with ethylene diamine followed by dansyl chloride do not exhibit any fluorescence, indicating the lack of any significant density of surface amines. However, XPS measurements did indicate the presence of primary amines in such samples, confirming the presence of a subsurface concentration of ethylene diamine. Absolute quantification of these subsurface amines is difficult, so we estimated their contribution to the XPS signal in two different ways. In the first method, we subtracted the concentration of primary amines measured in a sample prepared with a cover slip from the total primary amines in a sample prepared without a cover slip with the same exposure time. The degree of polymerization in the sample prepared with a cover slip is greater than in the sample prepared without a cover slip, and therefore the amount of diffusion of ethylene diamine into the former sample is an underestimate of the total subsurface concentration in the latter sample. Using this estimate, we find that there are 0.96 ethylene diamine nitrogen atoms per ring nitrogen atom at the surface. In the second method, we assumed that for samples treated with ethylene diamine after long exposure times, all primary amines detected are below the polymer surface. This

concentration of amines was subtracted from the XPS data at all different exposure times to estimate the surface density of primary amines. Using this method, we find that there are 0.61 ethylene diamine nitrogen atoms per ring nitrogen atom at the surface.

If each molecule of ethylene diamine reacts with one acrylate, then it will contain one primary amine and one secondary amine. Thus, half of the intensity of the ethylene diamine nitrogen peak arises from primary amines. The density of primary amines is approximately 0.5 per nm^2 based on the first method of estimation and 0.3 per nm^2 based on the second method.

4.4 Biocompatibility

To assess the biocompatibility of the amine-functionalized polymer, we used the ameboid *Dictyostelium discoideum,* a model cell line used for the study of cellular motility.[16] *D. discoideum* cells do not feature integrins, which require specific surface chemistry and mechanics to generate strong focal adhesion complexes. Instead, cells propel themselves over surfaces via weaker, non-specific interactions between cell and surface.

Figure 4.11 (a) shows *D. discoideum* migrating and aggregating on gray-scale, amine-functionalized surfaces that were patterned with the mask used in Figure 4.8 (c). Patterned polymer films with a UV exposure time of 1 minute were prepared for use with *D. discoideum* cells. The films were prepared, patterned and functionalized with amines as previously described. The film was baked for 10 min at 100 °C after

the final water rinse to remove any remaining liquid. To maintain consistency with previously used experimental protocols, the films were baked again under the same conditions immediately following removal of the patterning mask. Since the cells migrate within a buffer solution, each film was adhered to a plastic compartment such that its attached coverslip formed the bottom of a 2 cm wide square open chamber. Ax3 cells were grown in HL-5 medium (In one liter of water: 20g Maltose, 10g Bacto Proteose Peptone, 5g Bacto Yeast Extract, 0.965 g $Na_2HPO_4 \cdot 7H_2O$, 0.485g KH_2PO_4, 0.03g streptomycin) at 21.5 °C on first a Petri dish and then in shake suspension (200 rpm). Log-phase cells were harvested through centrifugation, washed in DB (5 mM KH_2PO_4, 5 mM $Na_2HPO_4 \cdot 7H_2O$, 2 mM $MgSO_4$, 0.2 mM $CaCl_2$), and then resuspended in DB at a concentration of 20 x 106 cells per mL. The cells were then pulsed with 20 nM cAMP every six minutes for 4.5 hours while being shaken at 150 rpm. After pulsing, the cells were washed in PB (5 mM KH_2PO_4, 5 mM $Na_2HPO_4 \cdot 7H_2O$), resuspended in PB at a concentration of 1.0 x 106 cells per mL, and then pipetted in 5 μL drops onto the polymer film. To prevent evaporation of the buffer, after 5 minutes, 1.5 mL of PB was added to the sample chamber. The migrating cells were imaged on an inverted microscope with a 10× objective using a μeye camera.

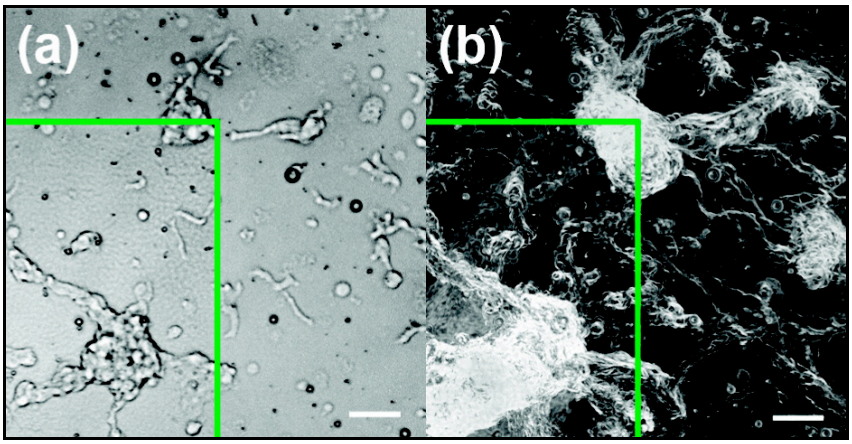

Figure 4.11 *Dictyostelium discoideum* cells aggregating on gray-scale, amine-functionalized patterned surfaces. The area bounded by green lines on the bottom left has a higher density of surface amines. (a) Snapshot of cells midway through aggregation. Both individual cells and cell aggregates are visible (10×); (b) Time averaged image illustrates that cell tracks (lines) do not change significantly with the density of surface amines (10×). Scale bars are 50 μm

The cell speeds on amine-functionalized and native polymer surfaces are similar to those measured on glass. The cell migration and aggregation patterns are independent of surface amine density, and are unaffected by boundaries between regions of different amine density (Figure 4.11b). As *D. discoideum* is a commonly used model cell line, our technique creates patterned surfaces that are also likely to be compatible with many cell types.

Since amine patterned surfaces themselves appear not to affect cell function, surface functionalization with biomolecules holds promise for generation of targeted interactions with cells. To demonstrate the capability for patterning biomolecules with our technique, we have synthesized peptides on amine-functionalized surfaces. Tripeptides composed of asparagine are known to bind Rhodamine B selectively from

aqueous solutions.[17] We synthesized acetyl-capped, NNN tripeptides with trityl-protected side chain amines using a protocol described previously.[18] Samples were then immersed in a dilute, aqueous solution of Rhodamine B for 60 hours with agitation. The samples were washed with water and dried before performing fluorescence imaging. As can be seen in Figure 4.12a, binary patterning of these peptides can be performed with resolution comparable to that achieved in the dansyl chloride experiments. The gray-scale Washington Monument pattern shown in Figure 4.12b was fabricated with mask shown in Figure 4.7c. The gray-scale Testudo in Figure 4.12c is also of comparable quality to the results obtained with dansyl chloride (Figure 4.8b). As a control experiment, the amines on patterned substrates were capped with acetyl groups and exposed to the Rhodamine B solution. No fluorescent patterns were present on these samples.

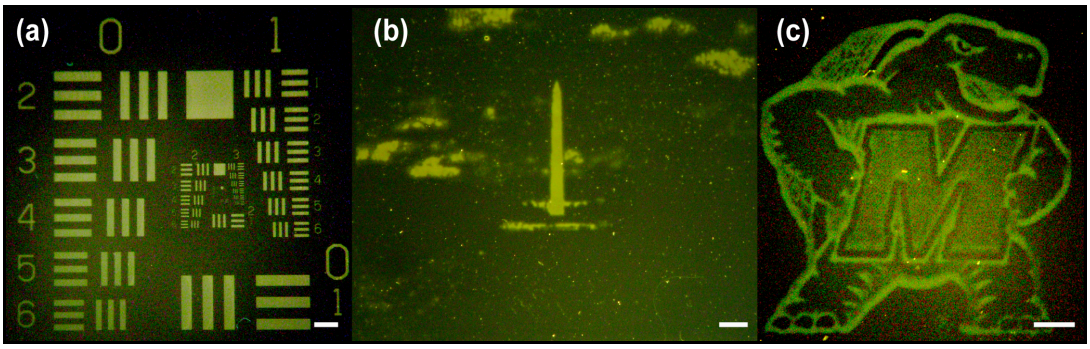

Figure 4.12 (a) Rhodamine B bound to a tripeptide synthesized on a binary Air Force test mask pattern; (b) (c) Rhodamine B bound to a tripeptide synthesized on a gray-scale image. The scale bars are 1 mm in all images.

4.5 Conclusion

The method presented here can be extended readily to the patterning of a large variety of materials beyond peptides and fluorophores, including metals, oxides, nucleic acids, antibodies, and small molecules. By using more complex amine-containing molecules, it will also be possible to pattern different types of initial chemical functionality on the polymer surfaces.

References:

(1) Muh, E.; Marquardt, J.; Klee, J. E.; Frey, H.; Mulhaupt, R., Bismethacrylate-based hybrid monomers via Michael-addition reactions. *Macromolecules* **2001,** *34* (17), 5778-5785.

(2) Muh, E.; Weickmann, H.; Klee, J. E.; Frey, H.; Mulhaupt, R., Acrylate-terminated macromonomers by Michael addition. *Macromolecular Chemistry and Physics* **2001,** *202* (18), 3484-3489.

(3) Farrer, R. A.; LaFratta, C. N.; Li, L. J.; Praino, J.; Naughton, M. J.; Saleh, B. E. A.; Teich, M. C.; Fourkas, J. T., Selective functionalization of 3-D polymer microstructures. *Journal of the American Chemical Society* **2006,** *128* (6), 1796-1797.

(4) Charbonnier, M.; Alami, M.; Romand, M., Electroless plating of polymers: XPS study of the initiation mechanisms. *Journal of Applied Electrochemistry* **1998,** *28* (4), 449-453.

(5) Charbonnier, M.; Romand, M.; Harry, E.; Alami, M., Surface plasma functionalization of polycarbonate: Application to electroless nickel and copper plating. *Journal of Applied Electrochemistry* **2001,** *31* (1), 57-63.

(6) Farrer, R. A.; Copeland, G. T.; Previte, M. J. R.; Okamoto, M. M.; Miller, S. J.; Fourkas, J. T., Production, analysis, and application of spatially resolved shells in solid-phase polymer spheres. *Journal of the American Chemical Society* **2002,** *124* (9), 1994-2003.

(7) Lafratta, C. N., Multiphoton Absorption Polymerization: Issues and Solutions. *Dissertation of Doctor of Phylosophy* **2006**.

(8) Efimenko, K.; Genzer, J., How to prepare tunable planar molecular chemical gradients. *Advanced Materials* **2001,** *13* (20), 1560-1563.

(9) Genzer, J., Templating surfaces with gradient assemblies. *Journal of Adhesion* **2005,** *81* (3-4), 417-435.

(10) Liu, H.; Xu, J.; Li, Y.; Li, B.; Ma, J.; Zhang, X., Fabrication and characterization of an organic-inorganic gradient surface made by polymethylsilsesquioxane (PMSQ). *Macromolecular Rapid Communications* **2006,** *27* (18), 1603-1607.

(11) Ruardy, T. G.; Schakenraad, J. M.; vanderMei, H. C.; Busscher, H. J., Preparation and characterization of chemical gradient surfaces and their application for the study of cellular interaction phenomena. *Surface Science Reports* **1997,** *29* (1), 3-30.

(12) Kim, M. S.; Seo, K. S.; Khang, G.; Lee, H. B., First preparation of biotinylated gradient polyethylene surface to bind photoactive caged streptavidin. *Langmuir* **2005,** *21* (9), 4066-4070.

(13) Chaudhury, M. K.; Whitesides, G. M., How to Make Water Run Uphill. *Science* **1992,** *256* (5063), 1539-1541.

(14) Kraus, T.; Stutz, R.; Balmer, T. E.; Schmid, H.; Malaquin, L.; Spencer, N. D.; Wolf, H., Printing chemical gradients. *Langmuir* **2005,** *21* (17), 7796-7804.

(15) Buxboim, A.; Bar-Dagan, M.; Frydman, V.; Zbaida, D.; Morpurgo, M.; Bar-Ziv, R., A single-step photolithographic interface for cell-free gene expression and active biochips. *Small* **2007,** *3* (3), 500-510.

(16) Parent, C. A.; Devreotes, P. N., A cell's sense of direction. *Science* **1999,** *284* (5415), 765-770.

(17) Wennemers, H.; Still, W. C., Peptide Complexation in Water. Sequence-Selective Binding with Simple Dye Molecules. *Tetrahedron Letters* **1994,** *35* (35), 6413-6416.

(18) Farrer, R. A.; Copeland, G. T.; Previte, M. J. R.; Okamoto, M. M.; Miller, S. J.; Fourkas, J. T., Production, Analysis, and Application of Spatially Resolved Shells in Solid-Phase Polymer Spheres. *Journal of the American Chemical Society* **2002,** *124* (9), 1994-2003.

Chapter 5: Multiphoton Absorption Induced Luminescence

5.1 Introduction

Photoinduced luminescence from metal nanostructures is attracting increasing attention for use in biomedical imaging because these nanostructures are readily synthesized with controlled diameters, relatively inert, and easily attached to biomolecules. Farrer and coworkers have demonstrated that multiphoton absorption induced luminescence (MAIL) from gold nanoparticles (AuNPs) can be generated efficiently at laser intensities lower than those typically used for two-photon imaging of living cells.[1] In MAIL, absorption of multiple photons from a near-infrared ultrafast laser can lead to efficient luminescence of a noble-metal nanostructure. This chapter will focus on the applications of MAIL, and will also briefly discuss the mechanism of MAIL.

5.1.1 Photoluminescence from metal

Visible single photon photoluminescence from metals was first reported in 1969.[2] The phenomena has been described as a three-step process as follows: (*i*) excitation of electrons from the occupied *d*-band to the *sp*-band to generate electron–hole pairs, (*ii*) electrons and holes move close to the Fermi level due to the

intraband scattering on the picosecond timescale, and (*iii*) electron–hole recombination resulting in photon emission.

Multiphoton luminescence from noble-metal surfaces was first reported in 1986.[3] Flat metal surfaces were found to be only weakly luminescent. However, significant enhancement of MAIL was observed on roughened surfaces.[3] More recently, MAIL has been observed from nanoparticles,[1, 4-6] nanorods[7-9] and other nanostructures[10-14] composed of noble metals. In the case of gold, MAIL has been observed to be a two-photon process for 800 nm excitation in most studies.[4, 7, 13, 14] However, some gold nanoparticles have been found to have extremely large MAIL signals, and in this case MAIL is a three-photon process with 800 nm excitation.[1] We have proposed that the efficient luminescence following three-photon excitation at 800 nm arises from nanoparticles that have asymmetric shapes. We believe this geometric asymmetry leads to particularly large electric field enhancements.[6]

5.1.2 MAIL in biomedical application

Several groups have demonstrated that MAIL is a useful tool for biomedical applications. Durr *et al*. have shown that luminescence from gold nanorods can be orders of magnitude brighter than autofluorescence from cancer cells.[7] Wang *et al*. were able to image gold nanorods within cancer cells in vitro and flowing in a mouse ear blood vessel *in vivo* using MAIL.[15] MAIL has been used to perform three-dimensional imaging of gold nanoshells within mouse tumor tissue.[16] Qu *et al*. employed MAIL to image AuNPs targeted to lymphoma cells.[17] In addition, Nagesha *et al*. have used MAIL to visualize AuNPs in *Dictyostelium discoideum* cells

and murine embryonic stem cells.[18]

We have demonstrated that MAIL can be used to monitor the targeting and endocytosis of AuNPs to human umbilical vein endothelial cells (HUVECs).[§] Gold nanoparticles are attractive for targeting applications because they are highly stable and biocompatible, have well-established surface chemistry, and can exhibit strong MAIL signals. We used MAIL to demonstrate that AuNPs functionalized with monocyclized RGDfK (which has a high degree of specificity for the $\alpha_v\beta_3$ integrin, a membrane protein that is over-expressed in the activated endothelium during angiogenesis,) can be targeted to, and endocytosed by, HUVECs. Following uptake, the AuNPs aggregate within endosomal and lysosomal vescicles. Our results suggest that AuNP uptake involves a specific binding event and that a receptor-mediated mechanism is the major pathway for endocytosis of the particles. This chapter will focus on the MAIL imaging part of this work.

5.1.3 Field-enhanced phenomena of MAIL

Compared with the signal generated by single-photon excitation, the photoluminescence produced upon multiphoton excitation can increase dramatically due to the field enhancement effects.[4] Although some theoretical explanations have been developed to model the field enhancement phenomena from nanostructures,[19, 20] well-designed experiments are still necessary to gain a deeper understanding of this process. An important experimental tool for understanding field enhancement is the

§ This project is based on collaboration with Prof. Philip DeShong's lab and Prof. Anjan Nan's lab. MAIL imaging was performed in our lab.

correlation of different field-enhanced phenomena with one another and with nanostructure geometry. We apply such an approach to two phenomena involving field enhancement, multiphoton-absorption-induced luminescence (MAIL) and metal-enhanced multiphoton absorption polymerization (MEMAP).[21]

5.2 MAIL apparatus

5.2.1 Experimental setup

Figure 5.1 shows the MAIL experimental setup. A tunable Ti:sapphire laser (Coherent Mira 900-F) produced pulses of 150 fs duration at a repetition rate of 76 MHz. The beam was introduced into an inverted microscope (Zeiss Axiovert 100) through the reflected light-source port and was directed to the objective by a dichroic mirror. A 1.45 NA, 100x, oil-immersion objective (Zeiss α Plan-FLUAR) was used for MAIL imaging and multiphoton fabrication. Scanning was performed with either a piezoelectric sample stage or with a set of galvanometric mirrors. The luminescence signal was collected by the same objective and sent to a polarizing beam cube. Signal with separated polarizations was then collected by a single-photon-counting avalanche photodiode (EG&G) and was transferred to a computer using a data acquisition board (National Instruments). Data collection and image construction were performed with software written in LabView (National Instruments). The user interface is shown in Figure 5.2.

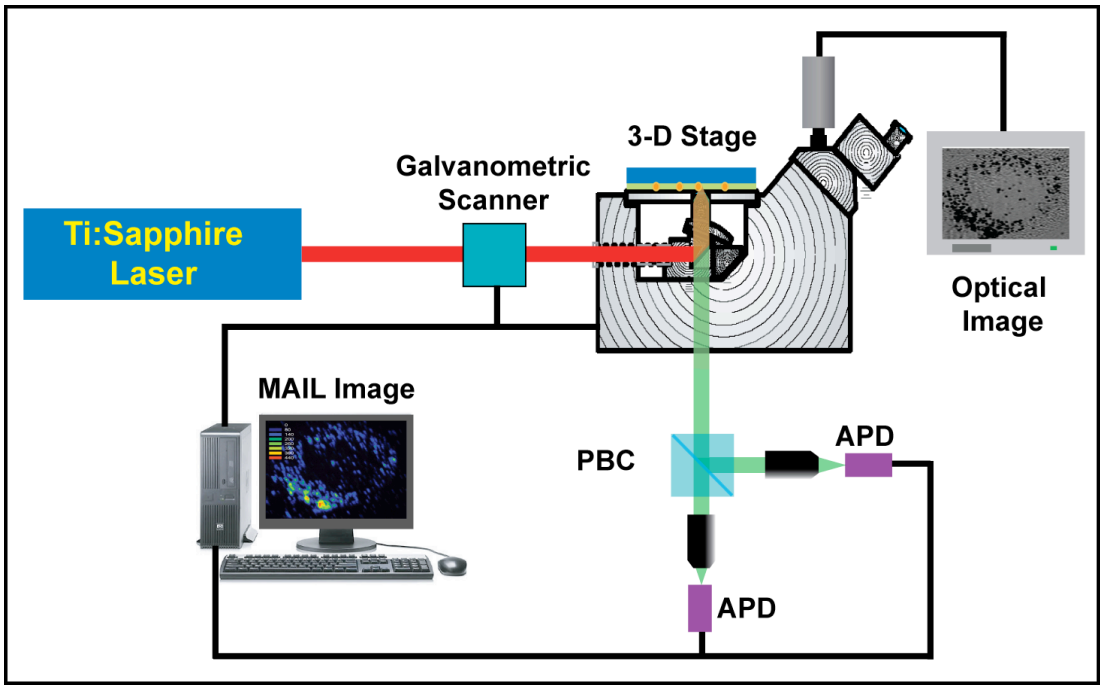

Figure 5.1 MAIL experimental setup. PBC = polarizing beam cube; QWP = quarter-wave plate; APD = avalanche photodiode.

5.2.2 Software

The software controls several components in the setup, including the scanning mirrors set, the motorized Ludl stage and the piezoelectric nanostage. A data acquisition board is used to collect MAIL signal and the data are displayed on the front panel of LabView program (green area in Figure 5.2). One can select which polarization of the signal to display by switching between tabs "count0" and "count1". The integration of the signal along a certain scanning plane can be shown if the tab "Int Ramp" or "Int DC" is selected. The grid in the display is helpful for stage or scanning mirror positioning. Final images are saved in both bitmap format and numeric data format allowing for reconstruction of images in other programs.

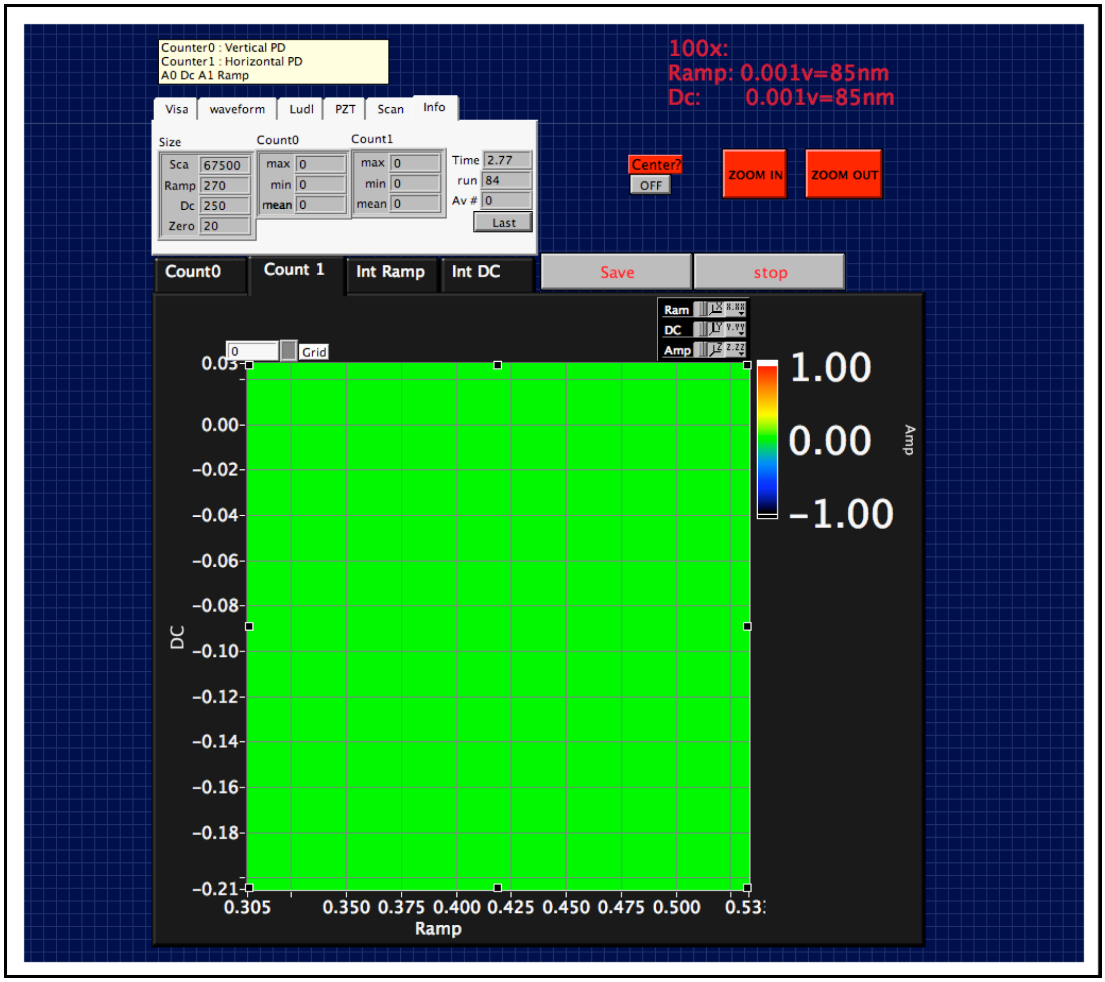

Figure 5.2 Front panel of the software of MAIL (written with LabView software).

Each of the five tabs near the top left corner of the panel (i.e. Visa, waveform, Ludl, etc.) has a corresponding display. For example, the "Visa" tab is used to display the instrument address panel, where the GPIB addresses of the stages are identified (Figure 5.3 (a)). In the "Waveform" panel, the scan rate and the number of scanning points are defined (Figure 5.3 (b)). The range of number of points per volt ranges from 250 to 30,000. This number determines the resolution of the final image. The scan range and center position are also controlled in this panel. The

inputs for these controls are in volts, and these inputs specify the voltages applied to the scanning mirrors. Based on a calibration by the piezostage, applying 1 mV to the mirror is equivalent to moving the stage by ~85 nm if using a 100x, 1.45 NA objective.

The two different stage control panels can be selected using the "Ludl" or "PZT" tabs (Figure 5.3 (c) and (d)). The Ludl stage can be moved either absolutely ("Abs Move") or relatively ("Rel Move"), while the piezoelectric nanostage can only be translated absolutely. The current positions of both stages are updated in real time.

The program can be used to specify a scan in the axial direction using the scanning mirrors and the piezoelectric stage. In Figure 5.3 (e), the left column is the control for XYZ scans, in which the scanning mirror set scans in an XY plane at a certain Z height and performs another XY scan at a different Z, moved by piezoelectric stage. This function enables the slicing scans to be performed for 3-D image buildup. The right column is the command for scanning in the XZ plane. The range and the number of segments of scanning in Z dimension can be identified in this tab. The last panel records the information of each scan. The images can be saved after averaging multiple times by pressing the "Last" button (Figure 5.3 (f)).

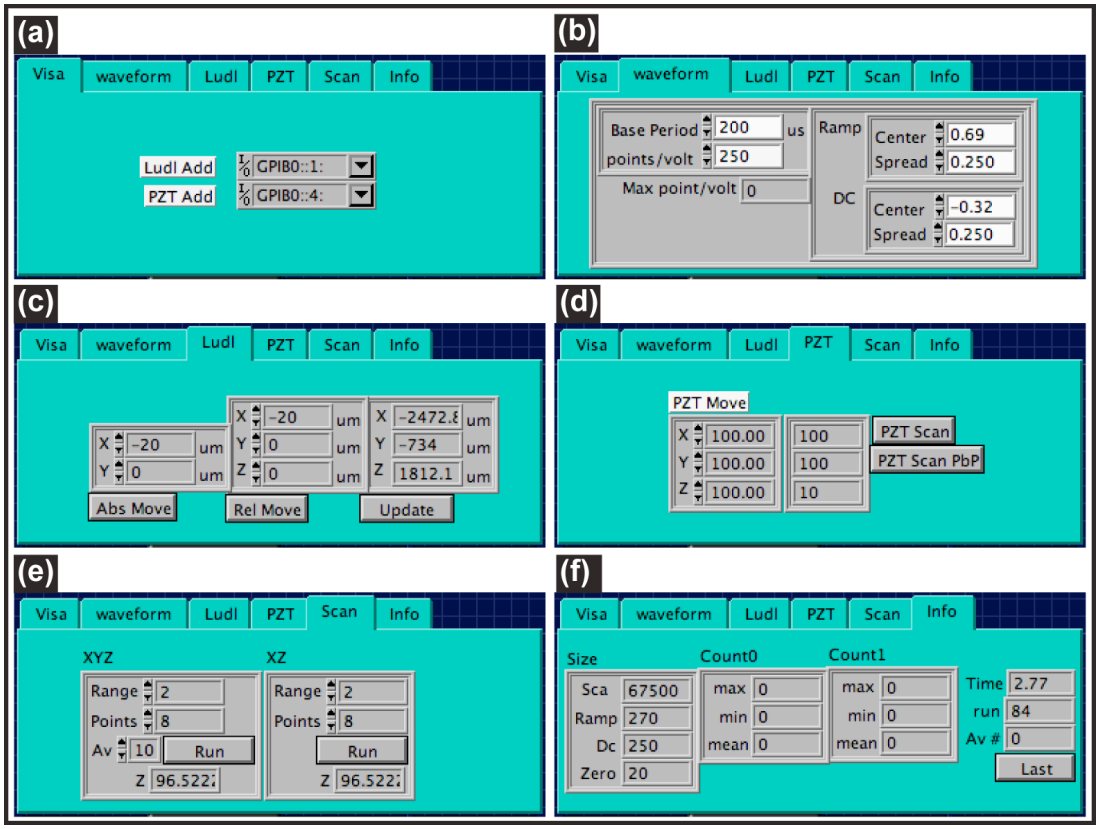

Figure 5.3 Individual functions of the MAIL software. (a) Instrument address panel; (b) Scanning control panel; (c) Ludl stage control panel; (d) Piezoelectric stage control panel; (e) Z-scan and 3-D slicing scan panel; (f) Information panel.

There are several other functions on the front panel. When the "center" function is selected (Figure 5.2), left clicking a certain point in the scanning area centers the image on that point. The "Zoom in" and "Zoom out" controls represent two preset scanning ranges that permit relatively quick scanning area selection. The preset range can be changed.

5.3 MAIL applications

5.3.1 Imaging of tumor-targeted gold nanopaticles

4.5 nm and 16 nm gold nanoparticles (AuNPs) were surface-modified with monocyclic RGDfK, a cyclized peptide that specifically targets the $\alpha_v\beta_3$ integrin, a membrane protein that is highly overexpressed in activated endothelial cells during angiogenesis. To determine whether the cyclic RGD could enhance the uptake of the AuNPs into activated endothelium, HUVECs (human umbilical vein endothelial cells) were used as model system. We studied uptake of gold nanoparticles with different surface modification with the MAIL imaging technique. The incubation time of the HUVECs in the different AuNPs was varied. The synthesis of the AuNPs and the cyclic RGD peptide conjugates, the cell growth and incubation were conducted in collaborating labs.[§] The details can be found in the appendix materials. Here, I will discuss the MAIL imaging portion of the cell study.

For MAIL imaging, cells were plated at a density of ~5 × 10^4 cells/ml in 4-chamber tissue culture slides (BD Falcon); each chamber had been treated with 1 ml of fibrinogen (200 μg/ml) for 24 h at 4 °C prior to seeding the cells. After 24 h of culture, the medium in the chambers was replaced with fresh medium containing nanoparticles of 3 varieties, separately: (1) bare Au citrate NPs, (2) linear RGD conjugated AuNPs and (3) monocyclic RGD conjugated AuNPs. One chamber per slide was refilled with fresh media containing no nanoparticles to serve as a control. After incubation for a particular time interval (2 h, 6 h, or 24 h), the media was removed from the chambers and cells were fixed by treatment with

§ Synthesis of the AuNPs and the cyclic RGD peptide conjugates were conducted in Prof. Philip DeShong's lab. Cells growth and incubation were performed in Prof. Anjan Nah's lab.

paraformaldehyde (4 % v/v in PBS) for 10 min. The cells were then washed twice with 25 mM glycine in PBS to remove any unreacted paraformaldehyde. Before the MAIL imaging, the glass slide with cells was rinsed in DI water twice to remove the buffer.

First, MAIL imaging was performed on HUVECs incubated for 6 h and 24 h with 4.5 nm AuNPs and with 16 nm AuNPs. Figure 5.4 shows the MAIL images and corresponding transmission optical images at 6 h incubation with 4 nm AuNPs. The images for HUVECs incubated with the same AuNPs for 24 h are shown in Figure 5.5. The cells incubated with the AuNPs with cyclic RGD conjugates (Figure 5.4 (a) and Figure 5.5 (a)) exhibit a much larger luminescence signal than do those incubated with either AuNPs with linear RGD conjugates (Figure 5.4 (b) and Figure 5.5 (b)) or bare citrate AuNPs (Figure 5.4 (c) and Figure 5.5 (c)). The results indicate that cyclic RGD modified AuNPs are taken into cells more efficient than the linear RGD modified AuNPs and bare particles.

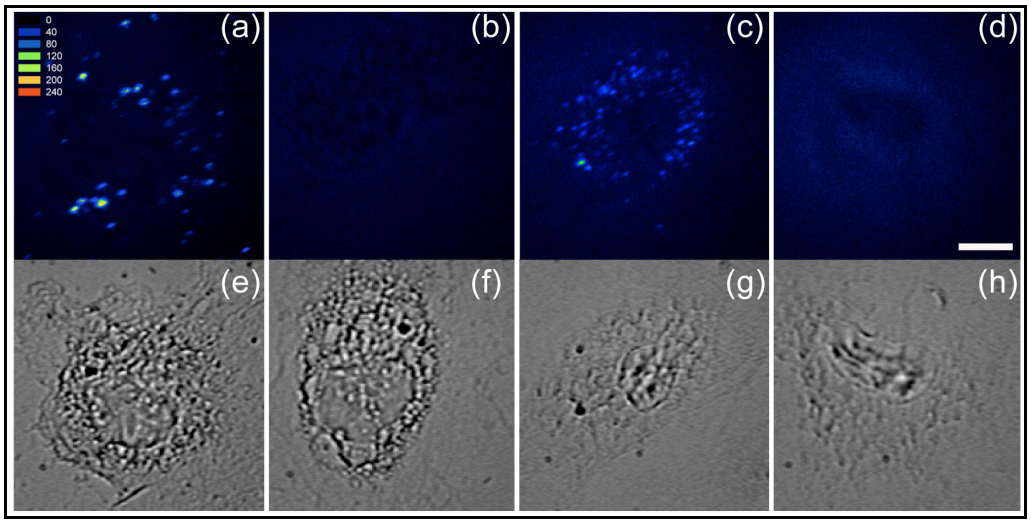

Figure 5.4 MAIL/Transmission (40x) images for 6 h uptake of targeted 4.5 nm AuNPs into HUVECs. (a) AuNPS with cyclic RGD conjugates; (b) AuNPs with linear RGD conjugates; (c) Bare 4 nm AuNPs; (d) Control: no AuNPs incubated with HUVECs; (e)-(h) correspond to the areas displayed in the MAIL images directly above in (a)-(d). The scale bar is 10 μm.

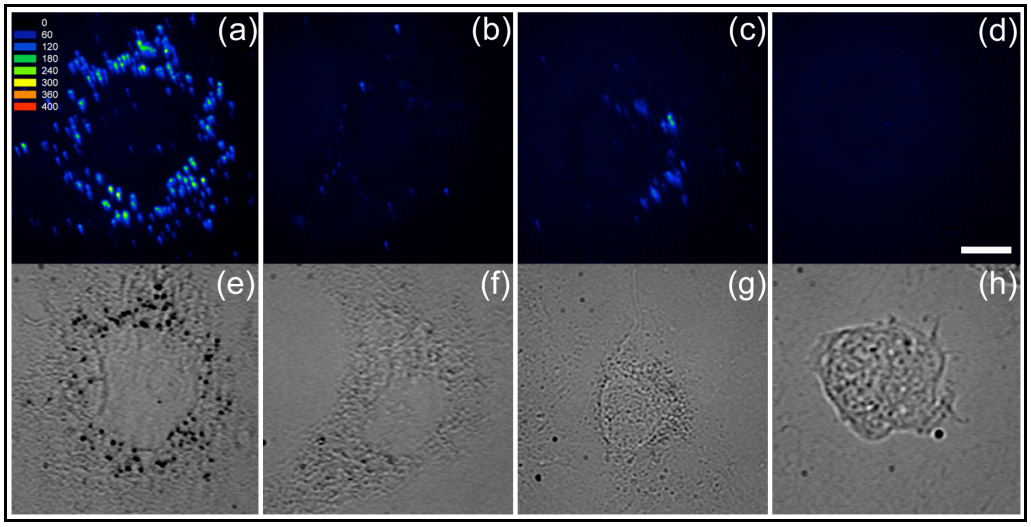

Figure 5.5 MAIL/Transmission (40x) images for 24 h uptake of targeted 4.5 nm AuNPs into HUVECs. (a) AuNPS with cyclic RGD conjugates; (b) AuNPs with linear RGD conjugates; (c) Bare 4 nm AuNPs; (d) Control: no AuNPs incubated with HUVECs; (e)-(h) correspond to the areas displayed in the MAIL images directly above in (a)-(d). The scale bar is 10 μm.

Figures 5.6 and 5.7 show images of HUVECs incubated with 16 nm AuNPs after 6 h and 24 h of incubation, respectively. Again, a considerably higher luminescence signal is observed in the samples containing the AuNPs with cyclic RGD conjugates (Figure 5.6 (a) and Figure 5.7 (a)), and uptake increases significantly over the 24 hour period. The MAIL signals for 16 nm AuNPs are stronger than those for 4.5 nm AuNPs. This effect could be intrinsic to the AuNPs, or could be due to a more effective exocytotic mechanism for smaller particles by the HUVECs. Note that the concentration of particles incubated with the HUVECs was 39 μg/ml, which was the upper limit value for the 72 h MTT assay.[§] Thus, a large number of the targeted AuNPs are getting into the cells, but they do not appear to harm the cells in any significant way.

[§] MTT assay is a laboratory test and a standard colorimetric assay (an assay which measures changes in color) for measuring the activity of enzymes.

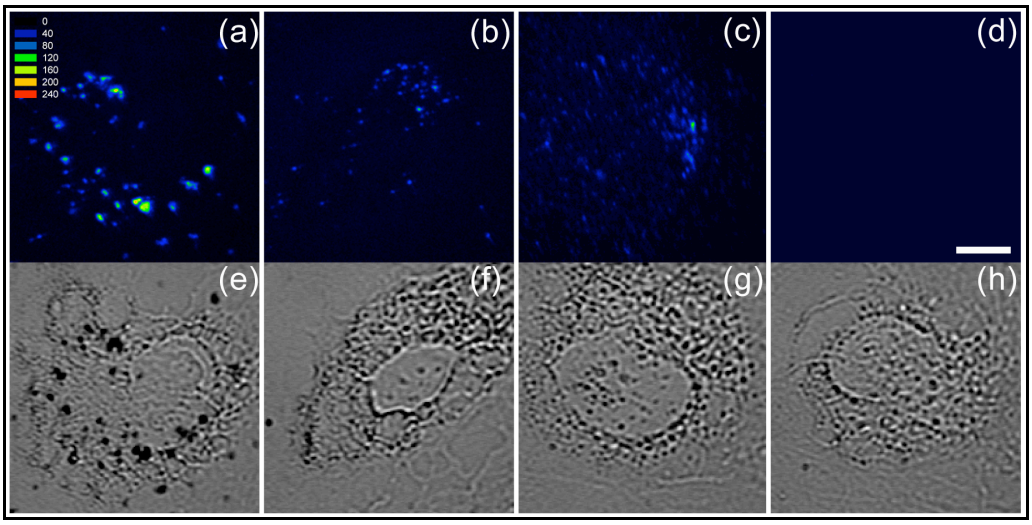

Figure 5.6 MAIL/Transmission (40x) images for 6 h uptake of targeted 16 nm AuNPs into HUVECs. (a) AuNPS with cyclic RGD conjugates; (b) AuNPs with linear RGD conjugates; (c) Bare 4 nm AuNPs; (d) Control: no AuNPs incubated with HUVECs; (e)-(h) correspond to the areas displayed in the MAIL images directly above in (a)-(d). The scale bar is 10 μm.

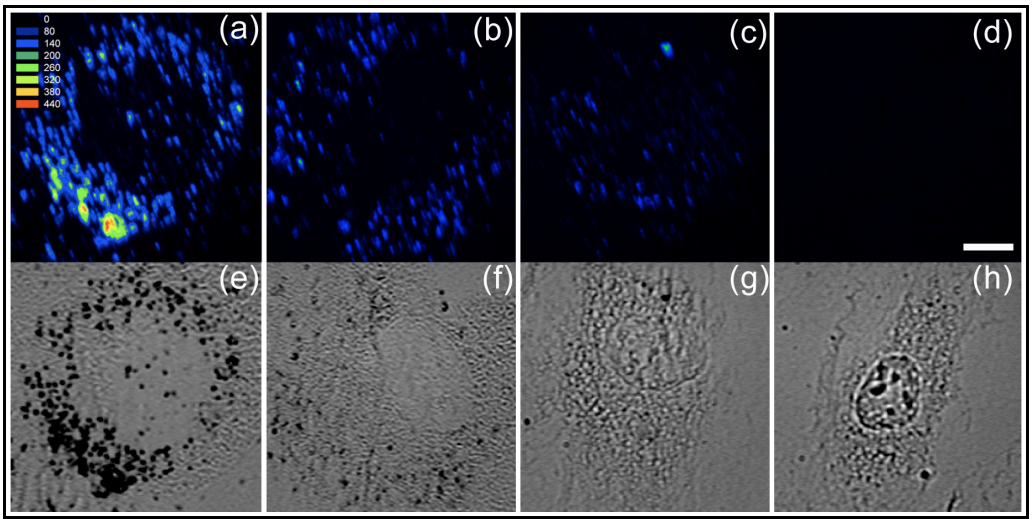

Figure 5.7 MAIL/Transmission (40x) images for 6 h uptake of targeted 16 nm AuNPs into HUVECs. (a) AuNPS with cyclic RGD conjugates; (b) AuNPs with linear RGD conjugates; (c) Bare 4 nm AuNPs; (d) Control: no AuNPs incubated with HUVECs; (e)-(h) correspond to the areas displayed in the MAIL images directly above in (a)-(d). The scale bar is 10 μm.

Figures 5.8 and 5.9 show HUVEC cells incubated with cyclic RGD-AuNPs for 24 h in the presence of different uptake-blocking agents for 4.5 nm and 16 nm AuNPs, respectively. The leftmost images are controls in which the HUVECs have not been treated with any blocking agent. Hence, the luminescence signals in Figure 5.8 (a) and 5.9 (a) are similar to those in Figure 5.4 (a) and 5.6 (a). In Figure 5.8 (b) and 5.9 (b), the cells have been treated with 0.1 wt% sodium azide for 10 min prior to addition of cyclic RGD-AuNPs. Uptake is inhibited significantly for both 4.5 nm and 16 nm AuNPs, although some small patches of luminescence are still observed for these samples. The cells in Figure 5.8 (c) and 5.9 (c) have been treated for 10 min with 3% BSA, which blocks all non-specific binding to the cells. For both samples, we see a smaller luminescence signal that is comparable to that of the untreated controls. This observation indicates that a large fraction of AuNPs is taken up into the cells via specific binding to a cell-surface receptor followed by receptor-mediated endocytosis.

Figure 5.8 (d) and 5.9 (d) demonstrate that treatment of the cells with 1 μM RGDfK to block αvβ3 integrins significantly decreases the luminescent signals relative to the untreated controls. This result implies that the majority of uptake must be through endocytosis via the αvβ3 integrin. The decrease in luminescence is not as dramatic as with the sodium azide treatment, which may be explained by the fact the over 24 h a significant number of new αvβ3 integrins will become available at the cell surface after all of the excess RGDfK has been washed away after the 10 min treatment period. We do observe a pronounced "ring" of luminescence around the edge of the cell in these images. This ring probably arises from a combination of

non-specific interactions with the cell surface and early interactions between targeted AuNPs and new surface-available αvβ3 integrins. In this scenario, the luminescence in Figure 5.8 (b) and 5.9 (b) is due to non-specific cell surface interactions and pinocytosis.

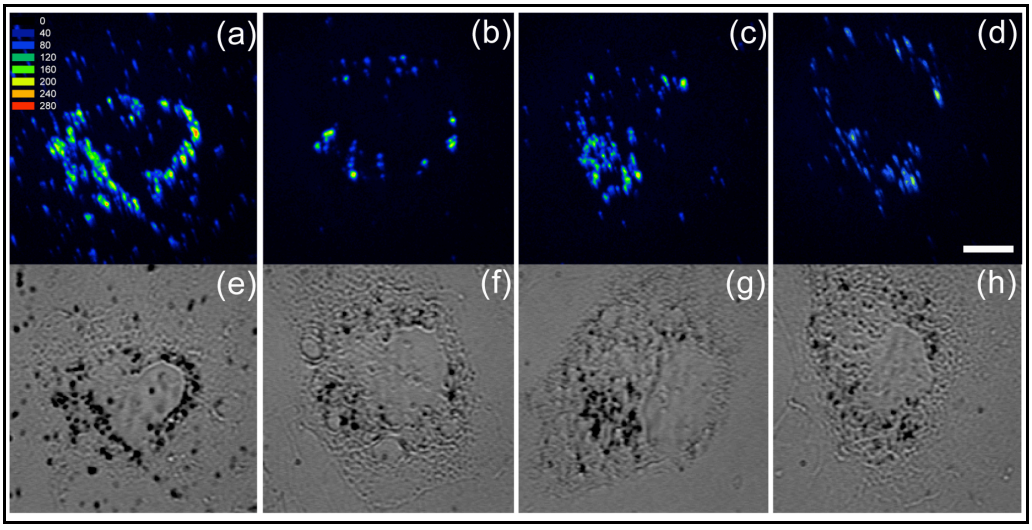

Figure 5.8 MAIL/Transmission (40x) images for 24 h uptake of targeted 4.5 nm AuNPs into HUVECs. (a) AuNPs with cyclic RGD conjugates (no treatment); (b) HUVECs treated with sodium azide; (c) HUVECs blocked with BSA; (d) HUVECs treated with free RGDfK; (e)-(f) correspond to the areas displayed in the MAIL images directly above in (a)-(d). The scale bar is 10 μm.

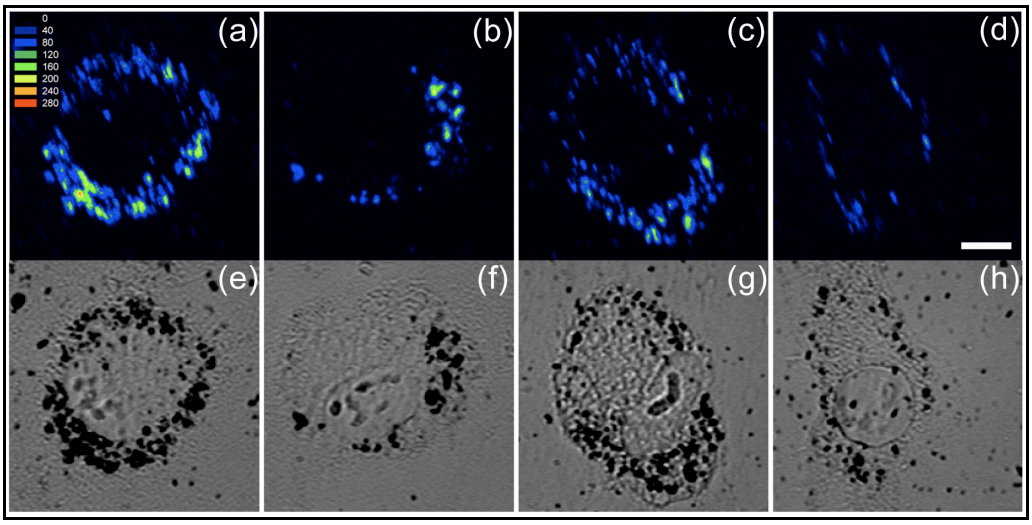

Figure 5.9 MAIL/Transmission (40x) images for 24 h uptake of targeted 16 nm AuNPs into HUVECs. (a) AuNPs with cyclic RGD conjugates (no treatment); (b) HUVECs treated with sodium azide; (c) HUVECs blocked with BSA; (d) HUVECs treated with free RGDfK; (e)-(f) correspond to the areas displayed in the MAIL images directly above in (a)-(d). The scale bar is 10 μm.

TEM studies show similar results to the MAIL studies. However, the MAIL technique uses a simpler instrument and has possibility of performing imaging in real time on live cells. In summary, by using MAIL, we have shown that AuNPs of two different diameters, 4.5 nm and 16 nm, can be targeted specifically to activated endothelial cells by covalent conjugation of monocylic RGDfK. This experiment demonstrated that MAIL is a powerful tool for studying targeting and determining uptake mechanisms of nanostructures. Given the capability of MAIL for rapid, three-dimensional imaging with high resolution, this technique shows great promise for applications in nanomedicine.

5.3.2 MAIL imaging of other structures

We have modified the surface of polystyrene (PS) microbeads with AuNPs.[§] These PS-AuNP microbeads were used to study cell mobility on the surfaces with different morphologies and different chemical treatments. We used MAIL as an easy tool to image the PS-AuNPs. Figure 5.10 shows the MAIL images of PS beads with AuNPs on the surface.

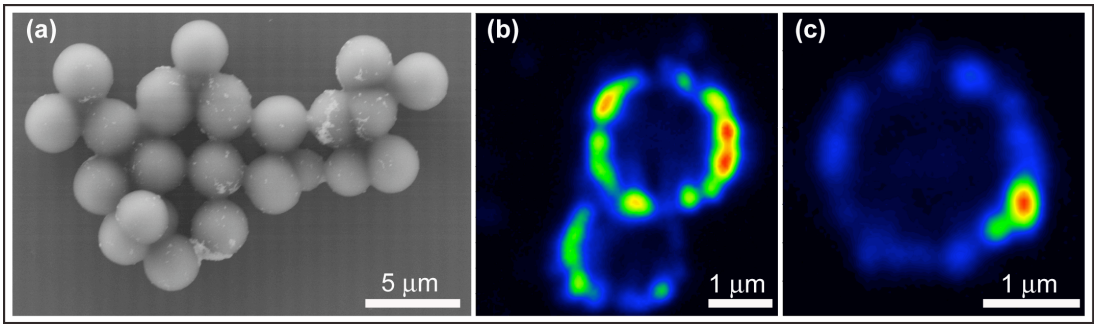

Figure 5.10 Images of polystyrene microbeads coated with AuNPs. (a) SEM image; (b) (c) MAIL images.

We have also used MAIL to study silica nanotubes modified with AuNPs at the entrance.[22**] The deposition of gold selectively on the nanotubes ensures the ability to fabricate nanostructures with multifunctionality. This capability is important for single- molecule sensing, bioseparations, and drug delivery.[22] Figure 5.11 shows images of silica nanotubes with AuNPs at the entrance.

[§] This work was done in collaboration with Prof. Wolfgang Losert's group.

[**] This work was done in collaboration with Prof. Sang Bok Lee's group.

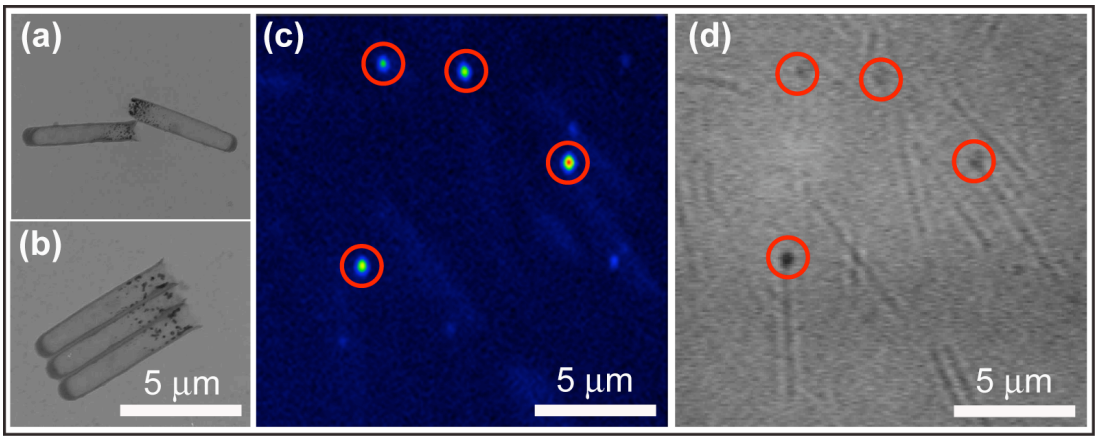

Figure 5.11 Silica nanotubes with AuNPs at the entrance, the other end is closed. (a) (b) TEM images of nanotubes; (c) MAIL images of the nanotubes; (d) corresponded optical image of the nanotubes. The red circles in (c) and (d) represent the AuNPs at the entrance of nanotubes, they match with each other on the MAIL and optical images.

5.3.3 Investigation of FE phenomena of AuNPs

Besides the imaging applications, we have employed MAIL for investigating field-enhanced phenomena of AuNPs. Interest in the field-enhanced phenomena of noble-metal nanostructures has experienced explosive growth in recent years.[19, 20] For instance, surface-enhanced Raman scattering (SERS)[23-25] has become a powerful analytical technique that is even capable of detecting signals from single molecules.[26-31] Similarly, surface-enhanced infrared absorption (SEIRA) can lead to increases in the absorption cross section of vibrations of up to three orders of magnitude.[32-36]

Field enhancement has also been used to enhance multiphoton absorption polymerization (MAP). Because MAP is a nonlinear optical process, its probability can be increased substantially by field enhancement. Metal nanostructure induced field enhancement is used to perform MAP at laser intensities that would normally be below the threshold for causing polymerization. The effect is called metal-enhanced multiphoton absorption polymerization, or MEMAP.[21] MEMAP has been reported on gold nanostructures created by shadow-sphere lithography,[37] in the controlled gaps of nanoscale gold structures,[13, 38] and at a metal-coated AFM tip.[39] MEMAP has also been observed in arrays of gold nanostructures excited with incoherent light.[38]

We performed the MEMAP with a system that includes AuNPs and the prepolymer resin we normally use for MAP fabrication. We employed an MAIL setup to scan the laser beam on AuNPs that were immersed in prepolymer resin (Figure 5.12). The polymerization on the AuNPs was occurred at a laser intensity lower than the threshold for MAP (Figure 5.13). However, we concluded this phenomenon was caused by the emission from the AuNPS (MAIL) rather than by direct field enhancement.

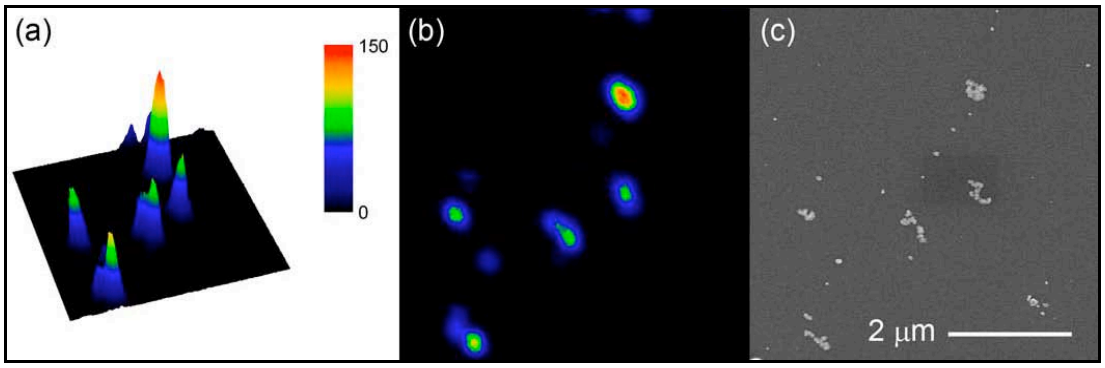

Figure 5.12 (a) 3D and (b) contour plots of MAIL from gold nanoparticles

deposited on a glass substrate, immersed in prepolymer resin, and excited with 800 nm light. The intensity scale is the same for both images. (c) A scanning electron micrograph of the same region of the sample.

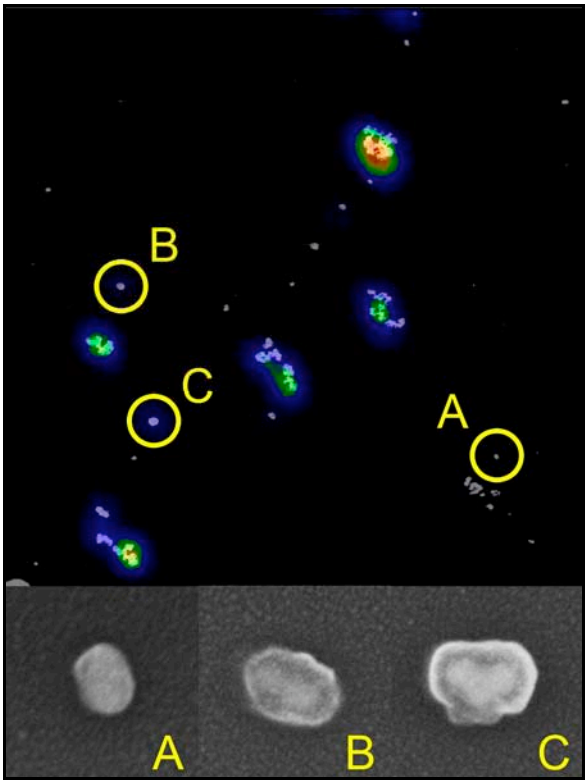

Figure 5.13 An overlay of the MAIL and SEM images from Figure 5.12 and close-up electron micrographs of selected particles and aggregates without a polymer shell (bottom left) and with a polymer shell (bottom center and bottom right). The magnifications of the close-ups vary.

We tuned the laser output wavelength to 890 nm to ensure it was outside the TPO-L two-photon absorption band. Exposing the resin to the 890 nm laser beam at very strong intensity resulted in no polymerization. We then performed a similar MEMAP experiment using the 890 nm excitation wavelength. Surprisingly, we found

the polymerization around the AuNPs (Figure 5.14). Since two-photon absorption by the photoinitiator promoted by the field enhancement cannot occur in this, it is probably excitation via MAIL emission that causes the polymerization.

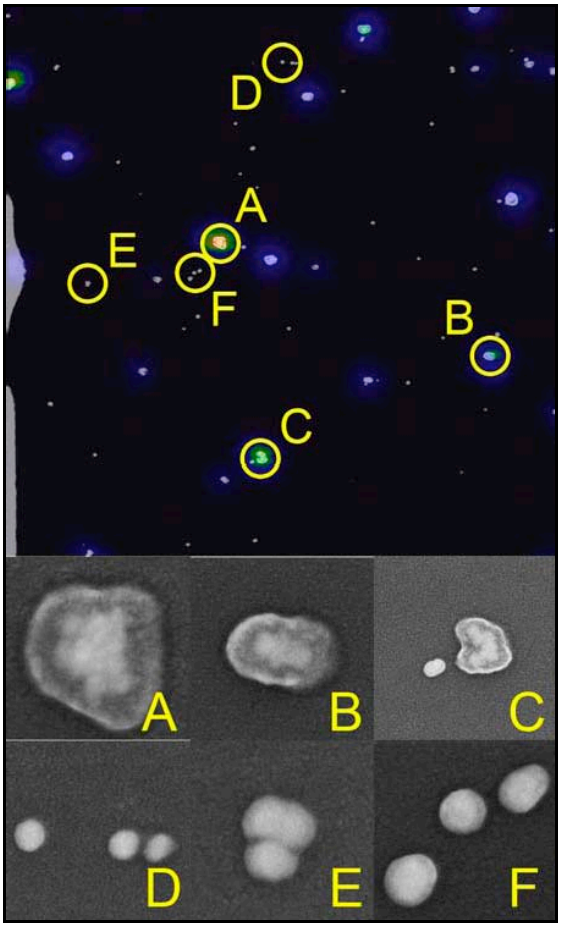

Figure 5.14 An overlay of the MAIL and SEM images and close-up electron micrographs of selected particles and aggregates with a polymer shell (middle) and without a polymer shell (bottom). The magnifications of the close-ups vary.

Also shown in Figure 5.14 are close-up SEM images of different particles and aggregates. Aggregates A, B and C all show strong MAIL emission and have polymerized shells around them. However, the particles and aggregates D, E and F do

not exhibit detectable MAIL emission at this excitation intensity and do not have polymerized shells about them. This is a direct correspondence between MAIL emission and MEMAP.

5.4 Conclusions

In this chapter, the MAIL technology and some of its application have been introduced. In one application, MAIL was used to investigate the uptake of AuNPs into HUVEC cells. In this study we found that significantly more efficient nanoparticle uptake with cyclic RGD conjugates when compared to AuNPs conjugated with linear RGD or bare AuNPs. Uptake results from MAIL studies indicate that the most of the endocytosed AuNPs aggregated in endosomal and lysosomal vesicles. Other applications including AuNPs coated microbeads, silica nanotubes have also been discussed.

This chapter also explored the connection between two field-enhanced phenomena of noble-metal nanostructures, MAIL and MEMAP. We have found a strong correlation between particles and aggregates that exhibit MAIL and MEMAP. Based on wavelength-dependent studies, we believe that the predominant mechanism for MEMAP in the systems studied here is MAIL-mediated excitation of the photoinitiator rather than field-enhanced two-photon absorption. This mechanism may be relevant for other field-enhanced phenomena of noble metal nanoparticles as well.

Reference:

(1) Farrer, R. A.; Butterfield, F. L.; Chen, V. W.; Fourkas, J. T., Highly efficient multiphoton-absorption-induced luminescence from gold nanoparticles. *Nano Letters* **2005,** *5* (6), 1139-1142.

(2) Mooradian, A., Photoluminescence of Metals. *Physical Review Letters* **1969,** *22* (5), 185.

(3) Boyd, G. T.; Yu, Z. H.; R., S. Y., Photoinduced Luminescence from the Noble-metal and its Enhancement on Roughened Surfaces. *Physical Review B* **1986,** *33* (12), 7923-7936.

(4) Beversluis, M. R.; Bouhelier, A.; Novotny, L., Continuum generation from single gold nanostructures through near-field mediated intraband transitions. *Physical Review B* **2003,** *68* (11), 115433.

(5) Eichelbaum, M.; Schmidt, B. E.; Ibrahim, H.; Rademann, K., Three-photon-induced luminescence of gold nanoparticles embedded in and located on the surface of glassy nanolayers. *Nanotechnology* **2007,** *18* (35), 355702.

(6) Kempa, T.; Farrer, R. A.; Giersig, M.; Fourkas, J. T., Photochemical synthesis and multiphoton luminescence of monodisperse silver nanocrystals. *Plasmonics* **2006,** *1* (1), 45-51.

(7) Durr, N. J.; Larson, T.; Smith, D. K.; Korgel, B. A.; Sokolov, K.; Ben-Yakar, A., Two-photon luminescence imaging of cancer cells using molecularly targeted gold nanorods. *Nano Letters* **2007,** *7* (4), 941-945.

(8) Wang, H.; Huff, T. B.; Zweifel, D. A.; He, W.; Low, P. S.; Wei, A.; Cheng, J.-X., In vitro and in vivo two-photon luminescence imaging of single gold nanorods. *Proceedings of the National Academy of Sciences of the United States of America* **2005,** *102* (44), 15752-15756.

(9) Mohamed, M. B.; Volkov, V.; Link, S.; El-Sayed, M. A., The 'lightning' gold nanorods: fluorescence enhancement of over a million compared to the gold metal. *Chemical Physics Letters* **2000,** *317* (6), 517-523.

(10) Kim, H.; Xiang, C.; Guell, A. G.; Penner, R. M.; Potma, E. O., Tunable two-photon excited luminescence in single gold nanowires fabricated by lithographically patterned nanowire electrodeposition. *Journal of Physical Chemistry C* **2008,** *112* (33), 12721-12727.

(11) Gong, H. M.; Zhou, Z. K.; Xiao, S.; Su, X. R.; Wang, Q. Q., Strong near-infrared avalanche photoluminescence from ag nanowire arrays. *Plasmonics* **2008,** *3* (2-3), 59-64.

(12) Su, X.; Li, M.; Zhou, Z.; Zhai, Y.; Fu, Q.; Huang, C.; Song, H.; Hao, Z., Microstructure and multiphoton luminescence of Au nanocrystals prepared by using glancing deposition method. *Journal of Luminescence* **2008,** *128* (4), 642-646.

(13) Sundaramurthy, A.; Schuck, P. J.; Conley, N. R.; Fromm, D. P.; Kino, G. S.; Moerner, W. E., Toward nanometer-scale optical photolithography: Utilizing the near-field of bowtie optical nanoantennas. *Nano Letters* **2006,** *6* (3), 355-360.

(14) Eichelbaum, M.; Kneipp, J.; Schmidt, B. E.; Panne, U.; Rademann, K., SERS and Multiphoton-Induced Luminescence of Gold Micro- and Nanostructures

Fabricated by NIR Femtosecond-Laser Irradiation. *ChemPhysChem* **2008,** *9* (15), 2163-2167.

(15) Wang, H. F.; Huff, T. B.; Zweifel, D. A.; He, W.; Low, P. S.; Wei, A.; Cheng, J. X., In vitro and in vivo two-photon luminescence imaging of single gold nanorods. *Proceedings of the National Academy of Sciences of the United States of America* **2005,** *102* (44), 15752-15756.

(16) Park, J.; Estrada, A.; Sharp, K.; Sang, K.; Schwartz, J. A.; Smith, D. K.; Coleman, C.; Payne, J. D.; Korgel, B. A.; Dunn, A. K.; Tunnell, J. W., Two-photon-induced photoluminescence imaging of tumors using near-infrared excited gold nanoshells. *Optics Express* **2008,** *16* (3), 1590-1599.

(17) Qu, X.; Wang, J.; Yao, C.; Zhang, Z., Two-photon imaging of lymphoma cells targeted by gold nanoparticles. *Chinese Optics Letters* **2008,** *6* (12), 879-881.

(18) Nagesha, D.; Laevsky, G. S.; Lampton, P.; Banyal, R.; Warner, C.; DiMarzio, C.; Sridhar, S., In vitro imaging of embryonic stem cells using multiphoton luminescence of gold anoparticles. *International Journal of Nanomedicine* **2007,** *2* (4), 813.

(19) Schwartzberg, A. M.; Zhang, J. Z., Novel optical properties and emerging applications of metal nanostructures. *Journal of Physical Chemistry C* **2008,** *112* (28), 10323-10337.

(20) Kelly, K. L.; Coronado, E.; Zhao, L. L.; Schatz, G. C., The optical properties of metal nanoparticles: The influence of size, shape, and dielectric environment. *Journal of Physical Chemistry B* **2003,** *107* (3), 668-677.

(21) Nah, S.; Li, L.; Fourkas, J. T., Field-enhanced phenomena of gold nanoparticles. *Journal of Physical Chemistry A* **2009,** *113* (16), 4416-22.

(22) Son, S. J.; Lee, S., Controlled Gold Nanoparticle Diffusion in Nanotubes: Platfom of Partial Functionalization and Gold Capping. *Journal of the American Chemical Society* **2006,** *128*, 15974-15975.

(23) Yang, W. H.; Schatz, G. C.; Van Duyne, R. P., Discrete dipole approximation for calculating extinction and Raman intensities for small particles with arbitrary shapes. *Journal of Chemical Physics* **1995,** *103* (3), 869-875.

(24) Bell, S. E. J.; Sirimuthu, N. M. S., Quantitative surface-enhanced Raman spectroscopy. *Chemical Society Reviews* **2008,** *37*, 1012-1024.

(25) Tian, Z. Q.; Ren, B.; Wu, D. Y., Surface-enhanced Raman scattering: From noble to transition metals and from rough surfaces to ordered nanostructures. *Journal of Physical Chemistry B* **2002,** *106* (37), 9463-9483.

(26) Kneipp, K.; Wang, Y.; Kneipp, H.; Perelman, L. T.; Itzkan, I., Single Molecule Detection Using Surface-Enhanced Raman Scattering (SERS). *Physical Review Letters* **1997,** *78* (9), 1667-1670.

(27) Zare, R. N., Probing Individual Molecules with Confocal Fluorescence Microscopy. *Science* **1994,** *266* (5187), 1018-1021.

(28) Qian, X. M.; Nie, S. M., Single-molecule and single-nanoparticle SERS: from fundamental mechanisms to biomedical applications. *Chemical Society Reviews* **2008,** *37*, 912-920.

(29) Pieczonka, N. P. W.; Aroca, R. F., Single molecule analysis by surfaced-enhanced Raman scattering. *Chemical Society Reviews* **2008,** *37*, 946-954.

(30) Kneipp, J.; Kneipp, H.; Kneipp, K., SERS—a single-molecule and nanoscale tool for bioanalytics. *Chemical Society Reviews* **2008,** *37*, 1052-1060.

(31) Camden, J. P.; Dieringer, J. A.; Wang, Y.; Masiello, D. J.; Marks, L. D.; Schatz, G.; Van Duyne, R. P., Probing the structure of single-molecule surface-enhanced Raman scattering hot spots. *Journal of the American Chemical Society* **2008,** *130* (38), 12616-12617.

(32) Osawa, M.; Ataka, K.-I.; Yoshii, K.; Nishikawa, Y., Surface-Enhanced Infrared Spectroscopy: The Origin of the Absorption Enhancement and Band Selection Rule in the Infrared Spectra of Molecules Adsorbed on Fine Metal Particles. *Applied Spectroscopy* **1993,** *47* (9), 1497-1502.

(33) Cai, W. B.; Amano, T.; Osawa, M., A comparison of surface-enhanced infrared and surface-enhanced Raman spectra of pyrazine adsorbed on polycrystalline gold electrodes. *Journal of Electroanalytical Chemistry* **2001,** *500*, 147-155.

(34) Osawa, M., Surface-Enhanced Infrared Absorption. *Topics in Applied Physics* **2001,** *81*, 163-187.

(35) Goutev, N.; Futamata, M., Attenuated Total Reflection Surface-Enhanced Infrared Absorption Spectroscopy of Carboxyl Terminated Self-Assembled Monolayers on Gold. *Applied Spectroscopy* **2003,** *57* (5), 506-513.

(36) Lal, S.; Grady, N.; Kundu, J.; Levin, C. S.; Lassiter, J. B.; Halas, N. J., Tailoring plasmonic substrates for surface enhanced spectroscopies. *Chemical Society Reviews* **2008,** *37*, 898-911.

(37) Postnikova, B. J.; Currie, J.; Doyle, T.; Hanes, R. E.; Anslyn, E. V.; Shear, J. B.; Vanden Bout, D. E., Towards nanoscale three-dimensional fabrication using

two-photon initiated polymerization and near-field excitation. *Microelectronic Engineering* **2003,** *69* (2-4), 459-465.

(38) Ueno, K.; Juodkazis, S.; Shibuya, T.; Yokota, Y.; Mizeikis, V.; Sasaki, K.; Misawa, H., Nanoparticle plasmon-assisted two-photon polymerization induced by incoherent excitation source. *Journal of the American Chemical Society* **2008,** *130* (22), 6928-9.

(39) Yin, X.; Fang, N.; Zhang, X.; Martini, I. B.; Schwartz, B. J., Near-field two-photon nanolithography using an apertureless optical probe. *Applied Physics Letters* **2002,** *81* (19), 3663-3665.

Chapter 6: Conclusions and Future Directions

6.1 Conclusions

Micro/nano-scale fabrication has make remarkable progress in the last several decades. However, independent of these progresses, feature sizes are still mainly restricted by the diffraction limit. The diffraction limit constrains the resolution in conventional photolithography to approximately one quarter of a wavelength of the light used to fabricate. Alternative means to photolithography with higher resolution usually requires expensive equipment and complicated conditions, such as electron beam lithography. Multiphoton absorption polymerization (MAP) offers another option for high-resolution fabrication. Using chemical and optical nonlinear effects MAP-based fabrication can generate features of 80-nm transverse dimension with 800-nm laser excitation, representing l/10 resolution. Moreover, MAP has the additional capability of fabricating arbitrary, complex three dimensional (3D) structures, which is essential in many applications, such as micro electromechanical systems (MEMS) and micro-total analysis system (μTAS).

This thesis has discussed the technique of multiphoton absorption polymerization. The mechanism and chemistry of MAP was described in the first

chapter, along with the experimental setup.[1] Several issues were also raised in the introduction, including the resolution of MAP and the lack of additional functionality.

In the second chapter, one of the applications of the MAP has been discussed. With MAP, we fabricated microring resonators that show a quality competitive with that of devices created with more complex techniques.[2] While the devices reported were made from a single polymer, it is readily possible to create different portions of devices from different polymeric materials while maintaining excellent registry. The ability to integrate two or more different polymers in these devices enables the introduction of additional functionality. The ability to use MAP to fabricate high-performance, polymeric microring resonators will make possible a wide range of new applications for these devices.

The next chapter introduced a new approach to improve the resolution of MAP, resolution augmentation through photo-induced deactivation, or RAPID lithography.[3] In RAPID, a pulsed laser beam is used to initiate polymerization in a photoresist through multiphoton absorption and a second laser beam is used simultaneously to deactivate the photopolymerization. The deactivation beam can either work at pulsed mode or continues wave (CW) mode. By spatial phase-shaping the deactivation beam, we demonstrated the fabrication of features with 40 nm resolutions *along the beam axis*. The aspect ratio of the voxels was correspondingly reduced from over 3 to 0.5.

The surface functionalization of polymeric microstructures was discussed in Chapter 4, in which two techniques were described to selectively pattern the

polymeric surface. The first technique starts with creating a 3-D acrylate-methacrylate microstructure with MAP. Amine functionality was then added selectively to the acrylic surface. The second technique uses single-photon polymerization, in which the density of acrylic groups is determined by the intensity of the exposed light.[4] Binary and gray-scale pattern of acrylated surface can be generated in this method. Amine groups were then patterned on the acrylic surface through Michael-addition reaction. This amine functionality can be used for applications requiring biocompatibility or as complexing agent to bind palladium. Reduction of bound palladium results in a highly catalytic surface for a number of reactions, including the electroless deposition of copper. Peptides were synthesized on the binary and gray-scale pattern of amines to demonstrated the biocompatibility.

In Chapter 5, an application for microscopic imaging based on multiphoton absorption was discussed. We have demonstrated that multiphoton absorption induced photoluminescence (MAIL) can be used to monitor the targeting and endocytosis of gold nanoparticles to human umbilical vein endothelial cells. The details of MAIL technique were introduced. We have also employed the same setup to investigate the field enhancement from the gold nanostructures.[5] We have fabricated polymeric shell on the gold nanoparticles. By doing this, we discovered that it is the emission from gold nanoparticles, rather than field enhancement, that initiates photopolymerization.

6.2 Future directions

6.2.1 Photonic devices

We have shown that MAP is capable of fabricating high-performance microring resonators. Even better devices are achievable if we take advantages of 3D fabrication ability of MAP. Figure 6.1(a) shows the cross section of a "Γ" shape waveguide. It has the pedestal offset to one side of the waveguide to prevent any mode leakage. Another architecture shown in Figure 6.1(b) is the cross section of a "T" shape waveguide. By fabricating them on the pedestals, the waveguides act as if they are effectively air-clad.

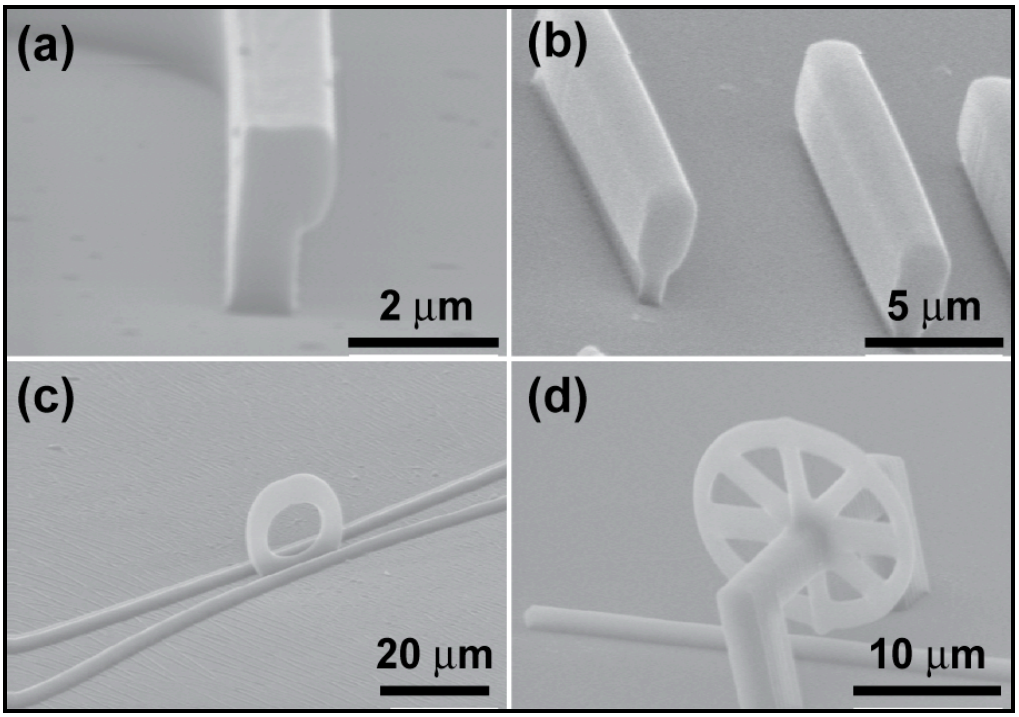

Figure 6.1 Examples of unique architectures that can be created readily with MAP. (a) A waveguide with a "Γ cross section; (b) A waveguide with a "T" cross section; (c) A standing-ring (on surface) waveguide device; (d) A device in which the microring is completely cladded by air.

Also shown in Figure 6.1 are two examples of 3-D devices that would be difficult to fabricate with conventional techniques. Vertical microrings such as the one shown in Figure 6.1(c) save space on the substrate and have different coupling to the bus waveguides than to coplanar microrings because the buses couple to one another through the ring. As shown in Figure 6.1(d), a suspending microring that is completely cladded by air can be fabricated with MAP.

6.2.2 Improvement for RAPID

We have demonstrated that RAPID is able to achieve λ/20 resolution in axial direction of the laser beam. The resolution in transverse dimension should be improved if a spiral phase mask is used to shape the deactivation beam. By combining a spiral phase-shaped and a π phase-shaped beam together for being used as deactivation beam, (Figure 6.2) the resolutions is expected to improve in all three dimensions.[6]

Careful designed experiments are needed for a better understanding of RAPID process. The wavelength of the deactivation beam used in my experiment was set at 800 nm. However, we have tested deactivation beams with wavelength ranging from 760 nm to 840 nm, in which all of the wavelengths were able to inhibit the polymerization. A color study is necessary to find out which wavelength works best for deactivating the polymerization. Another test is the efficiency of the photoinitiators that contain malachite green with different cationic bases. Studies have been performed with oxalate base, carbinol base and hydrochloride base. Most of the experiments were performed with malachite green carbinol base. More tests with other initiator can give more information of the physical process of RAPID.

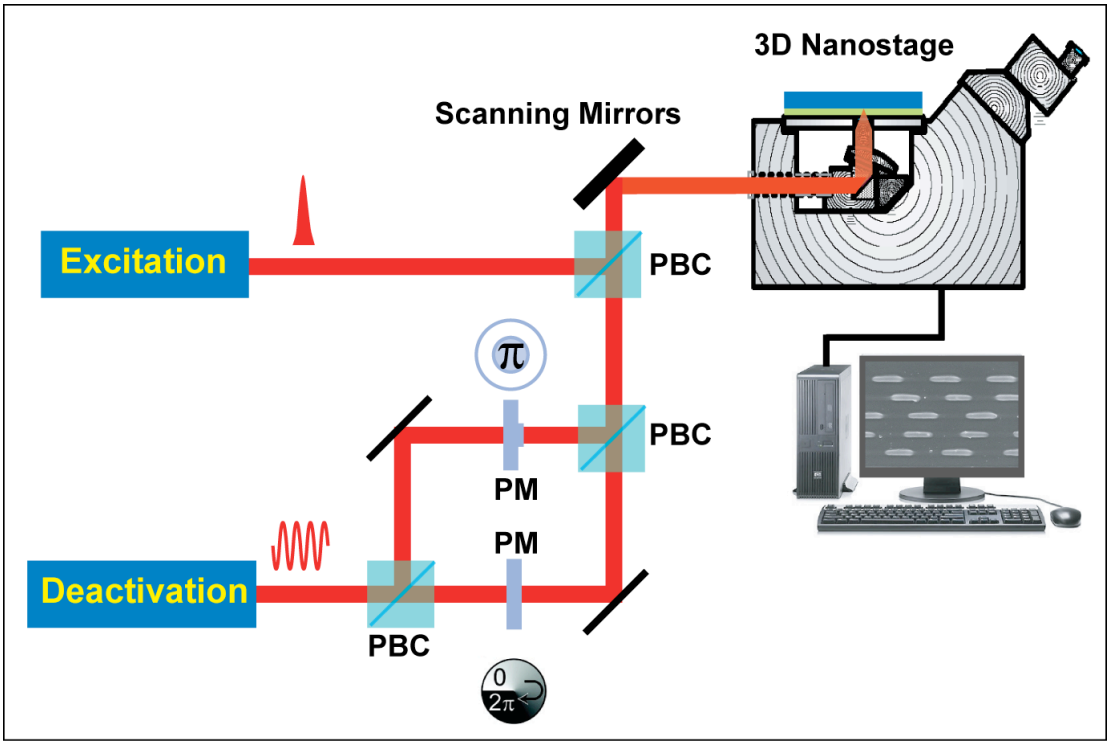

Figure 6.2 RAPID setup with two deactivation beams, in which one beam is used to compress voxels in Z dimension, the other deactivation beam is used to enhance resolution in XY dimension if a spiral phasemask is employed. PBC = polarizing beam cube, PM = phasemask.

We anticipate that the resolution of RAPID lithography can be improved to 10 nm, which is determined by the material. For 3D fabrication at 10 nm scale, the mechanical properties of acrylic polymer will be a limitation of the nanodevice since it is not strong enough to hold itself. Epoxy-based monomers have been tested for MAP fabrication. The good mechanical property of epoxy-based monomers makes it a potential candidate for future resist of RAPID.

6.2.3 Improvement for MAIL

We have shown that MAIL is a great technique for imaging of human cells modified with gold nanoparticles. It is also essential to understand how the AuNPs uptake into the cell and the time scale of the process. An improvement for MAIL to image cells in real-time has been initiated. A sample chamber that contains microfluidic system will be used. The cells will be put in the reservoir on the sample chamber and the AuNPs will be then injected.

The same microfluidic system can also be used for fabrication of Au/polymer core/shell structures. The acrylic monomers and TPO-L initiator used for MAP are insoluble in water, which prohibits its use in microfluidic system. We have synthesized a water soluble photoinitiator that can be mixed in a water soluble monomer, ethoxylated trimethylolpropane triacrylate (SR-9035, Sartomer). This resist with AuNPs will be flown through the sample chamber, while a laser beam is focused in the sample to selectively polymerize around the surface of the AuNPs. The polymer coated AuNPs will then be functionalized later for biological applications.

References:

(1) Li, L.; Fourkas, J. T., Multiphoton polymerization. *Materials Today* **2007,** *10* (6), 30-37.

(2) Li, L.; Gershgoren, E.; Kumi, G.; Chen, W.; Ho, P.; Herman, W. N.; Fourkas, J. T., High-Performance Microring Resonators Fabricated with Multiphoton Absorption Polymerization. *Advanced Materials* **2008,** *20* (19), 3668-3671.

(3) Li, L.; Gattass, R. R.; Gershgoren, E.; Hwang, H.; Fourkas, J. T., Achieving λ/20 Resolution by One-Color Initiation and Deactivation of Polymerization. *Science* **2009**, released online in *Science Express*.

(4) Li, L.; Driscoll, M.; Kumi, G.; Hernandez, R.; Gaskell, K. J.; Losert, W.; Fourkas, J. T., Binary and gray-scale patterning of chemical functionality on polymer films. *Journal of the American Chemical Society* **2008,** *130* (41), 13512-13513.

(5) Nah, S.; Li, L. J.; Fourkas, J. T., Field-Enhanced Phenomena of Gold Nanoparticles. *Journal of Physical Chemistry A* **2009,** *113* (16), 4416-4422.

(6) Harke, B.; Ullal, C. K.; Keller, J.; Hell, S. W., Three-dimensional nanoscopy of colloidal crystals. *Nano letters* **2008,** *8* (5), 1309-1313.

Appendix A: Experiment details of cell growth and uptake of AuNPs

Preparation of Citrate-Stabilized Gold Nanoparticles

4.5 nm-Diameter Gold Nanoparticles. A solution of $HAuCl_4$ (1.00 mL, 29.4 mM in H_2O, Alfa Aesar) was added into 90 mL of H_2O at room temperature. After being stirred for 1 min, a solution of sodium citrate (2.00 mL, 38.8 mM in H_2O) was added, followed by a fresh solution of $NaBH_4$ (1.00 mL, 0.0750 % in 38.8 mM of sodium citrate). The red-colored solution was stirred for 10 min and stored at 4 ^oC.

16 nm-Diameter Gold Nanoparticles. To a refluxing solution of $HAuCl_4$ (100 mL, 1.47 mM in H_2O) was added a solution of sodium citrate (2.00 mL, 0.340 M in H_2O). The resulting red-colored solution was stirred at reflux for 20 min, cooled to room temperature, and stored at 4 ^oC.

Procedure for the Synthesis of RGD Peptide Conjugates

A solution of RGD peptide (1.0 equiv) in HEPES buffer (0.1 M, pH 7.4) was mixed with a solution of the *N*-hydroxy succinimidyl thioctic ester (1.3 equiv) in acetone. The resulting mixture was stirred at room temperature for 24 h, and the acetone was removed *in vacuo*. The aqueous layer was acidified with aq. HCl (0.2 M) to pH 3, washed with organic solvent (EtOAc or ether), and neutralized with aq. NaOH (0.2 M). The remaining organic solvent was removed *in vacuo*, and the final solution was syringe-filtered (0.2 μm). This solution was used for the surface functionalization of AuNPs without further purification.

Linear RGD Peptide Conjugate. Linear RGD peptide (5.0 mg, GRGDSP, Calbiochem) in 4.0 mL of buffer and *N*-hydroxy succinimidyl thioctic ester (3.4 mg) in 2.0 mL of acetone. After purification, the final solution was syringe-filtered with a total volume of 5.0 mL.

Cyclic RGD Peptide Conjugate. Cyclic RGD peptide (2.4 mg, RGDfK, Anaspec) in 2.0 mL of buffer and thioctic ester (1.6 mg) in 2.0 mL of acetone. After purification, the final solution was syringe-filtered with a total volume of 7.0 mL.

Procedure for the Surface Functionalization of Gold Nanoparticles with RGD Peptide Conjugates

A solution of citrate-stabilized gold nanoparticles was mixed with a solution of RGD peptide conjugate. Self-assembly of peptide conjugate onto the surface of gold nanoparticles was accomplished by leaving the solution at room temperature for 24 h. The functionalized particles were then purified by centrifugal filtering (Centriplus YM-30, Amicon). The process was repeated two times with H_2O. The residue in the centriplus filter was additionally purified by gel filtration (pre-packed column, PD-10, GE Healthcare). The final volume of particle solution was adjusted with H_2O and stored at 4 ^oC.

4.5 nm-Diameter Gold Nanoparticles Functionalized with Linear RGD Peptide. To a solution of citrate-stabilized gold nanoparticles (5.0 mL) was added a solution of linear RGD peptide conjugate (0.25 mL). The final volume of purified particle solution is 5.0 mL.

4.5 nm-Diameter Gold Nanoparticles Functionalized with Cyclic RGD Peptide. To a solution of citrate-stabilized gold nanoparticles (5.0 mL) was added a solution of cyclic RGD peptide conjugate (0.50 mL). The final volume of purified particle solution is 5.0 mL.

16 nm-Diameter Gold Nanoparticles Functionalized with Linear RGD Peptide. A solution of citrate-stabilized gold nanoparticles (4.0 mL) was mixed with a mixture of linear RGD peptide conjugate (0.5 mL) and HEPES buffer (7.5 mL, 20 mM, pH 7.4). The final volume of purified particle solution is 16 mL.

16 nm-Diameter Gold Nanoparticles Functionalized with Cyclic RGD Peptide. A solution of citrate-stabilized gold nanoparticles (2.0 mL) was mixed with a mixture of cyclic RGD peptide conjugate (0.5 mL) and HEPES buffer (3.5 mL, 20 mM, pH 7.4). The final volume of purified particle solution is 8.0 mL.

Cell Lines

HUVECs (Human Umbilical Vein Endothelial Cells, Cambrex Biosciences, Walkersville, MD) were cultured in endothelial growth media at 37°C in a humidified atmosphere of 5% CO_2 (v/v). The growth media consisted of 500 mL of endothelial cell basal media (EBM) supplemented with 10 ng/ml recombinant epidermal growth factor (hEGF), 1 μg/ml hydrocortisone, 12 μg/ml bovine brain extract, 25 U/ml heparin, 50 μg/ml amphotericin B, and 2% fetal bovine serum. The cells were detached and harvested using 0.05% trypsin/ 0.02% EDTA in PBS.

References:

(1) Kilby, J. S., Miniaturized Self-Contained Circuit Modules and Method of Fabrication. *U.S. Patent* **1964,** *3,138,744*.

(2) Noyce, R. N., Semiconductor Device-and Lead Structure. *U. S. Patent* **1961,** *No. 2,981,877*.

(3) Intel Corporation, Next-generation Intel® Itanium® processor (codenamed Tukwila) is the world's first 2-billion transistor microprocessor. 2008.

(4) Grabiec, P.; Domanski, K.; Janus, P.; Zaborowski, M.; Jaroszewicz, B., Microsystem technology as a road from macro to nanoworld. *Bioelectrochemistry* **2005,** *66* (1-2), 23-28.

(5) Esashi, M.; Ono, T., From MEMS to nanomachine. *Journal of Physics D: Applied Physics* **2005,** *38* (13), R223-R230.

(6) Elders, J. S., Vincent; Walsh, Steve Microsystems Technology (MST) and MEMS Applications: An Overview. *MRS Bulletin* **2001,** *26* (4), 4.

(7) Craighead, H. G., Nanoelectromechanical systems. *Science* **2000,** *290* (5496), 1532-1536.

(8) Petersen, K., From microsensors to microinstruments. *Sensors and Actuators, A: Physical* **1996,** *A56* (1-2), 143-149.

(9) Daw, R.; Finkelstein, J., Lab on a chip. *Nature* **2006,** *442* (7101), 367-367.

(10) Psaltis, D.; Quake, S. R.; Yang, C., Developing optofluidic technology through the fusion of microfluidics and optics. *Nature* **2006,** *442* (7101), 381-386.

(11) Whitesides, G. M., The origins and the future of microfluidics. *Nature* **2006,** *442* (7101), 368-373.

(12) LaFratta, C. N.; Fourkas, J. T.; Baldacchini, T.; Farrer, R. A., Multiphoton fabrication. *Angewandte Chemie International Edition* **2007,** *46* (33), 6238-6258.

(13) Gratson, G. M.; Garcia-Santamaria, F.; Lousse, V.; Xu, M.; Fan, S.; Lewis, J. A.; Braun, P. V., Direct-write assembly of three-dimensional photonic crystals: conversion of polymer scaffolds to silicon hollow-woodpile structures. *Advanced Materials* **2006,** *18* (4), 461-465.

(14) Therriault, D.; Shepherd, R. F.; White, S. R.; Lewis, J. A., Fugitive inks for direct-write assembly of three-dimensional microvascular networks. *Advanced Materials* **2005,** *17* (4), 395-399.

(15) Wang, T. C.; Cohen, R. E.; Rubner, M. F., Metallodielectric photonic structures based on polyelectrolyte multilayers. *Advanced Materials (Weinheim, Germany)* **2002,** *14* (21), 1534-1537.

(16) Fleming, J. G.; Lin, S. Y.; El-Kady, I.; Biswas, R.; Ho, K. M., All-metallic three-dimensional photonic crystals with a large infrared bandgap. *Nature* **2002,** *417* (6884), 52-55.

(17) Zhao, X. M.; Xia, Y.; Whitesides, G. M., Fabrication of three-dimensional microstructures. Microtransfer molding. *Advanced Materials* **1996,** *8* (10), 837-840.

(18) Tolfree, D. W. L., Microfabrication using synchrotron radiation. *Reports on Progress in Physics* **1998,** *61* (4), 313-351.

(19) Hruby, J., LIGA technologies and applications. *MRS Bulletin* **2001,** *26* (4), 337-340.

(20) Xing, J. F.; Dong, X. Z.; Chen, W. Q.; Duan, X. M.; Takeyasu, N., Improving spatial resolution of two-photon microfabrication by using photoinitiator with high initiating efficiency. *Applied Physics Letters* **2007,** *90*, 3.

(21) Whitesides, G. M.; Grzybowski, B., Self-assembly at all scales. *Science* **2002,** *295* (5564), 2418-2421.

(22) Black, C. T.; Ruiz, R.; Breyta, G.; Cheng, J. Y.; Colburn, M. E.; Guarini, K. W.; Kim, H.; Zhang, Y., Polymer self assembly in semiconductor microelectronics. *IBM Journal of Research and Development* **2007,** *51* (5), 605-633.

(23) Mao, Y.; Park, T.; Zhang, F.; Zhou, H.; Wong, S. S., Environmentally friendly methodologies of nanostructure synthesis. *Small* **2007,** *3* (7), 1122-1139.

(24) Che, G. L.; Lakshmi, B. B.; Fisher, E. R.; Martin, C. R., Carbon nanotubule membranes for electrochemical energy storage and production. *Nature* **1998,** *393* (6683), 346-349.

(25) Wirtz, M.; Martin, C. R., Template-fabricated gold nanowires and nanotubes. *Advanced Materials* **2003,** *15* (5), 455-458.

(26) Hou, S. F.; Wang, J. H.; Martin, C. R., Template-synthesized protein nanotubes. *Nano letters* **2005,** *5* (2), 231-234.

(27) Bauer, L. A.; Reich, D. H.; Meyer, G. J., Selective functionalization of two-component magnetic nanowires. *Langmuir* **2003,** *19* (17), 7043-7048.

(28) Cerrina, F., Application of Xrays to Nanolithography. *Proceedings of the IEEE* **1997,** *84* (4), 644-651.

(29) Madou, M. J., *Fundamentals of Microfabrication: the Science of Miniaturization*. 2 ed.; CRC Press: 2002; p 723.

(30) Becker, E. W.; Ehrfeld, W.; Muenchmeyer, D. *Accuracy of x-ray lithography using synchrotron radiation for the fabrication of technical separation nozzle elements*; Inst. Kernverfahrenstech.,Kernforschungszent. Karlsruhe G.m.b.H.,Karlsruhe,Fed. Rep. Ger.: 1984; p 92 pp.

(31) Ehrfeld, W.; Becker, E. W., The LIGA process for fabricating microstructure devices with extreme aspect ratio and great structural height. *KFK-Nachrichten* **1987,** *19* (4), 167-79.

(32) Ito, T.; Okazaki, S., Pushing the limits of lithography. *Nature* **2000,** *406* (6799), 1027-1031.

(33) Chen, K.-S.; Lin, I.-K.; Ko, F.-H., Fabrication of 3D polymer microstructures using electron beam lithography and nanoimprinting technologies. *Journal of Micromechanics and Microengineering* **2005,** *15*, 1894-1903.

(34) Chou, S. Y.; Keimel, C.; Gu, J., Ultrafast and direct imprint of nanostructures in silicon. *Nature* **2002,** *417*, 835-837.

(35) Yamazaki, K.; Namatsu, H., Two-axis-of-rotation drive system in electron-beam lithography apparatus for nanotechnology applications. *Microelectronic Engineering* **2004,** *73-74*, 85-89.

(36) Chou, S. Y.; Krauss, P. R.; Renstrom, P. J., Imprint Lithography with 25-Nanometer Resolution. *Science* **1996,** *272* (5258), 85-87.

(37) Schift, H., Nanoimprint lithography: An old story in modern times? A review. *Journal of Vacuum Science and Technology B* **2008,** *26* (2), 458-480.

(38) Gates, B. D.; Xu, Q.; Stewart, M.; Ryan, D.; Willson, C. G.; Whitesides, G. M., New Approaches to Nanofabrication: Molding, Printing, and Other Techniques. *Chemical Reviews* **2005,** *105* (4), 1171-1196.

(39) Xia, Y.; Whitesides, G. M., Soft lithography. *Angewandte Chemie International Edition* **1998,** *37* (5), 550-575.

(40) Rogers, J. A.; Nuzzo, R. G., Recent progress in soft lithography. *Materials Today* **2005,** *8* (2), 50-56.

(41) LaFratta, C. N.; Li, L.; Fourkas, J. T., Soft-lithographic replication of 3D microstructures with closed loops. *Proceedings of the National Academy of Sciences of the United States of America* **2006,** *103* (23), 8589-8594.

(42) Bertsch, A.; Jiguet, S.; Bernhard, P.; Renaud, P., Microstereolithography: A review. *Materials Research Society Symposium Proceedings* **2003,** *758* (Rapid Prototyping Technologies), 3-15.

(43) Piner, R. D.; Zhu, J.; Xu, F.; Hong, S. H.; Mirkin, C. A., "Dip-pen" nanolithography. *Science* **1999,** *283* (5402), 661-663.

(44) Salaita, K.; Wang, Y.; Fragala, J.; Vega, R. A.; Liu, C.; Mirkin, C. A., Massively Parallel Dip-Pen Nanolithography with 55 000-Pen Two-Dimensional Arrays. *Angewandte Chemie International Edition* **2006,** *45* (43), 7220-7223.

(45) Kawata, S.; Sun, H.-B.; Tianaka, T.; Takada, K., Finer features for functional microdevices. *Nature* **2001,** *412* (6848), 697-698.

(46) Li, L.; Fourkas, J. T., Multiphoton polymerization. *Materials Today* **2007,** *10* (6), 30-37.

(47) Maruo, S.; Fourkas, J. T., Recent progress in multiphoton microfabrication. *Laser Photonics Reviews* **2008,** *2* (1-2), 100-111.

(48) Baldacchini, T.; LaFratta, C. N.; Farrer, R. A.; Teich, M. C.; Saleh, B. E. A.; Naughton, M. J.; Fourkas, J. T., Acrylic-based resin with favorable properties for three-dimensional two-photon polymerization. *Journal of Applied Physics* **2004,** *95* (11), 6072-6076.

(49) Goppert-Mayer, M., Annalen der Physik. *(Berlin, Germany)* **1931,** *9*, 273.

(50) Kaiser, W.; Garrett, C. G. B., Two-photon excitation in CaF2:Eu++. *Physical Review Letters* **1961,** *7*, 229-31.

(51) Denk, W.; Strickler, J. H.; Webb, W. W., Two-photon laser scanning fluorescence microscopy. *Science* **1990,** *248* (4951), 73-6.

(52) Soeller, C.; Cannell, M. B., Two-photon microscopy: imaging in scattering samples and three-dimensionally resolved flash photolysis. *Microscopy Research and Technique* **1999,** *47* (3), 182-195.

(53) Schafer, K. J.; Hales, J. M.; Balu, M.; Belfield, K. D.; Van Stryland, E. W.; Hagan, D. J., Two-photon absorption cross-sections of common photoinitiators. *Journal of Photochemistry and Photobiology, A: Chemistry* **2004,** *162* (2-3), 497-502.

(54) Cumpston, B. H.; Ananthavel, S. P.; Barlow, S.; Dyer, D. L.; Ehrlich, J. E.; Erskine, L. L.; Heikal, A. A.; Kuebler, S. M.; Lee, I. Y. S.; McCord-Maughon, D.; Qin, J.; Rockel, H.; Rumi, M.; Wu, X.-L.; Marder, S. R.; Perry,

J. W., Two-photon polymerization initiators for three-dimensional optical data storage and microfabrication. *Nature (London)* **1999,** *398* (6722), 51-54.

(55) Belfield, K. D.; Ren, X.; Van Stryland, E. W.; Hagan, D. J.; Dubikovsky, V.; Miesak, E. J., Near-IR Two-Photon Photoinitiated Polymerization Using a Fluorone/Amine Initiating System. *Journal of the American Chemical Society* **2000,** *122* (6), 1217-1218.

(56) Teh, W. H.; Duerig, U.; Drechsler, U.; Smith, C. G.; Guentherodt, H. J., Effect of low numerical-aperture femtosecond two-photon absorption on (SU-8) resist for ultrahigh-aspect-ratio microstereolithography. *Journal of Applied Physics* **2005,** *97* (5), 054907/1-054907/11.

(57) Witzgall, G.; Vrijen, R.; Yablonovitch, E.; Doan, V.; Schwartz, B. J., Single-shot two-photon exposure of commercial photoresist for the production of three-dimensional structures. *Optics Letters* **1998,** *23* (22), 1745-1747.

(58) Yu, T.; Ober, C. K.; Kuebler, S. M.; Zhou, W.; Marder, S. R.; Perry, J. W., Chemically amplified positive resists for two-photon three-dimensional microfabrication. *Advanced Materials (Weinheim, Germany)* **2003,** *15* (6), 517-521.

(59) LaFratta, C. N.; Lim, D.; O'Malley, K.; Baldacchini, T.; Fourkas, J. T., Direct Laser Patterning of Conductive Wires on Three-Dimensional Polymeric Microstructures. *Chemistry of Materials* **2006,** *18* (8), 2038-2042.

(60) Formanek, F.; Takeyasu, N.; Tanaka, T.; Chiyoda, K.; Ishikawa, A.; Kawata, S., Three-dimensional fabrication of metallic nanostructures over large areas by two-photon polymerization. *Optics Express* **2006,** *14* (2), 800-809.

(61) Formanek, F.; Takeyasu, N.; Tanaka, T.; Chiyoda, K.; Ishikawa, A.; Kawata, S., Selective electroless plating to fabricate complex three-dimensional metallic micro/nanostructures. *Applied Physics Letters* **2006,** *88* (8), 083110/1-083110/3.

(62) Farrer, R. A.; LaFratta, C. N.; Li, L.; Praino, J.; Naughton, M. J.; Saleh, B. E. A.; Teich, M. C.; Fourkas, J. T., Selective functionalization of 3-D polymer microstructures. *Journal of the American Chemical Society* **2006,** *128* (6), 1796-1797.

(63) Juodkazis, S.; Mizeikis, V.; Seet, K. K.; Miwa, M.; Misawa, H., Two-photon lithography of nanorods in SU-8 photoresist. *Nanotechnology* **2005,** *16* (6), 846-849.

(64) Sun, H.-B.; Maeda, M.; Takada, K.; Chon, J. W. M.; Gu, M.; Kawata, S., Experimental investigation of single voxels for laser nanofabrication via two-photon photopolymerization. *Applied Physics Letters* **2003,** *83* (5), 819-821.

(65) Tan, D.; Li, Y.; Qi, F.; Yang, H.; Gong, Q.; Dong, X. Z.; Duan, X. M., Reduction in feature size of two-photon polymerization using SCR500. *Applied Physics Letters* **2007,** *90*, 071106/1-071106/3.

(66) Li, L.; Gershgoren, E.; Kumi, G.; Chen, W.; Ho, P.; Herman, W. N.; Fourkas, J. T., High-Performance Microring Resonators Fabricated with Multiphoton Absorption Polymerization. *Advanced Materials* **2008,** *20* (19), 3668-3671.

(67) Sun, H. B.; Kawata, S., Two-photon laser precision microfabrication and its applications to micro-nano devices and systems. *IEEE/OSA Journal of Lightwave Technology* **2003,** *21* (3), 624-633.

(68) Marder, S. R.; Bredas, J. L.; Perry, J. W., Materials for multiphoton 3D microfabrication. *MRS Bulletin* **2007,** *32*, 561-565.

(69) Yang, D.; Jhaveri, S. J.; Ober, C. K., Three-dimensional microfabrication by two-photon lithography. *MRS Bulletin* **2005,** *30* (12), 976-982.

(70) Deubel, M.; Freymann, G. v.; Wegener, M.; Pereira, S.; Busch, K.; Soukoulis, C. M., Direct laser writing of three-dimensional photonic-crystal templates for telecommunications. *Nature Materials* **2004,** *3* (7), 444-447.

(71) Tétreault, N.; Freymann, G. v.; Deubel, M.; Hermatschweiler, M.; Pérez-Willard, F.; John, S.; Wegener, M.; Ozin, G. A., New Route to Three-Dimensional Photonic Bandgap Materials: Silicon Double Inversion of Polymer Templates. *Advanced Materials* **2006,** *18*, 457-460.

(72) Guo, R.; Xiao, S.; Zhai, X.; Li, J.; Xia, A.; Huang, W., Micro lens fabrication by means of femtosecond two photon photopolymerization. *Optics Express* **2006,** *14* (2), 810-816.

(73) Yokoyama, S.; Nakahama, T.; Miki, H.; Mashiko, S., Fabrication of three-dimensional microstructure in optical-gain medium using two-photon-induced photopolymerization technique. *Thin Solid Films* **2003,** *438-439*, 452-456.

(74) Ishihara, J.; Komatsu, K.; Sugihara, O.; Kaino, T., Fabrication of three-dimensional calixarene polymer waveguides using two-photon assisted polymerization. *Applied Physics Letters* **2007,** *90*, 033511/ -033511/3.

(75) Klein, S.; Barsella, A.; Leblond, H.; Bulou, H.; Fort, A.; Andraud, C.; Lemercier, G.; Mulatier, J. C.; Dorkenoo, K., One-step waveguide and optical circuit writing in photopolymerizable materials processed by two-photon absorption. *Applied Physics Letters* **2005,** *86* (21), 211118/1-211118/3.

(76) Serbin, J.; Gu, M., Superprism phenomena in waveguide-coupled woodpile structures fabricated by two-photo polymerization. *Optics Express* **2006,** *14* (8), 3563-3568.

(77) Chen, L.; Sherwood-Droz, N.; Lipson, M., Compact bandwidth-tunable microring resonators. *Optics letters* **2007,** *32* (22), 3361-3.

(78) Ibrahim, T. A.; Grover, R.; Kuo, L. C.; Kanakaraju, S.; Calhoun, L. C.; Ho, P. T., All-optical AND/NAND logic gates using semiconductor microresonators. *IEEE Photonics Technology Letters* **2003,** *15* (10), 1422-1424.

(79) Xiao, S.; Khan, M. H.; Shen, H.; Qi, M., Compact silicon microring resonators with ultra-low propagation loss in the C band. *Optics Express* **2007,** *15* (22), 14467-14475.

(80) Vander Rhodes, G. H.; Goldberg, B. B.; Ünlü, M. S.; Chu, S. T., Internal Spatial Modes in Glass Microring Resonators. *IEEE Journal of Selected Topics in Quantum Electronics* **2000,** *6* (1), 46-53.

(81) Chen, W. Y.; Grover, R.; Ibrahim, T. A.; Van, V.; Herman, W. N.; Ho, P. T., High-finesse laterally coupled single-mode benzocyclobutene microring resonators. *IEEE Photonics Technology Letters* **2004,** *16* (2), 470-472.

(82) Chen, W.; Van, V.; Herman, W. N.; Ho, P., Periodic microring lattice as a bandstop filter. *IEEE Photonics Technology Letters* **2006,** *18* (17-20), 2041-2043.

(83) Poon, J. K. S.; Huang, Y. Y.; Paloczi, G. T.; Yariv, A., Soft lithography replica molding of critically coupled polymer microring resonators. *IEEE Photonics Technology Letters* **2004,** *16* (11), 2496-2498.

(84) Song, H. C.; Oh, M. C.; Ahn, S. W.; Steier, W. H.; Fetterman, H. R., Flexible low-voltage electro-optic polymer modulators. *Applied Physics Letters* **2003,** *82* (25), 4432-4434.

(85) Li, C.; Zhou, L.; Poon, A. W., Silicon microring carrier-injection-based modulators/switches with tunable extinction ratios and OR-logic switching by using waveguide cross-coupling. *Optics Express* **2007,** *15* (8), 5069-5076.

(86) Mikroulis, S.; Simos, H.; Roditi, E.; Syvridis, D., Ultrafast all-optical AND logic operation based on four-wave mixing in a passive InGaAsP-InP microring resonator. *IEEE Photonics Technology Letters* **2005,** *17* (9), 1878-1880.

(87) Chao, C. Y.; Guo, L. J., Biochemical sensors based on polymer microrings with sharp asymmetrical resonance. *Applied Physics Letters* **2003,** *83* (8), 1527-1529.

(88) Zhu, H.; White, I.; Suter, J.; Zourob, M.; Fan, X., Opto-fluidic micro-ring resonator for sensitive label-free viral detection. *Analyst* **2008,** *133* (3), 356-360.

(89) Yalcin, A.; Popat, K. C.; Aldridge, J. C.; Desai, T. A.; Hryniewicz, J. V.; Chbouki, N.; Little, B. E.; King, O.; Van, V.; Chu, S. T.; Gill, D.; Anthes-Washburn, M.; Unlu, M. S., Optical sensing of biomolecules using microring resonators. *IEEE Journal of Selected Topics in Quantum Electronics* **2006,** *12* (1), 148-155.

(90) Little, B. E.; Foresi, J. S.; Steinmeyer, G.; Thoen, E. R.; Chu, S. T.; Haus, H. A.; Ippen, E. P.; Kimerling, L. C.; Greene, W., Ultra-compact Si-SiO2 microring resonator optical channel dropping filters. *IEEE Photonics Technology Letters* **1998,** *10* (4), 549-551.

(91) Laine, J. P.; Little, B. E.; Haus, H. A., Etch-eroded fiber coupler for whispering-gallery-mode excitation in high-Q silica microspheres. *IEEE Photonics Technology Letters* **1999,** *11* (11), 1429-1430.

(92) Turner, A. C.; Foster, M. A.; Gaeta, A. L.; Lipson, M., Ultra-low power parametric frequency conversion in a silicon microring resonator. *Optics Express* **2008,** *16* (7), 4881-4887.

(93) Deri, R. J. K., E., Low-Loss III-V Semiconductor Optical Waveguides. *IEEE Journal of Quantum Electronics* **1991,** *27* (3), 626-640.

(94) Chen, W., Benzocyclobutene Microring Resonators. *Ph.D. Thesis* **2007**.

(95) Robitaille, L. C., Claire L.; Noad, Julian P., Polymer waveguide devices for WDM applications. *SPIE Proceedings Series* **1998,** *3281*, 14-24.

(96) Chao, C. Y.; Guo, L. J., Polymer microring resonators fabricated by nanoimprint technique. *Journal of Vacuum Science and Technology B* **2002,** *20* (6), 2862-2866.

(97) Zhou, J.; Pyayt, A.; Dalton, L. R.; Luo, J.; Jen, A. K. Y.; Chen, A., Photobleaching fabrication of microring resonator in a chromophore-containing polymer. *IEEE Photonics Technology Letters* **2006,** *18* (21-24), 2221-2223.

(98) Zhuang, Y. X.; Hansen, O.; Knieling, T.; Wang, C.; Rombach, P.; Lang, W.; Benecke, W.; Kehlenbeck, M.; Koblitz, J., Thermal stability of vapor phase deposited self-assembled monolayers for MEMS anti-stiction. *Journal of Micromechanics and Microengineering* **2006,** *16* (11), 2259-2264.

(99) Van, V.; Absil, P. P.; Hryniewicz, J. V.; Ho, P. T., Propagation loss in single-mode GaAs-AlGaAs microring resonators: measurement and model. *Journal of Lightwave Technology* **2001,** *19* (11), 1734-1739.

(100) Eldada, L.; Shacklette, L. W., Advances in polymer integrated optics. *IEEE Journal of Selected Topics in Quantum Electronics* **2000,** *6* (1), 54 - 68.

(101) Kim, D. H.; Im, J. G.; Lee, S. S.; Ahn, S. W.; Lee, K. D., Polymeric microring resonator using nanoimprint technique based on a stamp incorporating a

smoothing buffer layer. *IEEE Photonics Technology Letters* **2005,** *17* (11), 2352-2354.

(102) Thompson, S. E.; Parthasarathy, S., Moore's law: the future of Si microelectronics. *Materials Today* **2006,** *9* (6), 20-25.

(103) Ito, H.; Marty, J. D.; Mauzac, M., *Microlithography, molecular imprinting*. Springer-Verlag Berlin: Berlin, 2005; Vol. 172.

(104) Li, L.; Gattass, R.; Gershgoren, E.; Hwang, H.; Fourkas, J. T., Achieving λ/20 Resolution by One-Color Initiation and Deactivation of Polymerization *Science* **2009**.

(105) Haske, W.; Chen, V. W.; Hales, J. M.; Dong, W.; Barlow, S., 65 nm feature sizes using visible wavelength 3-D multiphoton lithography. *Optics Express* **2007,** *15* (6), 3426-3436.

(106) Sun, H. B.; Tanaka, T.; Kawata, S., Three-dimensional focal spots related to two-photon excitation. *Applied Physics Letters* **2002,** *80* (20), 3673-3675.

(107) Klar, T. A.; Jakobs, S.; Dyba, M.; Egner, A.; Hell, S. W., Fluorescence microscopy with diffraction resolution barrier broken by stimulated emission. *Proceedings of the National Academy of Sciences of the United States of America* **2000,** *97* (15), 8206-8210.

(108) Hell, S. W., Far-field optical nanoscopy. *Science* **2007,** *316*, 1153-1158.

(109) Hell, S. W., Microscopy and its focal switch. *Nature Methods* **2009,** *6* (1), 24-32.

(110) Colley, C. S.; Grills, D. C.; Besley, N. A.; Jockusch, S.; Matousek, P.; Parker, A. W.; Towrie, M.; Turro, N. J.; Gill, P. M. W.; George, M. W., Probing the

reactivity of photoinitiators for free radical polymerization: Time-resolved infrared spectroscopic study of benzoyl radicals. *Journal of American Chemical Society* **2002,** *124* (50), 14952-14958.

(111) Hirschfelder, J. O.; Curtiss, C. F.; Bird, R. B., *Molecular theory of gases and liquids*. Wiley: New York, 1954; p 890.

(112) Farrer, R. A.; Butterfield, F. L.; Chen, V. W.; Fourkas, J. T., Highly efficient multiphoton-absorption-induced luminescence from gold nanoparticles. *Nano Letters* **2005,** *5* (6), 1139-1142.

(113) Sun, H. B.; Maeda, M.; Takada, K.; Chon, J. W. M.; Gu, M.; Kawata, S., Experimental investigation of single voxels for laser nanofabrication via two-photon photopolymerization. *Applied Physics Letters* **2003,** *83* (5), 819-821.

(114) Beijersbergen, M. W.; Coerwinkel, R. P. C.; Kristensen, M.; Woerdman, J. P., Helical-wave-front Laser-beams Produced with a Spiral Phaseplate. *Optics Communications* **1994,** *112* (5-6), 321-327.

(115) Harke, B.; Ullal, C. K.; Keller, J.; Hell, S. W., Three-dimensional nanoscopy of colloidal crystals. *Nano Letters* **2008,** *8* (5), 1309-1313.

(116) Muh, E.; Marquardt, J.; Klee, J. E.; Frey, H.; Mulhaupt, R., Bismethacrylate-based hybrid monomers via Michael-addition reactions. *Macromolecules* **2001,** *34* (17), 5778-5785.

(117) Muh, E.; Weickmann, H.; Klee, J. E.; Frey, H.; Mulhaupt, R., Acrylate-terminated macromonomers by Michael addition. *Macromolecular Chemistry and Physics* **2001,** *202* (18), 3484-3489.

(118) Charbonnier, M.; Alami, M.; Romand, M., Electroless plating of polymers: XPS study of the initiation mechanisms. *Journal of Applied Electrochemistry* **1998,** *28* (4), 449-453.

(119) Charbonnier, M.; Romand, M.; Harry, E.; Alami, M., Surface plasma functionalization of polycarbonate: Application to electroless nickel and copper plating. *Journal of Applied Electrochemistry* **2001,** *31* (1), 57-63.

(120) Farrer, R. A.; Copeland, G. T.; Previte, M. J. R.; Okamoto, M. M.; Miller, S. J.; Fourkas, J. T., Production, analysis, and application of spatially resolved shells in solid-phase polymer spheres. *Journal of the American Chemical Society* **2002,** *124* (9), 1994-2003.

(121) Lafratta, C. N., Multiphoton Absorption Polymerization: Issues and Solutions. *Dissertation of Doctor of Phylosophy* **2006**.

(122) Efimenko, K.; Genzer, J., How to prepare tunable planar molecular chemical gradients. *Advanced Materials* **2001,** *13* (20), 1560-1563.

(123) Genzer, J., Templating surfaces with gradient assemblies. *Journal of Adhesion* **2005,** *81* (3-4), 417-435.

(124) Liu, H.; Xu, J.; Li, Y.; Li, B.; Ma, J.; Zhang, X., Fabrication and characterization of an organic-inorganic gradient surface made by polymethylsilsesquioxane (PMSQ). *Macromolecular Rapid Communications* **2006,** *27* (18), 1603-1607.

(125) Ruardy, T. G.; Schakenraad, J. M.; vanderMei, H. C.; Busscher, H. J., Preparation and characterization of chemical gradient surfaces and their application for the study of cellular interaction phenomena. *Surface Science Reports* **1997,** *29* (1), 3-30.

(126) Kim, M. S.; Seo, K. S.; Khang, G.; Lee, H. B., First preparation of biotinylated gradient polyethylene surface to bind photoactive caged streptavidin. *Langmuir* **2005,** *21* (9), 4066-4070.

(127) Chaudhury, M. K.; Whitesides, G. M., How to Make Water Run Uphill. *Science* **1992,** *256* (5063), 1539-1541.

(128) Kraus, T.; Stutz, R.; Balmer, T. E.; Schmid, H.; Malaquin, L.; Spencer, N. D.; Wolf, H., Printing chemical gradients. *Langmuir* **2005,** *21* (17), 7796-7804.

(129) Buxboim, A.; Bar-Dagan, M.; Frydman, V.; Zbaida, D.; Morpurgo, M.; Bar-Ziv, R., A single-step photolithographic interface for cell-free gene expression and active biochips. *Small* **2007,** *3* (3), 500-510.

(130) Parent, C. A.; Devreotes, P. N., A cell's sense of direction. *Science* **1999,** *284* (5415), 765-770.

(131) Wennemers, H.; Still, W. C., Peptide Complexation in Water. Sequence-Selective Binding with Simple Dye Molecules. *Tetrahedron Letters* **1994,** *35* (35), 6413-6416.

(132) Mooradian, A., Photoluminescence of Metals. *Physical Review Letters* **1969,** *22* (5), 185.

(133) Boyd, G. T.; Yu, Z. H.; R., S. Y., Photoinduced Luminescence from the Noble-metal and its Enhancement on Roughened Surfaces. *Physical Review B* **1986,** *33* (12), 7923-7936.

(134) Beversluis, M. R.; Bouhelier, A.; Novotny, L., Continuum generation from single gold nanostructures through near-field mediated intraband transitions. *Physical Review B* **2003,** *68* (11), 115433.

(135) Eichelbaum, M.; Schmidt, B. E.; Ibrahim, H.; Rademann, K., Three-photon-induced luminescence of gold nanoparticles embedded in and located on the surface of glassy nanolayers. *Nanotechnology* **2007,** *18* (35), 355702.

(136) Kempa, T.; Farrer, R. A.; Giersig, M.; Fourkas, J. T., Photochemical synthesis and multiphoton luminescence of monodisperse silver nanocrystals. *Plasmonics* **2006,** *1* (1), 45-51.

(137) Durr, N. J.; Larson, T.; Smith, D. K.; Korgel, B. A.; Sokolov, K.; Ben-Yakar, A., Two-photon luminescence imaging of cancer cells using molecularly targeted gold nanorods. *Nano Letters* **2007,** *7* (4), 941-945.

(138) Wang, H.; Huff, T. B.; Zweifel, D. A.; He, W.; Low, P. S.; Wei, A.; Cheng, J.-X., In vitro and in vivo two-photon luminescence imaging of single gold nanorods. *Proceedings of the National Academy of Sciences of the United States of America* **2005,** *102* (44), 15752-15756.

(139) Mohamed, M. B.; Volkov, V.; Link, S.; El-Sayed, M. A., The 'lightning' gold nanorods: fluorescence enhancement of over a million compared to the gold metal. *Chemical Physics Letters* **2000,** *317* (6), 517-523.

(140) Kim, H.; Xiang, C.; Guell, A. G.; Penner, R. M.; Potma, E. O., Tunable two-photon excited luminescence in single gold nanowires fabricated by lithographically patterned nanowire electrodeposition. *Journal of Physical Chemistry C* **2008,** *112* (33), 12721-12727.

(141) Gong, H. M.; Zhou, Z. K.; Xiao, S.; Su, X. R.; Wang, Q. Q., Strong near-infrared avalanche photoluminescence from ag nanowire arrays. *Plasmonics* **2008,** *3* (2-3), 59-64.

(142) Su, X.; Li, M.; Zhou, Z.; Zhai, Y.; Fu, Q.; Huang, C.; Song, H.; Hao, Z., Microstructure and multiphoton luminescence of Au nanocrystals prepared by using glancing deposition method. *Journal of Luminescence* **2008,** *128* (4), 642-646.

(143) Sundaramurthy, A.; Schuck, P. J.; Conley, N. R.; Fromm, D. P.; Kino, G. S.; Moerner, W. E., Toward nanometer-scale optical photolithography: Utilizing the near-field of bowtie optical nanoantennas. *Nano Letters* **2006,** *6* (3), 355-360.

(144) Eichelbaum, M.; Kneipp, J.; Schmidt, B. E.; Panne, U.; Rademann, K., SERS and Multiphoton-Induced Luminescence of Gold Micro- and Nanostructures Fabricated by NIR Femtosecond-Laser Irradiation. *ChemPhysChem* **2008,** *9* (15), 2163-2167.

(145) Wang, H. F.; Huff, T. B.; Zweifel, D. A.; He, W.; Low, P. S.; Wei, A.; Cheng, J. X., In vitro and in vivo two-photon luminescence imaging of single gold nanorods. *Proceedings of the National Academy of Sciences of the United States of America* **2005,** *102* (44), 15752-15756.

(146) Park, J.; Estrada, A.; Sharp, K.; Sang, K.; Schwartz, J. A.; Smith, D. K.; Coleman, C.; Payne, J. D.; Korgel, B. A.; Dunn, A. K.; Tunnell, J. W., Two-photon-induced photoluminescence imaging of tumors using near-infrared excited gold nanoshells. *Optics Express* **2008,** *16* (3), 1590-1599.

(147) Qu, X.; Wang, J.; Yao, C.; Zhang, Z., Two-photon imaging of lymphoma cells targeted by gold nanoparticles. *Chinese Optics Letters* **2008,** *6* (12), 879-881.

(148) Nagesha, D.; Laevsky, G. S.; Lampton, P.; Banyal, R.; Warner, C.; DiMarzio, C.; Sridhar, S., In vitro imaging of embryonic stem cells using multiphoton luminescence of gold anoparticles. *International Journal of Nanomedicine* **2007,** *2* (4), 813.

(149) Schwartzberg, A. M.; Zhang, J. Z., Novel optical properties and emerging applications of metal nanostructures. *Journal of Physical Chemistry C* **2008,** *112* (28), 10323-10337.

(150) Kelly, K. L.; Coronado, E.; Zhao, L. L.; Schatz, G. C., The optical properties of metal nanoparticles: The influence of size, shape, and dielectric environment. *Journal of Physical Chemistry B* **2003,** *107* (3), 668-677.

(151) Nah, S.; Li, L.; Fourkas, J. T., Field-enhanced phenomena of gold nanoparticles. *Journal of Physical Chemistry A* **2009,** *113* (16), 4416-22.

(152) Son, S. J.; Lee, S., Controlled Gold Nanoparticle Diffusion in Nanotubes: Platfom of Partial Functionalization and Gold Capping. *Journal of the American Chemical Society* **2006,** *128*, 15974-15975.

(153) Yang, W. H.; Schatz, G. C.; Van Duyne, R. P., Discrete dipole approximation for calculating extinction and Raman intensities for small particles with arbitrary shapes. *Journal of Chemical Physics* **1995,** *103* (3), 869-875.

(154) Bell, S. E. J.; Sirimuthu, N. M. S., Quantitative surface-enhanced Raman spectroscopy. *Chemical Society Reviews* **2008,** *37*, 1012-1024.

(155) Tian, Z. Q.; Ren, B.; Wu, D. Y., Surface-enhanced Raman scattering: From noble to transition metals and from rough surfaces to ordered nanostructures. *Journal of Physical Chemistry B* **2002,** *106* (37), 9463-9483.

(156) Kneipp, K.; Wang, Y.; Kneipp, H.; Perelman, L. T.; Itzkan, I., Single Molecule Detection Using Surface-Enhanced Raman Scattering (SERS). *Physical Review Letters* **1997,** *78* (9), 1667-1670.

(157) Zare, R. N., Probing Individual Molecules with Confocal Fluorescence Microscopy. *Science* **1994,** *266* (5187), 1018-1021.

(158) Qian, X. M.; Nie, S. M., Single-molecule and single-nanoparticle SERS: from fundamental mechanisms to biomedical applications. *Chemical Society Reviews* **2008,** *37*, 912-920.

(159) Pieczonka, N. P. W.; Aroca, R. F., Single molecule analysis by surfaced-enhanced Raman scattering. *Chemical Society Reviews* **2008,** *37*, 946-954.

(160) Kneipp, J.; Kneipp, H.; Kneipp, K., SERS—a single-molecule and nanoscale tool for bioanalytics. *Chemical Society Reviews* **2008,** *37*, 1052-1060.

(161) Camden, J. P.; Dieringer, J. A.; Wang, Y.; Masiello, D. J.; Marks, L. D.; Schatz, G.; Van Duyne, R. P., Probing the structure of single-molecule surface-enhanced Raman scattering hot spots. *Journal of the American Chemical Society* **2008,** *130* (38), 12616-12617.

(162) Osawa, M.; Ataka, K.-I.; Yoshii, K.; Nishikawa, Y., Surface-Enhanced Infrared Spectroscopy: The Origin of the Absorption Enhancement and Band Selection Rule in the Infrared Spectra of Molecules Adsorbed on Fine Metal Particles. *Applied Spectroscopy* **1993,** *47* (9), 1497-1502.

(163) Cai, W. B.; Amano, T.; Osawa, M., A comparison of surface-enhanced infrared and surface-enhanced Raman spectra of pyrazine adsorbed on polycrystalline gold electrodes. *Journal of Electroanalytical Chemistry* **2001,** *500*, 147-155.

(164) Osawa, M., Surface-Enhanced Infrared Absorption. *Topics in Applied Physics* **2001,** *81*, 163-187.

(165) Goutev, N.; Futamata, M., Attenuated Total Reflection Surface-Enhanced Infrared Absorption Spectroscopy of Carboxyl Terminated Self-Assembled Monolayers on Gold. *Applied Spectroscopy* **2003,** *57* (5), 506-513.

(166) Lal, S.; Grady, N.; Kundu, J.; Levin, C. S.; Lassiter, J. B.; Halas, N. J., Tailoring plasmonic substrates for surface enhanced spectroscopies. *Chemical Society Reviews* **2008,** *37*, 898-911.

(167) Postnikova, B. J.; Currie, J.; Doyle, T.; Hanes, R. E.; Anslyn, E. V.; Shear, J. B.; Vanden Bout, D. E., Towards nanoscale three-dimensional fabrication using two-photon initiated polymerization and near-field excitation. *Microelectronic Engineering* **2003,** *69* (2-4), 459-465.

(168) Ueno, K.; Juodkazis, S.; Shibuya, T.; Yokota, Y.; Mizeikis, V.; Sasaki, K.; Misawa, H., Nanoparticle plasmon-assisted two-photon polymerization induced by incoherent excitation source. *Journal of the American Chemical Society* **2008,** *130* (22), 6928-9.

(169) Yin, X.; Fang, N.; Zhang, X.; Martini, I. B.; Schwartz, B. J., Near-field two-photon nanolithography using an apertureless optical probe. *Applied Physics Letters* **2002,** *81* (19), 3663-3665.

(170) Harke, B.; Ullal, C. K.; Keller, J.; Hell, S. W., Three-dimensional nanoscopy of colloidal crystals. *Nano letters* **2008,** *8* (5), 1309-1313.